Techniques for fast screening of 3D heterogeneous shale barrier configurations and their impacts
on SAGD production behavior

by

Chang Gao

A thesis submitted in partial fulfillment of the requirements for the degree of

Master of Science

in

PETROLEUM ENGINEERING

Department of Civil and Environmental Engineering
University of Alberta

ABSTRACT

Steam-assisted gravity drainage (SAGD) recovery process is strongly impacted by the spatial distributions of heterogeneous shale barriers. Though detailed compositional flow simulators are available for SAGD recovery performance evaluation, the simulation process is usually quite computationally demanding, rendering their use over a large number of reservoir models for assessing the impacts of heterogeneity (uncertainties) to be impractical. In recent years, data-driven proxy has been widely proposed to reduce the computational effort; nevertheless, the proxy must be trained using a large data set consisting of many flow simulation cases that is, ideally, spanning the model parameter spaces. The question remains: is there a more efficient way to quickly screen a large number of heterogeneous SAGD models? Such techniques could help to construct a training data set with less redundancy; they can also be used to quickly identify a subset of heterogeneous models for detailed flow simulation. In this work, three particular distance measures, flow-based and static-based, are formulated to quantify the similarity among a set of 3D heterogeneous SAGD models.

First, to formulate the flow-based distance measure, a physics-based particle tracking model is employed: Darcy's law and energy balance are integrated to mimic the steam chamber expansion process; steam particles that are located at the edge of the chamber would release their energy to the surrounding cold bitumen, while detailed fluid displacements are not explicitly simulated. The steam chamber evolution is modeled, and a flow-based distance between two given reservoir models is defined as the difference in their chamber sizes over time. Second, to formulate the static-based distance, the Hausdorff distance is employed: it is often used in image processing to compare two images according to their corresponding spatial arrangement and shapes of various objects. The static quality calculation is also employed: estimating the potential recoverable reserves based on the connectivity to the production well.

A suite of 3D models is constructed using representative petrophysical properties and operating constraints extracted from several pads in Suncor's Firebag project. The computed distance measures are used to partition the models into different groups. To establish a baseline for comparison, flow simulations are performed on these models to predict the actual chamber evolution and production profiles. The grouping results according to the proposed flow- and static-based distance measures match reasonably well to those obtained from detailed flow simulations.

Significant improvement in computational efficiency is achieved with the proposed techniques. They can be used to efficiently screen a large number of reservoir models and facilitate the classification of these models into groups with distinct shale heterogeneity characteristics. It presents a significant potential to be integrated with other data-driven approaches for reducing the computational load typically associated with detailed flow simulations involving multiple heterogeneous reservoir realizations.

PREFACE

This thesis is an original work by Chang Gao. Parts of the thesis have been previously published as conference papers, and they are ready for the peer review journal submission after the conference.

Chapter 3 and 5 are composed in part by Gao, C., & Leung, J. Y., (2020), "Techniques for fast screening of 3D heterogeneous shale barrier configurations and their impacts on SAGD production behavior", paper presented at *SPE Canada Heavy Oil Technical Conference*, Calgary, AB, Canada. I was responsible for method formulation, coding development, result analysis, and manuscript preparation. Leung, J. Y. was the supervisory author and involved in method formulation and manuscript preparation.

Chapter 4 is initially composed in part by Gao, C., Ma, Z., & Leung, J.Y., (2019), "A novel particle-tracking based proxy for capturing SAGD Production features under reservoir heterogeneity", paper presented at *SPE Western Regional Meeting*, San Jose, United State; and modified in part by Gao, C., & Leung, J. Y., (2020), "Techniques for fast screening of 3D heterogeneous shale barrier configurations and their impacts on SAGD production behavior", paper presented at *SPE Canada Heavy Oil Technical Conference*, Calgary, AB, Canada. For both conference papers, I was responsible for method formulation, coding development, result analysis, and manuscript preparation. Leung, J. Y. was the supervisory author and involved in method formulation and manuscript preparation. For the paper presented at *SPE Western Regional Meeting*, Ma, Z. was the assisting author and involved in result analysis and manuscript preparation.

Chapters 6 and 7 are originally written by Chang Gao and have not been published before.

ACKNOWLEDGEMENT

I would first like to thank my supervisor, Dr. Juliana Y. Leung, for her continuous support, encouragement and invaluable advice throughout my studies and research. This thesis would not have been possible without her guidance. I also want to thank my MSc examining committee, Dr. Yuxiang Chen, Dr. Japan Trivedi, and Dr. Nobuo Maeda, for attending my final defense and providing insightful comments towards my thesis.

I also want to thank all my colleagues of Dr. Leung's research group for providing an enjoyable research environment and all the inspiring discussions.

What is more, I appreciate the financial support by the University of Alberta Future Energy Systems (FES), which was established from the Government of Canada's First Research Excellence Fund (CFREF) with project number T707-C02; and the academic licenses provided by Computer Modeling Group (CMG) and MathWorks.

Finally, I would like to express my profound gratitude to my parents and my boyfriend Nan Yang for their endless love, support, and encouragement.

TABLE OF CONTENTS

LIST OF TABLES

LIST OF FIGURES

LIST OF SYMBOLS

A_{ij} = Cross-sectional area between the injector cell, i, and the neighboring cell, j, m^2

C_p = Specific isobaric heat capacity, kJ/(kg °C)

d = Euclidean distance

D = The shortest distance of a flow path, m

f = Modifying factor

f_{cs} = Facies code

h = Directed Hausdorff distance

H = Enthalpy, kJ/kg

H_f = Hausdorff distance

I = Binary temperature index, 1 or 0

K = Permeability of a cell, Darcy

k_{ij} = Average permeability between two neighboring grid cells

L_{ij} = Distance between the centers of two neighboring grid cells, m

l = Realization number

N = Mass of steam particles, kg

$netf_{cs}$ = Net facies code

nc = Total number of non-producer cells in a realization

nw = Total number of producer cells in a realization

P_{ij} = Transitional probability

p = Geometric average permeability along a flow path, Darcy

S = Saturation

T = Temperature, °C

T_{ij} = Transmissibility between cell i and j

V = Volume, m^3

w = Weighting fator, 1/month^2

***Greek letters*:**

μ_g = Steam viscosity, Pa·s

ρ = Density, kg/m^3

ω = Calibration parameter

ϕ = Porosity

Subscripts:

c	= Cutoff value
ch	= Chamber
d	= Length along the flow path
$global$	= Globally connected
inj	= Injection steam
$local$	= Locally connected
n	= Time level n
net	= Net connected
o	= Oil
os	= Oil sand
p	= Permeability along the flow path
$prod$	= Oil production
r	= Rock
rp	= Rock type
sh	= Shale
w	= Water

CHAPTER 1: INTRODUCTION

1.1 Background and Motivations

Steam-assisted gravity drainage (SAGD) is a widely-adopted thermal bitumen recovery process. A pair of horizontal wells, which are drilled approximately 5 meters apart, are placed at the bottom of the formation. High-temperature and high-pressure steam is continuously injected into the reservoir to form a steam chamber; as the chamber expands, the bitumen is contacted by the steam and its viscosity is reduced due to latent heat transfer. Both the water condensate and mobilized oil would drain along the chamber edge due to gravity toward the producer (Butler et al., 1981; Butler, 2004).

It is widely acknowledged that the steam chamber expansion and production performance are strongly impacted by the reservoir heterogeneities. This was observed during the first SAGD pilot at the Underground test facility in Fort McMurray, Canada (Edmunds et al. 1989). To quantify the impacts of reservoir heterogeneities on the steam chamber development, many techniques have been developed. The most commonly used techniques to estimate the extent of chamber growth are experimental analysis, analytical/semi-analytical models, geological static measures and detailed numerical simulators. Despite their advantages, they also come with some limitations. For experimental analysis, it is hard to capture certain field-scale heterogeneities, since the operational conditions are difficult to reproduce during experiments at the lab scale (Shin and Polikar, 2006). For analytical/semi-analytical models, such as Butler's equation (Butler et al., 1981; Butler, 1985) and its subsequent improvements (Reis, 1992; Akin, 2005; Sharma and Gates, 2010), it is difficult to capture the dynamic influences of reservoir heterogeneities due to many simplifications in the models. For the geological static measures, such as the original hydrocarbon in place (OOIP) (Tang and Liu, 2008) or connected hydrocarbon volume in place (CHV), despite of their ease of computation, these measures

generally capture information related to the connectivity of the reservoir, (Gilman, 2005) and often fail to capture the dynamic response due to fluid flow (McLennan and Deutsch, 2005). For full-physics thermal flow simulators, though they are able to offer some insights about the influences of field-scale heterogeneities (Zheng, et al. 2018a, 2018b), these computational costs associated with executing these simulations can be quite high (Saad, 1996).

To further investigate the effect of reservoir heterogeneities, many recent studies have proposed incorporating various data-driven model techniques in the analysis workflow (Amirian et al. 2014; Ma et al., 2015; Zheng et al., 2018a). One issue with these data-driven model techniques is that they require a large training data set consisting of many randomly choosing heterogeneity geological realizations that is, ideally, spanning the model parameter spaces.

1.2 Problem Statement

When dealing with a large number of SAGD heterogeneous models, the same question would commonly arise: "*are there ways to quickly screen a large number of heterogeneous SAGD models?*" This question is particularly relevant in many data-driven modeling workflows. With the increasing popularity of data analytics and machine learning (ML), many studies have proposed the incorporating of these data-driven approaches in the modeling workflow (Amirian et al. 2014; Ma et al., 2015; Zheng et al., 2018a). For example, if a data-driven model (proxy) is trained using a sufficiently large set of flow simulations, the model can be used for performance production, significantly reducing the computational costs (Saad, 1996). In the case of heterogeneous reservoirs, a particular challenge, though, is that the training data set consisting of various heterogeneity realizations must be large enough to sufficiently span the entire model parameter space (i.e., many shale barrier arrangements encompassing a variety of shale proportions and continuity). Unfortunately, quantifying the (dis)similarities among many 3D

realizations is not a trivial task.

1.3   Research Objectives

The main object of this work is *to develop a novel workflow and investigate different techniques for fast screening a large set of 3D heterogeneous shale barrier configurations and their impacts on SAGD production behavior.* The specific objectives of this work are:

(1) Develop a workflow to fast access the impacts of reservoir heterogeneities by integrating dynamic/static distance measures and Multidimensional scaling (MDS), as well as -mean cluster analysis.

(2) Develop a simplified flow model based on particle-tracking principles for approximating the development of a steam chamber and key SAGD production features in a three-dimensional heterogeneous SAGD reservoir.

(3) Formulate a dynamic distance measure based on the principles of particle tracking: Darcy's law (momentum balance) and energy balance are integrated to mimic the steam chamber expansion process. The main idea is that the injected steam particles (analogous to exothermic tracers) would travel to the edge of the chamber and release their energy to the surrounding cold bitumen. The movements of the steam particles, as well as the chamber evolution, are modeled. A flow-based distance between a pair of heterogeneous models is calculated as the difference in chamber sizes over time.

(4) Contrast the performance of the dynamic distance measure with the other two widely-adopted static measures. One is the static distance measure which is calculated based on the Hausdorff distance: it captures the difference related to the spatial arrangement and shapes of

various objects (i.e., shale berries) between a pair of images (i.e., heterogeneous realizations). The other one is the static quality calculation: it estimates an expected steam chamber drainage volume with considering the effective connection between the steam chamber and the surrounding reservoir.

(5) Quantify the dissimilarities between different realizations with clustering techniques and investigate the reservoir architecture among realizations in each cluster with similar shale configurations. Following the approach in Zheng et al., (2018b), three difference distance matrices are constructed (based on the flow-based, static distance measures, and the static volumetric measures), and Multidimensional scaling (MDS), as well as K-mean cluster analysis, are applied to classify these realizations into groups with distinct shale heterogeneity characteristics.

(6) Last, demonstrate the feasibility of the proposed workflows:

(1) Efficiently screen a large number of reservoir models and facilitate the classification of these models into groups with distinct shale heterogeneity characteristics.

(2) Quickly identify a subset of heterogeneous models for detailed flow simulation, which is particularly useful for many data-driven modeling tasks.

1.4   Thesis Outline

This work consists of 7 chapters, and it is organized as follows:

Chapter 1 presents a general introduction of this thesis including background information and research motivations, problem statement, research objectives, and thesis outline.

Chapter 2 presents the literature review including an overview of the SAGD extraction process, impacts of reservoir heterogeneity on SAGD production performance, techniques for assessing the impact of reservoir heterogeneities.

Chapter 3 presents the workflow for fast assessing the impact of reservoir heterogeneities, including model setups, methodologies of the two widely-adopted static distance measures, and Multidimensional scaling (MDS) and cluster analysis. The test results are compared with the results obtained from a detailed flow simulation. The comparisons are also discussed in this chapter.

Chapter 4 presents an improvement of heterogeneities characterizations using the proposed dynamic distance measure based on the particle tracking algorithm. The methodology of the novel particle-tracking based model is described in this chapter.

Chapter 5 presents the proposed particle-tracking model's visual and numerical comparisons with the results generated from a detailed flow simulation.

Chapter 6 presents the comparison of clustering results obtained corresponding to different distance measures.

Chapter 7 presents the conclusions and contributions to this study. The recommendations for future work are also shown at the end of this chapter.

CHAPTER 2: LITERATURE REVIEW

This chapter presents a brief description of the SAGD technique, impacts of reservoir heterogeneity on SAGD production performance, techniques for assessing the impact of reservoir heterogeneities.

2.1 SAGD Technique

Steam-assisted gravity drainage (SAGD) is a widely-adopted in-situ thermal heavy oil recovery technique in Canada. This technique is first invented by Butler in 1970. Figure 9-1 shows a typical SAGD well configuration where a pair of horizontal wells are drilled and placed near the bottom of the formation. High-temperature and pressurized steam is continuously injected into the reservoir through the injection well, which is located 5 to 10 meters above the production well. A steam chamber is formed and grows both vertically and laterally, while the crude oil along the boundary of the chamber absorbs the latent heat released from the steam and becomes less viscous. The steam condensate and mobile oil would drain along the chamber edge due to gravity and be extracted from the production well (Butler et al., 1981; Butler, 2004).
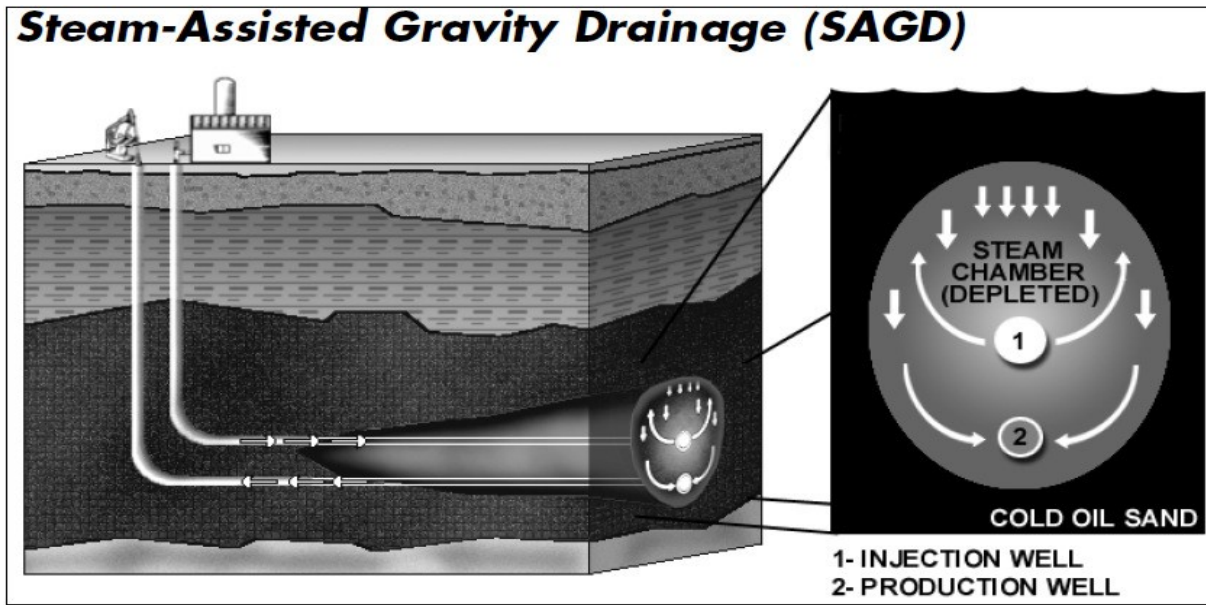
Figure 9-2. **An example of the SAGD extraction process. (National Energy Board, 2006)**

2.2   SAGD Reservoir Heterogeneities

It was first reported by Edmunds et al. (1989) for the SAGD UTF (Underground Test Facility) pilot. One of the issues shown by this field test is that low-permeability facies, which is shale barriers, hinder the communication between the hot steam and the cold bitumen. Such reservoir heterogeneities could adversely affect the lateral and vertical expansion of the steam chamber, leading to poor SAGD production performance (Figure 9-3). Later, the similar issue is observed by Birrell and Putnam (2000) as they applied the graphic method to detect changes in steam rise rates over the UFT pilots and by Zhang et al. (2005) as they use 4D seismic surveillance monitor temperature changes with time over the Christina Lake SAGD project. Reservoir heterogeneities do negatively affect steam chamber development and oil recovery. Additionally, in both experiments, researchers observed that, first, the flow of hot fluid in the near-well region is significantly influenced by the presence, shape and orientation of shale barriers; second, the steam chamber expansion is sensitive to the presence of long, continuous shale or high shale proportion in the

vicinity of the well pair.

To better understand the effects of heterogeneities in SAGD performance, many experimental (Yang and Butler, 1992; Shin and Polikar, 2006) and modeling studies (Butler et al., 1981; Butler, 1985; Reis, 1992; Rose, 1993; Pooladi-Darvish, 1994; Akin, 2005; McLennan and Deutsch, 2005; Bagci, 2006; Chen et al., 2008; Sharma and Gates, 2010; Wang and Leung, 2014; 2015; Amirian et al. 2014; Ma et al., 2015; Wang et al., 2018) have been proposed. Yang and Butler (1992) conducted a series of lab experiments to represent various heterogeneous SAGD conditions by inserting sealed phenolic resin dividers (i.e., shale barriers) into a bed of glass beads (i.e., clean sand). They observed that the horizontal shale barriers would negatively impact the production rate. Similar conclusions were also presented in the simulation studies by Kisman and Yeung (1995), Bagci (2006) and Chen et al. (2008). Additionally, these numerical simulation studies further conclude that the effect of reservoir heterogeneity on steam chamber development and well productivity are minor, unless the shale barriers are laterally extensive and continuous. What is more, the numerical investigation using a stochastic model of shale distribution conducted by Chen et al. (2008) reveals that steam chamber expansion and production performance is highly sensitive to the distribution of shale barriers in the near-well region. Similarly, sensitivity analysis using models with different shale proportions performed by Le Ravalec et al. (2009) further shows that the effects of reservoir heterogeneities to SAGD production performance mainly depend on shale barriers' size, proportions and relative locations to well pairs, and the most detrimental ones are the shale barriers (no matter if they are small and discontinuous) located in between the well pair. Later, researchers, such as Wang and Leung (2014) and Lee et al. (2015), constructed sets of geostatistical models with stochastically distributed shale layers of different portions, sizes, and degrees of continuity; once again, experiments concluded that as the volume or proportion or

continuity of shale barriers increases, or the distance between the shale barriers and well pairs decreases, the more severe the impact on the steam chamber evolution would be.
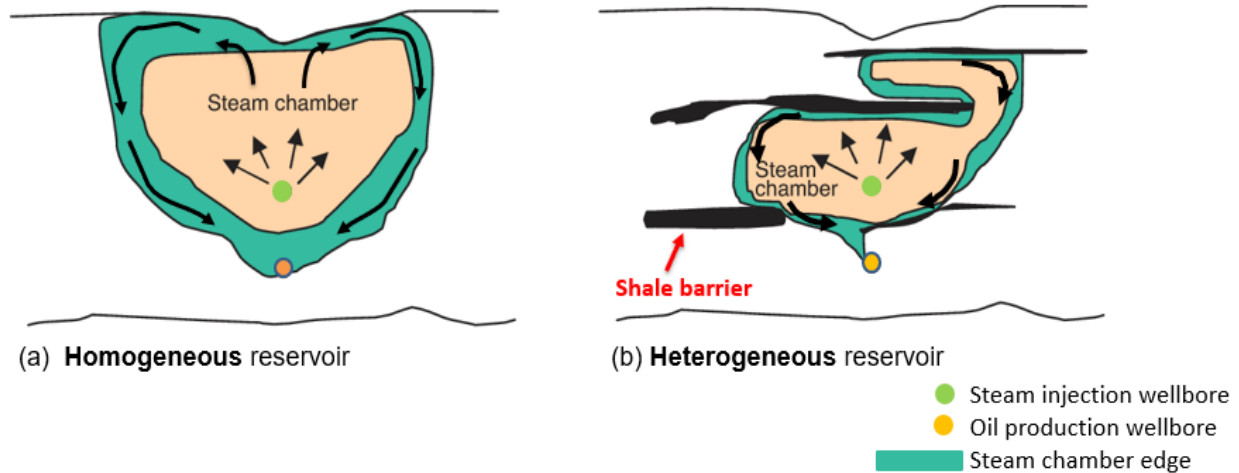
Figure 9-4. Impact of shale barriers on SAGD production performance. (Le Ravalec et al., 2009)

2.3 Techniques Assessing the Impacts of SAGD Reservoir Heterogeneities

Knowing that the SAGD process is pronouncedly impacted by the distributions of shale heterogeneities, it is important to quantify the impacts of shale heterogeneities on the steam chamber development and oil production performance. Analytical/semi-analytical models, experimental analysis, and detailed numerical simulators are the three most commonly used approaches to estimate the extent of the chamber expansion. Despite their advantages, these also come with some limitations. For analytical/semi-analytical models, such as Butler's equation (Butler et al., 1981; Butler, 1985) and its subsequent improvements (Reis, 1992; Akin, 2005; Sharma and Gates, 2010), the effects of reservoir heterogeneities are usually overly simplified. For experimental analysis, only certain operational conditions and field-scale heterogeneities can be reproduced in the lab-scale (Shin and Polikar, 2006). For full-physics thermal flow simulators,

though they are able to offer some insights about the influences of field-scale heterogeneities (Zheng, et al. 2018a, 2018b), the computational costs are high (Saad, 1996).

In order to reduce the computational costs associated with running many numerical simulations, many recent studies have proposed incorporating various data-driven model techniques in the modeling workflow (Ma et al., 2015; Zheng et al., 2018a). A practical challenge for applying these data-driven modeling techniques is that a large training data set consisting of many different heterogeneity realizations is necessary to sufficiently span the entire model parameter space. However, quantifying the (dis)similarities among these realizations is often challenging, particularly if 3D models are involved.

Multidimensional scaling (MDS) and K-means clustering have been applied in many previous studies to visualize or assess (dis)similarities among a set of realizations (Arpat 2005; Borg & Groenen, 2005; Park & Caers, 2007; Suzuki & Caers, 2008; Scheidt & Caers, 2009; Honarkhah & Caers, 2010; Alpak et al. 2010; Tavakoli et al., 2014; Lee et al., 2017; McKenna et al., 2019). In simple terms, MDS transforms a dissimilarity matrix into a configuration of points in an *n*-dimensional Euclidean space (Cox & Cox, 2001). Various distance functions have been employed in those previous studies to compute the dissimilarity matrix; in addition to several flow-based measures, other static measures, such as the Hausdorff distance (Hausdorff, 1914), were also adopted (Suzuki & Caers, 2010). Generally speaking, MDS provides a direct visual representation of the distances among a set of objects, such as various heterogeneous reservoir models in the current context. Recently, Zheng et al. (2018b) adopted a similar MDS/clustering procedure to categorize different SAGD production time-series data according to their shale barrier distributions; in that workflow, realizations are systematically added/removed to/from the training data set, with the intent of maximizing the spanning of the model parameter space, without exhaustively sampling

similar realizations; a flow-based distance function comparing the production responses between any two realizations was computed; then, the resultant distance matrix was mapped into an n-dimensional Euclidean space via multidimensional scaling (MDS), and cluster analysis was applied to group these realizations into multiple categories or clusters. The results were employed to revise the original data set by adding new realizations to clusters with insufficient members and removing realizations from clusters exhibiting excessive redundancy. Although their workflow was capable of screening new realizations for potential redundancy among the existing data set, a relatively large number of flow simulation runs were still required. Other static measures, such as connected hydrocarbon volume in place (CHV) (Fenik et al., 2009), static quality (QS) (Li et al., 2012) or fraction of locally connected hydrocarbon area/volume (Fenik et al., 2009), may offer a cheaper formulation for the distance function. However, despite of their ease of computation, these measures often fail to capture the dynamic response due to fluid flow (McLennan and Deutsch, 2005). Alternative dynamic measure formulations based on simplified flow physics are available; for example, particle tracking (e.g., tracer measures) simulations have been employed in other subsurface modeling applications to approximate flow paths, streamline lines, production patterns (Saad et al., 1996; Ochi and Vernoux, 1999; Siqueria et al., 2003; Srinivasan et al., 2010; Le Borgne et al., 2011; Niu et al., 2011; Vishal and Leung, 2015; 2017; 2018); random-walk measures are applied to approximate the dynamic continuity/connectivity between the well pair (Deutsch and Srinivasan, 1996; McCarthy, 1993); Time-to-Flight algorithm is used to measure the connectivity of a flow path or a streamline line by estimating the traveling time of a neutral tracer along a flow path/streamline (Wang and Kovscek, 2002); streamline simulation, such as swept volume calculation measure, is utilized to rank realizations with regards to the production history (Ates, et al., 2003; Wang and Kovscek, 2002; Idrobo et al., 2000).

CHAPTER 3: Workflow for Fast Assessing the Impact of Reservoir Heterogeneities

The primary objective of this chapter is to develop a workflow to fast assess and visualize (dis)similarities among a set of realizations with different shale barrier configurations in terms of the spatial properties or other forms related to the production behaviors. The idea of the cluster analysis workflow is originally proposed by Zheng et al. (2018b) and several key modifications and improvements have since been implemented. For example, in addition to the conventional history-matching routines, other simple distance functions, such as static distance measures, are utilized. The proposed workflow consists (1) distance measures that is applicable to SAGD recovery process, such as Hausdorff distance, and static quality (Qs) – a optimization of connected hydrocarbon in volume (CHV), to fast access the (dis)similarities among a set of reservoir models; and (2) multidimensional scaling (MDS) and K-mean cluster analysis technique to cluster the test models in different group in accordance to their steam chamber development behavior and shale barrier characteristics. To establish a baseline for comparison, reservoir models are also subjected to detailed numerical flow simulations to predict the actual chamber evolution and production profiles. Clustering results of the two static geologically measures and the detailed flow simulation are also shown in this chapter. Due to the focus of each distance measures is different, the clustering results would represent the influences of shale barriers on the production performance differently.

---

[1] The content in Chapter 3 of this thesis is derived from the following paper:

Gao, C., & Leung, J.Y. (2020). Techniques for fast screening of 3D heterogeneous shale barrier configurations and their impacts on SAGD production behavior, Paper presented at *SPE Canada Heavy Oil Technical Conference*, Calgary, AB, Canada.

3.1   Work Flow

The workflow for fast assessing the influence of reservoir heterogeneities is presented in Figure 10-1. This workflow is designed to:

(1) Efficiently screen a large number of reservoir models.

(2) Facilitate the classification of these models into groups with distinct shale heterogeneity characteristics.

(3) Sufficiently span the feature space.

A set of N 3D models with different shale barrier configurations is constructed using representative petrophysical properties and operating constraints extracted from several pads in Suncor's Firebag project. Then, the models are subjects to either static geological measures or dynamic flow simulations. To establish a baseline for comparison, these models are also subjected to detailed numerical flow simulators to predict the actual chamber evolution and production profiles. For each simulation, a distance function that measures the dissimilarity in production responses between any two realizations is defined, and an N×N dissimilarity matrix is set up. Next, the resultant distance matrix is mapped into an n-dimensional Euclidean space via multidimensional scaling (MDS) and multiple clusters with distinct reservoir architecture feature is revealed via K-means cluster analysis. Models that locate relatively closed in the transformed space generally have similar reservoir heterogeneities and are likely to be redundant. To span the feature space, only a subset of these models is retained. For cluster(s) with insufficient members, new realizations could be added to the cluster(s).
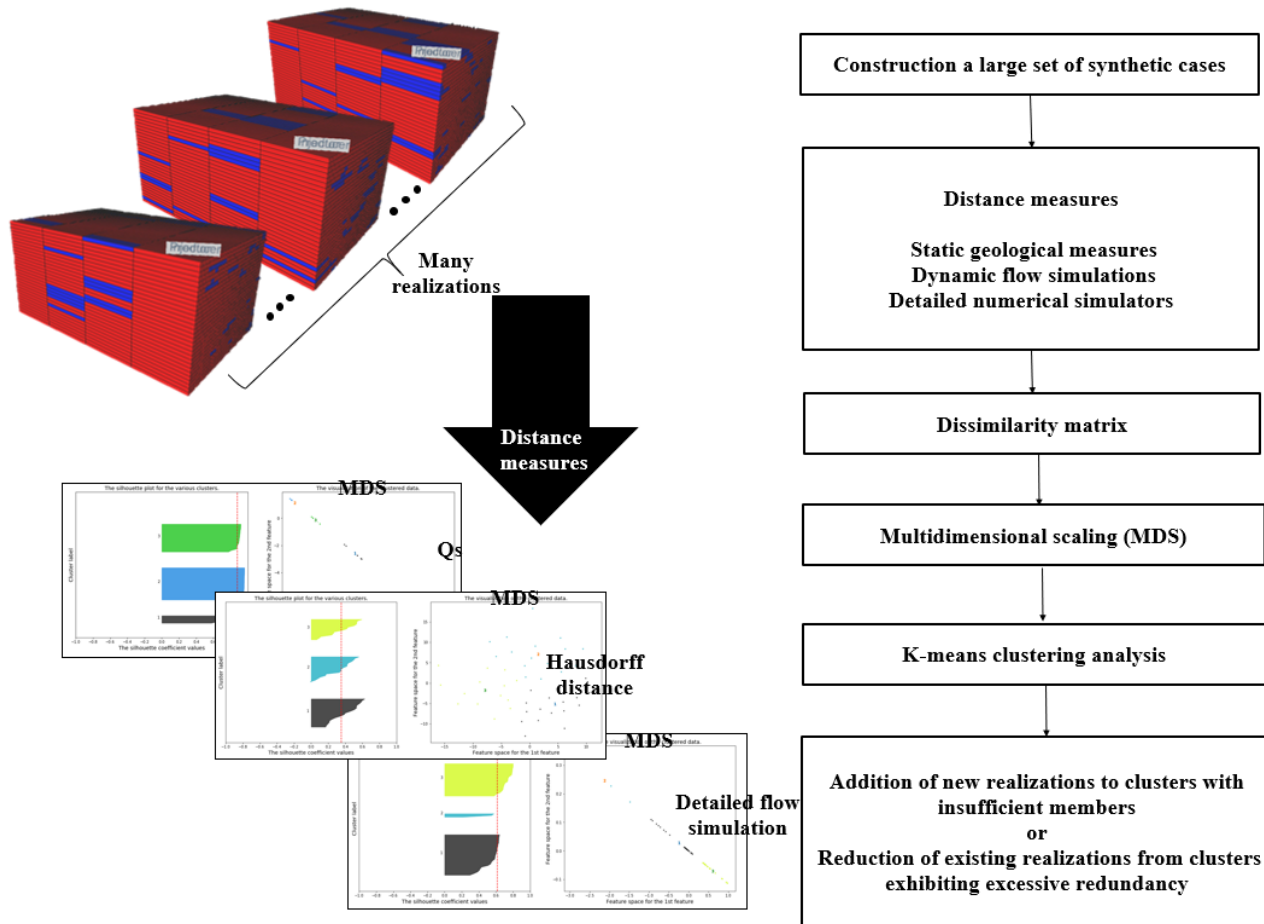
Figure 10-1. A workflow for fast assessing the impact of reservoir heterogeneities

3.2   SAGD Base Model

A total of two types of base models are constructed for this work. For both models, the petrophysical properties and operating constraints are extracted from Suncor's Firebag project whose filed data is considered representative of Athabasca oil sands reservoirs, as presented in Zheng et al. (2018a, 2018b). It should be noted that the properties within the sand/shale domains are set to be uniform in this study, since the focus of this work is to capture a bigger impact of the distribution of sand/shale. For base model 1, it is constructed following the same procedures as

Zheng et al. (2018a, 2018b). For base model 2, it is generated using a sequential indicator simulation, as implemented in SGeMS (2009). The main difference between the two base models is that, for base model 1, instead of constructing physical shales with exact size and shape, it uses sets of arbitrary shales with different size and geometry to represent zones with low permeability (influence of shale barriers).

3.2.1 Base Model 1

Two hundred 3D heterogeneous SAGD models are constructed, following the same procedure and utilizing the same field data (extracted from Suncor's Firebag project) as presented in Zheng, et al. (2018a, 2018b). The corresponding reservoir properties and operating constraints are presented in Table 1. Figure 10-2 shows an example of the 3D heterogeneous model, which is 50 m × 80 m × 40 m in the x-, y-, and z-directions. In each realization, two horizontal wells are placed along the y-direction. Only half the distance between two well pairs is modeled. In consideration of the trade-off between model resolution and problem complexity, only 80 m along the y-direction and 50 m along the y-direction are modeled. To simulate the heterogeneities, each realization is stacked by four 2D segments with $\Delta y = 20$ m, and each section is further divided into 4 zones. The shale heterogeneities are modeled based on the parameterization scheme proposed by Zheng et al. (2018b): superimposing sets of fundamental building blocks with different geometry (thickness and lateral extent) in different zones of the 2D segments to represent a combination of a set of small shales. Different fundamental building blocks are combined along x- or y- direction to mimic the lateral extensive shale barrier influence. To mimic the vertical extensive shale barrier influence, numerous fundamental building block is stacked along the z-direction.

Table 10-1. The reservoir properties and operating constraints for the base model type 1.

	Shale		Sand	
Porosity	0.25		0.32	
Permeability	3×10^{-8}	Darcy	3	Darcy
Oil Saturation	0		0.52	
Water Saturation	1	(fraction)	0.15	(fraction)
Formation Volumetric Heat Capacity	2.35×10^{6}	J/m³-ºC	2.35×10^{6}	J/m³-ºC
Formation Compressibility	2×10^{6}	1/kPa	2×10^{6}	1/kPa
Formation Thermal Expansion Coefficient	6×10^{5}	1/C	6×10^{5}	1/C
Formation Thermal Conductivity	1.5×10^{5}	J/m-day-ºC	1.5×10^{5}	J/m-day-ºC
Oil Density @ Initial Conditions	1010	kg/m³		
Oil Viscosity @ Initial Conditions	1.8×10^{6}	cP		
Oil Specific Heat Capacity	1060	J/kg·K		
Initial Reservoir Temperature	8	ºC		
Initial Reservoir Pressure	800	kPa		
Steam Temperature	225	ºC		
Injected Steam Pressure	1500	kPa		
Injected Steam Quality	0.95			
Well Spacing	5	m		
Well Length	80	m		
Net Pay Thickness	40	m		
Thermal Conductivity of water	5.35×10^{4}	J/m-day-ºC		
Thermal Conductivity of oil	1.5×10^{4}	J/m-day-ºC		

(a) 3D view   (a) xz plane view

(a) Laterally-extensive shale barrier along y-direction

(b) Laterally-extensive shale barrier along x-direction

(c) Vertically-extensive shale barrier along z-direction

■ Area putting the low permeability value ■ Sand
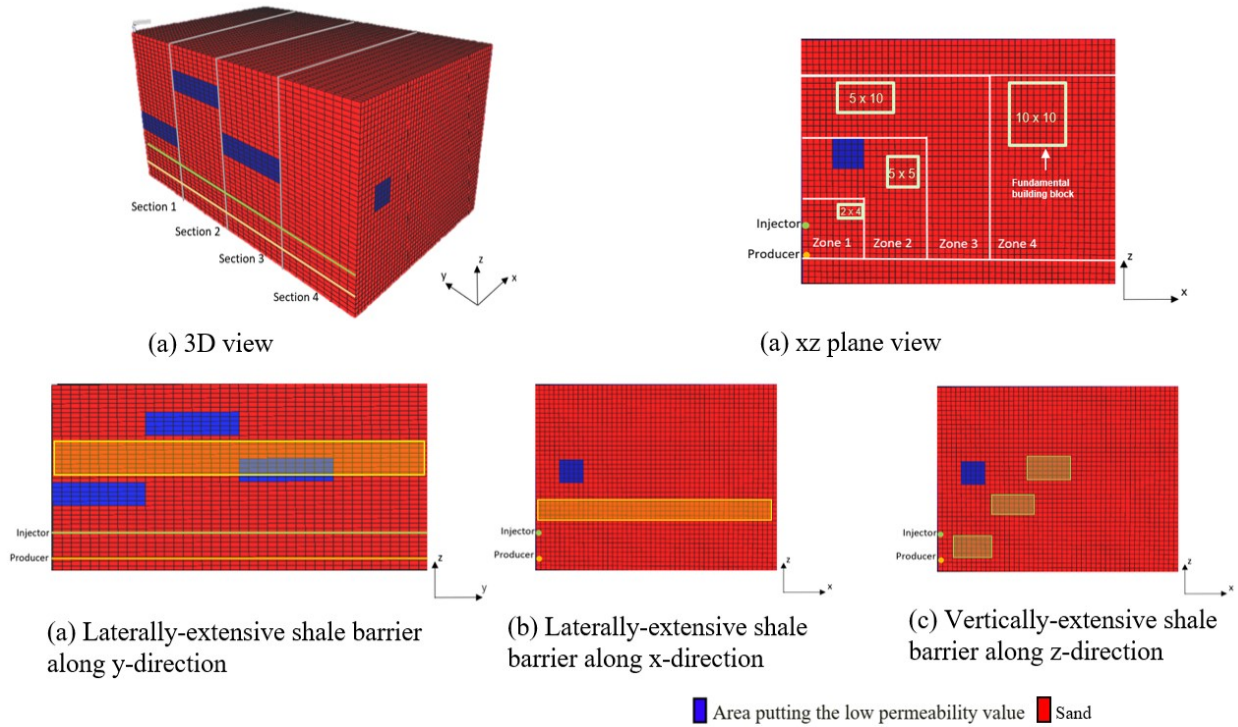
Figure 10-2. An example of the 3D heterogeneous SAGD model based on the parameterization scheme proposed in previous research.

3.2.2 Base Model 2

Fifty realizations of sand/shale distribution are generated using sequential indicator simulation, as implemented in SGeMS (2009). Different from base model type 1, in base model type 2, the sand to shale ratio is fixed and it is set as 10%. Constant porosity, permeability, and saturation values are assigned to each of the two rock types. The petrophysical properties and operating constraints (Table 10-2) are extracted from Suncor's Firebag project, as presented in Zheng et al. (2018a, 2018b).

Each model is 50 m × 80 m × 30 m ($\Delta x = \Delta y = \Delta y = 1$ m) in the *x*-, *y*-, and *z*-directions. A pair of horizontal wells are placed near the bottom of the pay zone, and the horizontal trajectory is aligned along the *y*-direction. It is assumed that all 80 perforations are distributed uniformly along

17

the horizontal well length, thus a point source (injection or production) is placed in each of the 80

cells along the *y*-direction. In consideration of the trade-off between model resolution and problem

complexity, only half the distance between two well pairs (i.e., 50 m) is modeled, assuming

symmetry around the *z*-axis; in addition, only 80 m along the *y*-direction is modeled (i.e., only a

portion of the horizontal well length is captured). Since the shale barriers are generally more

continuous along the lateral (horizontal) direction than the vertical, the following anisotropy

(correlation length) is applied when constructing these realizations: 15 m, 40 m, and 2 m along the

x-, *y*-, and *z*-directions, respectively; to facilitate the model construction, the *y*-direction (along

which the shale is most continuous) is divided into 4 segments.

Table 10-2. The reservoir properties and operating constraints for the base model type 2.

	Shale		Sand	
Proportions by volume	10	%	90	%
Porosity	0.25		0.32	
Permeability	3×10^{-8}	Darcy	3	Darcy
Oil Saturation	0		0.52	
Water Saturation	1	(fraction)	0.15	(fraction)
Formation Volumetric Heat Capacity	2.35×10^6	J/m³-°C	2.35×10^6	J/m³-°C
Formation Compressibility	2×10^6	1/kPa	2×10^6	1/kPa
Formation Thermal Expansion Coefficient	6×10^5	1/C	6×10^5	1/C
Formation Thermal Conductivity	1.5×10^5	J/m-day-°C	1.5×10^5	J/m-day-°C
Oil Density @ Initial Conditions	1010	kg/m³		
Oil Viscosity @ Initial Conditions	1.8×10^6	cP		
Oil Specific Heat Capacity	1060	J/kg·K		
Initial Reservoir Temperature	8	°C		
Initial Reservoir Pressure	800	kPa		
Steam Temperature	225	°C		
Injected Steam Pressure	1500	kPa		
Injected Steam Quality	0.95			
Well Spacing	4	m		
Well Length	80	m		
Net Pay Thickness	30	m		
Thermal Conductivity of water	5.35×10^4	J/m-day-°C		
Thermal Conductivity of oil	1.5×10^4	J/m-day-°C		

(a) 3D view   (b) Shale barriers in x-z plane   (c) Shale barriers in y-z plane
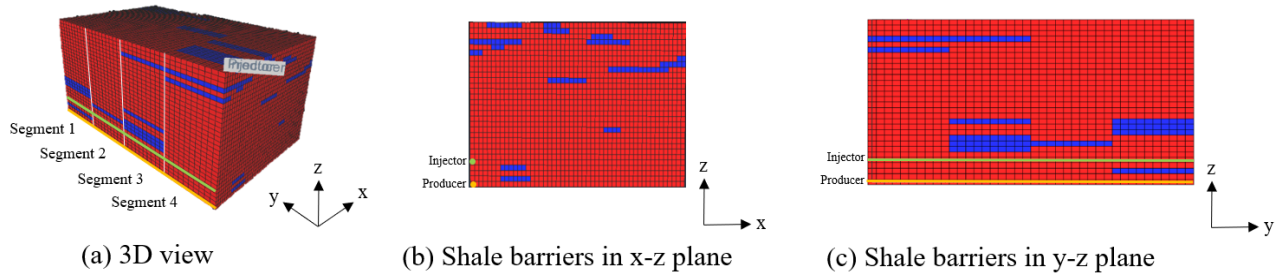
Figure 10-3. An example of the 3D heterogeneous SAGD model.

3.3   Static Geological measures

Static geological measures is the simplest approach to efficiently screen through a large set of reservoir models and quantify the (dis)similarities among these realizations, in order to reduce the number of models for further processing by a detailed numerical simulator or to help to assemble training data sets for data-driven proxy analyses. Compared to dynamic flow simulations, static geological measures are not required to solve complex fluid flow equations (Saad,1996; Ates,2005; McLennan and Deutsch, 2005). Compared to detailed numerical flow simulations, static geological measures offer a much cheaper formulation for the distance function.

Static geological measures are generally classified in the following categories (McLennan and Deutsch, 2005):

(1)   Statistical measures, such as average porosity, average permeability, and average fluid saturation.

(2)   Global connectivity measures, such as fraction of globally connected cells (globally connected hydrocarbon area/volume), average tortuosity.

(3)   Local connectivity measures, such as fraction of locally connected cells (locally connected hydrocarbon area/volume) to specific well locations.

(4) Volumetric measures, such as original hydrocarbon in place (OOIP) (Tang and Liu, 2008), net oil in place (OIPnet) (McLennan and Deutsch, 2005), connected hydrocarbon volume in place (CHV) (Fenik et al., 2009), static quality (QS) (Li et al., 2012).

It should be noted that not all static geological measures are applicable to the SAGD recovery process. According to the paper published by McLennan and Deutsch (2005), it is known that all statistical measures and global connectivity measures, as well as some volumetric measures, are not useful for the SAGD process. Only static geological measures considered local connectivity can be applied for the SAGD process, since this process depends on the efficient connection of the steam chamber to the surrounding reservoir (Laurel and Hovadik, 2006). Additionally, according to Suzuki and Caers (2008; 2010) and Lee et al. (2017), Hasudorff distance is correlated directly with the difference in flow response. Therefore, in this work, QS and Hausdorff distance are selected.

3.3.1 Static Quality (Qs)

A static quality (Q_S^l) (Li et al., 2012) is applied to approximate the potential recoverable reserves for a SAGD extraction process in a realization l. The preliminary formulations for static quality are local connectivity and the original-hydrocarbon-in-place ($OOIP^l$) -a measure based on volumetric. In order to better correlate the estimated hydrocarbon volume in a reservoir to the true oil production, two modifying factors have been implemented into the static quality calculation. As a result, the static quality not only addresses the factors that could significantly affect the production

performance, such as the spatial distribution of facies, permeability and porosity, it also accounts for the location of a cell relative to the producer, and quality of sand along the flow path.

3.3.1.1 Theory and General Mathematical Formulation

It is known that, in the SAGD process, oil production is correlated to the amount of hydrocarbon in the reservoir. Thus, original-hydrocarbon-in-place ($OOIP^l$) is a reasonable initial approximation (Tang and Liu, 2008). The $OOIP^l$ calculated for each realization l is defined as:

$$OOIP^l = \sum_{iw=1}^{nw} \sum_{j=1}^{nc} V_j^l (1 - S_{wj}^l) \phi_j^l \quad \text{...} \quad (10\text{-}1)$$

Where V_j^l, S_{wj}^l and ϕ_j^l are the volume, water saturation and porosity of a cell j in a realization l. nc refers to the total number of non-producer cells in a realization l, and nw refers to the total number of producer cells in a realization l.

Then, as an improvement in the $OOIP^l$ calculation, a net-hydrocarbon-in-place ($OOIP_{net}^l$) calculation is proposed (McLennan and Deutsch, 2005). This new approximation only considered the hydrocarbon volume in cells satisfying a set of net cutoff criteria that: first, the rock type of the cells is not shale; second, the porosity and permeability threshold are above a cutoff value. The n $OOIP_{net}^l$ calculated for each realization l is defined as:

$$OOIP_{net}^l = \sum_{iw=1}^{nw} \sum_{j=1}^{nc} V_j^l (1 - S_{wj}^l) \phi_j^l i_{net\, j}^l \quad \text{...} \quad (10\text{-}2)$$

Where the indicator for a cell j in a realization l, $i^l_{net\,j}$, is defined as:

$$I^l_{net\,j} = \begin{cases} 1, & \begin{aligned} if \quad & f^l_{cs\,j} = netf_{cs_{rp}}\,;and \\ & \phi^l_j > \phi_c\,;and \\ & K^l_j > K_c \end{aligned} \\ 0, & otherwise \end{cases} \quad \text{...} \quad (10\text{-}3)$$

Where K^l_j and $f^l_{cs\,j}$ are the permeability and the facies code of a cell j in a realization l. $netf_{cs_{rp}}$ refers to the net facies codes of $p=1, \ldots, P$, and each facies code, p, represents a distinct category of rock type. ϕ_c and K_c are the porosity and permeability cutoff value.

Since the SAGD production depends on the efficient connection of the steam chamber to the surrounding reservoir, the connectivity should also be accounted for (Laurel and Hovadik, 2006). Thus, a global connectivity indicator is introduced (Deutsch and Srinivasan, 1996a; 1996b; McLennan and Deutsch, 2005). A cell is considered globally connected if: first, the cell is a net cell ($I^l_{net\,j} = 1$). It meets a combination of facies, porosity and permeability cutoff criteria. Second, the cell connected to at least one neighboring net cell by sharing either a face, a corner or an edge with the neighboring net cell.

Figure 10-4 shows an example of global connectivity. Cell #1, #2, #3 and #4 are globally connected, since they are net cells and they are connecting to at least one neighboring net cell; whereas, cell #5 and #6 are not globally connected, since cell #5 is not a net cell and cell #6 does not connect to a net cell.

$$I_{global\,j}^{l} = \begin{cases} 1, & connected \\ 0. & nonconnected \end{cases} \quad \text{.. (10-4)}$$

As illustrated in Figure 10-5, all cells in blue are globally connected. This indicates that global connectivity essentially considers the entire reservoir as one connected geo-object. However, in a SAGD process, a steam chamber is not able to visit all parts of the reservoir. It is only able to reach and recover oil within an expected drainage volume. A local connectivity indicator is developed by limiting the calculation of connectivity within an expected steam chamber drainage volume (local window) (McLennan and Deutsch, 2005). Later, Fenik et al. (2009) extended the work of McLennan and Deutsch (2005). Net cells, that located outside of the expected drainage volume (local window) but located along a direct line-of-sight and directly connected to the production well, are also considered locally connected. In summary, a cell is considered locally connected if: first, the cell is a net cell ($I_{net\,j}^{l} = 1$) and it connects to one or more neighboring net cells ($I_{global\,j}^{l} = 1$). Second, it is either a cell directly connected to a production well within an expected drainage volume around that production well, or a cell directly connected to the production well along a direct line-of-sight.

Figure 10-6 shows an example of local connectivity in a 2D plane. A window is defined around a production well. Cell #1, #2 and #5 are locally connected. Cell #1 is a cell directly connected to a production well within a window tolerance, as well as a cell directly connected to the production well along a direct line-of-sight. Cell #2 is a cell directly connected to a production well within a window tolerance. Cell #5 is a cell directly connected to the production well along a direct line-of-sight. On the contrary, cell #3, #4 and #6 are not locally connected. Due to the presence of a thick shale unit draped over the entire window width, steam is not able to reach the

upper area of the defined window. As a result, for cells located at the net reservoir above the shale, such as cell #3, they are not locally connected. Though cell #4 is a net cell located on a direct line-of-sight, it is not directly connected to the producer. Thus, it cannot be considered as a locally connected cell. Cell #6 is not a net cell, so it is not locally connected.

$$I_{local\,j}^{l} = \begin{cases} 1, & connected \\ 0. & nonconnected \end{cases} \dots\dots\dots\dots\dots\dots\dots\dots\dots\dots\dots\dots\dots\dots\dots\dots\dots\dots\dots\dots\dots\dots\dots \text{(10-5)}$$

By obtaining the connectivity of a realization, the oil production of the realization can be estimated based on the connected hydrocarbon volume in place (CHV). CHV^{l} measures the amount of hydrocarbon that is connected to the production well and can be produced for a realization l (Fenik et al., 2009) and it is defined as:

$$CHV^{l} = \sum_{iw=1}^{nw} \sum_{j=1}^{nc} I_{local\,j}^{l} V_{j} (1 - S_{wj}^{l}) \phi_{j}^{l} \dots\dots\dots\dots\dots\dots\dots\dots\dots\dots\dots\dots\dots\dots\dots\dots\dots\dots\dots \text{(10-6)}$$

Besides the connectivity, additional modifying factors could potentially capture more significant flow respond and improve the ranking measure (Li et al., 2012). Wilde and Deutsch (2012) proposed several possible modifying factors, such as the number of flow steps from a cell to the production well, the angle measured from vertical between a cell and the production well, permeability along a flow path, and distance from any particular cell to the production well. The static quality (Q_{s}^{l}) (Li et al., 2012) is developed based on CHV by adding two modifying factors,

permeability along a flow path and length of the flow path between productive cells to the production well. The static quality (Q_S^l) is defined as,

$$Q_S^l = \sum_{iw=1}^{nw} \sum_{j=1}^{nc} f_{dj}^l f_{pj}^l I_{local\,j}^l V_j (1 - S_{wj}^l) \phi_j^l \quad\text{...}\quad (10\text{-}7)$$

Where f_{dj}^l is the modifying factors related to the length of a flow path between a productive cell to a selected producer cell. f_{pj}^l is the modifying factors related to permeability along a flow path from a productive cell to a selected producer cell. More details for these two modifying factors are presented in section 3.3.1.3 and 3.3.1.4
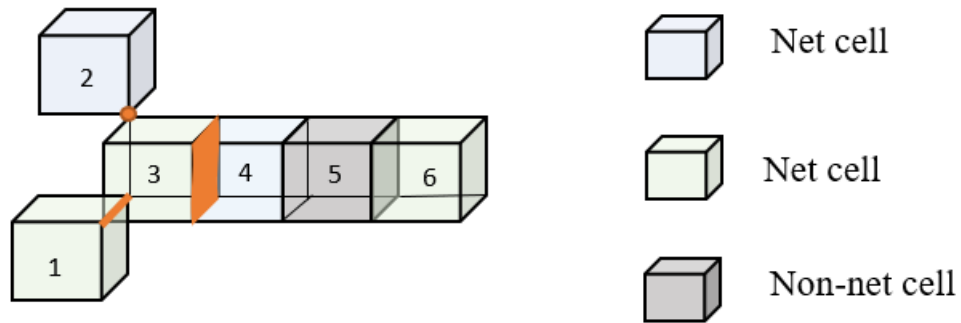
Figure 10-4. An example of global connectivity between cells.
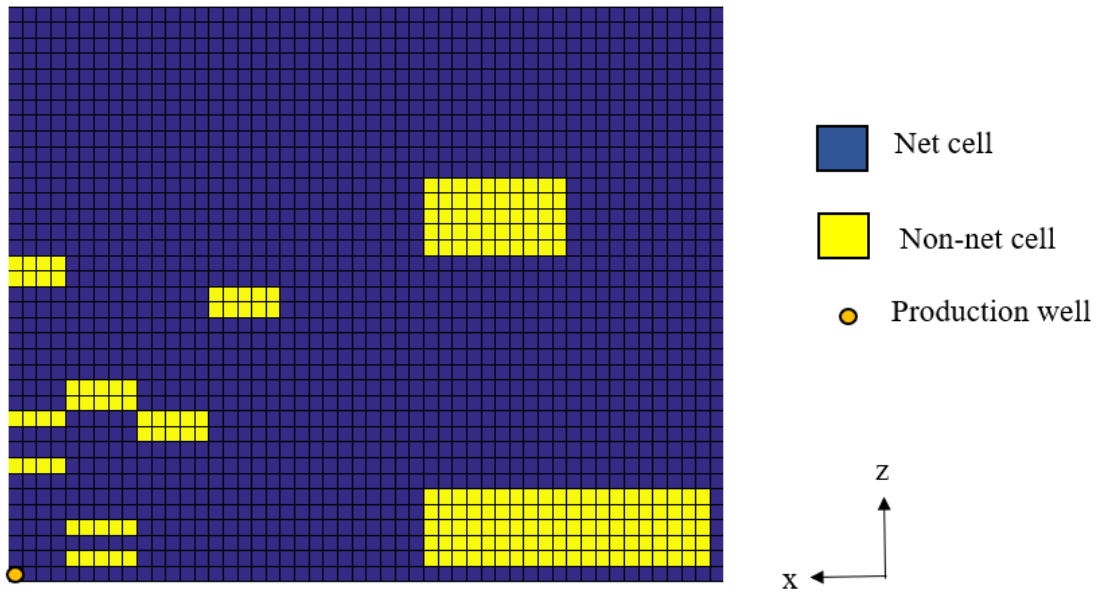
Figure 10-5. An example of global connectivity in the x-z plane.
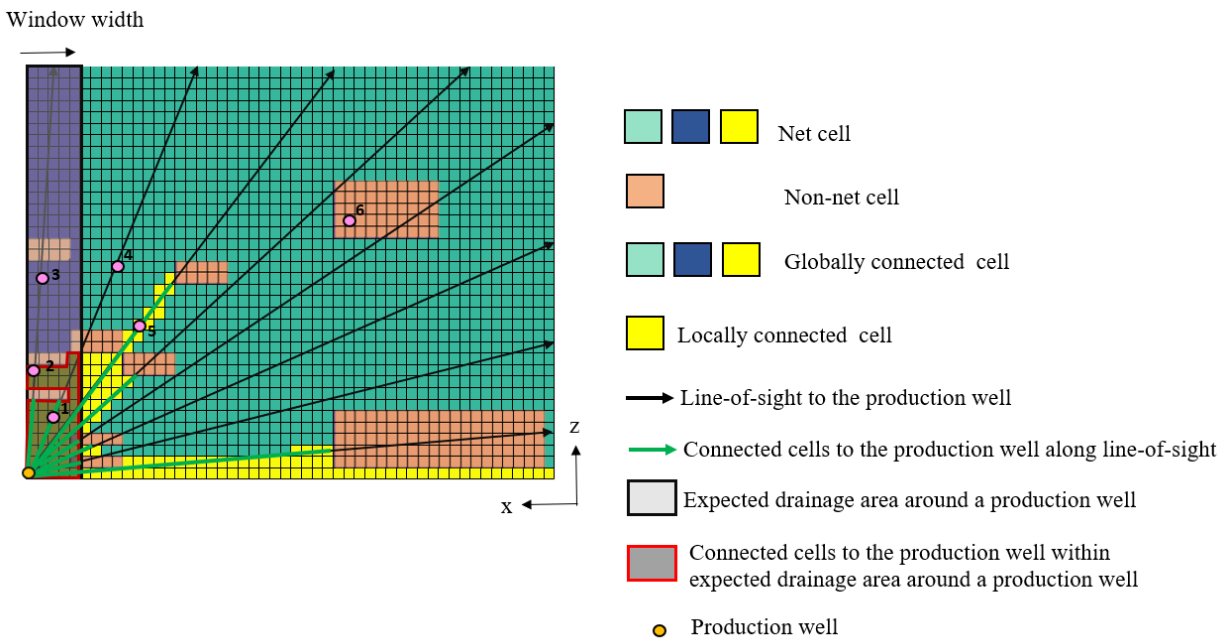
Figure 10-6. An example of local connectivity in the x-z plane.

3.3.1.2 Local Window

A local window is defined as the expected drainage area/volume around a specific well location. It represents an interval for calculating the connected hydrocarbon to a producer. The window width is the width of the expected drainage area or the thickness of the expected drainage volume. Figure 10-7 shows examples of window size under different scenarios. In 2D, the window starts from the producer and takes the two directions along an axis which is normal to the horizontal well. In 3D, if the well trajectory is not considered, the window width refers to the thickest connected interval to the producer; otherwise, it is set to be normal to the well trajectory (Fenik et al., 2009).

The results are sensitive to the window size selection; thus, in this work, a set of window width in the range of 5 to 25 meters is considered.

(a) A example of window width in 2D

(b) A example of window width in 3D if the well trajectory is not considered   (c) A example of window width in 3D if the well trajectory is considered
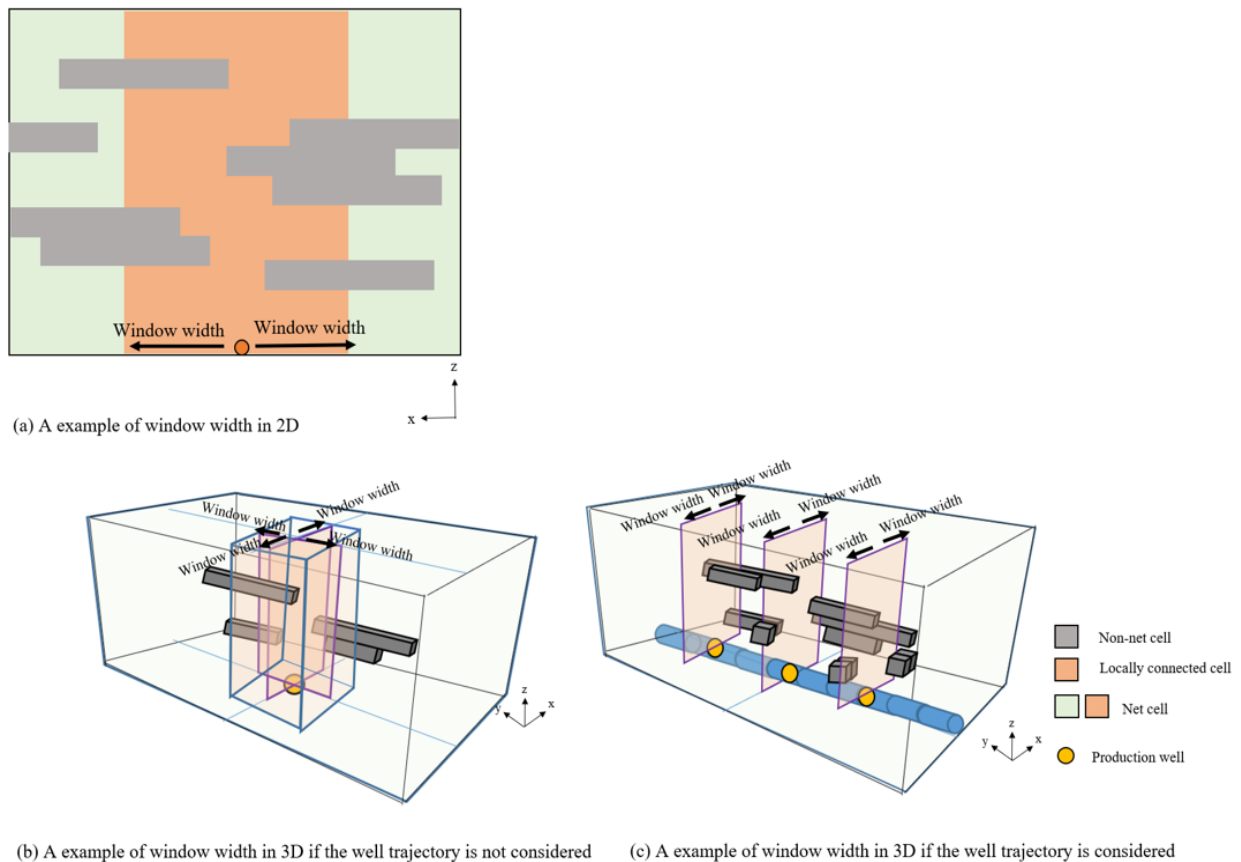
Figure 10-7. Examples of window width under different scenarios.

3.3.1.3 Procedures to Determine Locally Connected Cells to a Selected Producer Cell

Figure 10-8 shows the workflow to find all locally connected cells to a selected producer cell in a realization. First, remove all cells located lower than the producer. Then, construct boundaries for the realization. To find connected cells to a selected producer cell along a direct line-of-sight, first of all, the Bresenham algorithm (Bresenham, 1963) is applied for the producer cell to any cell belong to the boundary plane. Then, coordinates of cells along the Bresenham line (also known as a line-of-sight to the producer cell) are recorded in order of an increasing distance to the producer cell. This step is repeated until all cells on the boundary planes were evaluated. After obtaining paths of all line-of-sight for the selected producer cell, locations of non-net cells in the list are denoted as N/A. For each line-of-sight to the producer cell, coordinate information beyond the first N/A value is removed from the list. For example, in Figure 10-8 (d), only locations of cells along the line segment a would be recorded in the list. For locations of non-net cells (cells belong to b) and cells located beyond the first appearance non-net cell (cells along line segment c) would be removed from the list. To find all connected cells to the selected producer cell within an expected drainage volume, first, a volume around the producer cell is created with a user-specified window width, w, on x-z plane; a depth, d, which is twice to the width on y-z plane; and a height, h, which is the same as the height of the selected realization. Then, construct boundaries for this volume. For cells within the lowest region(s) enclosed by non-net cells and the boundary cells, their coordinate information is recorded into a new list. Take Figure 10-8 (f) as an example, the expected drainage volume is divided into three separated regions (regions a, b, and c) by non-net cells and the boundary cells. Since only cells in the lowest region (region a) are connected to the producer; the net cells within the region a are considered locally connected. After combining the two lists and

28

removing the redundant locations, the final list contains locations for all locally connected cells to the selected producer cell.
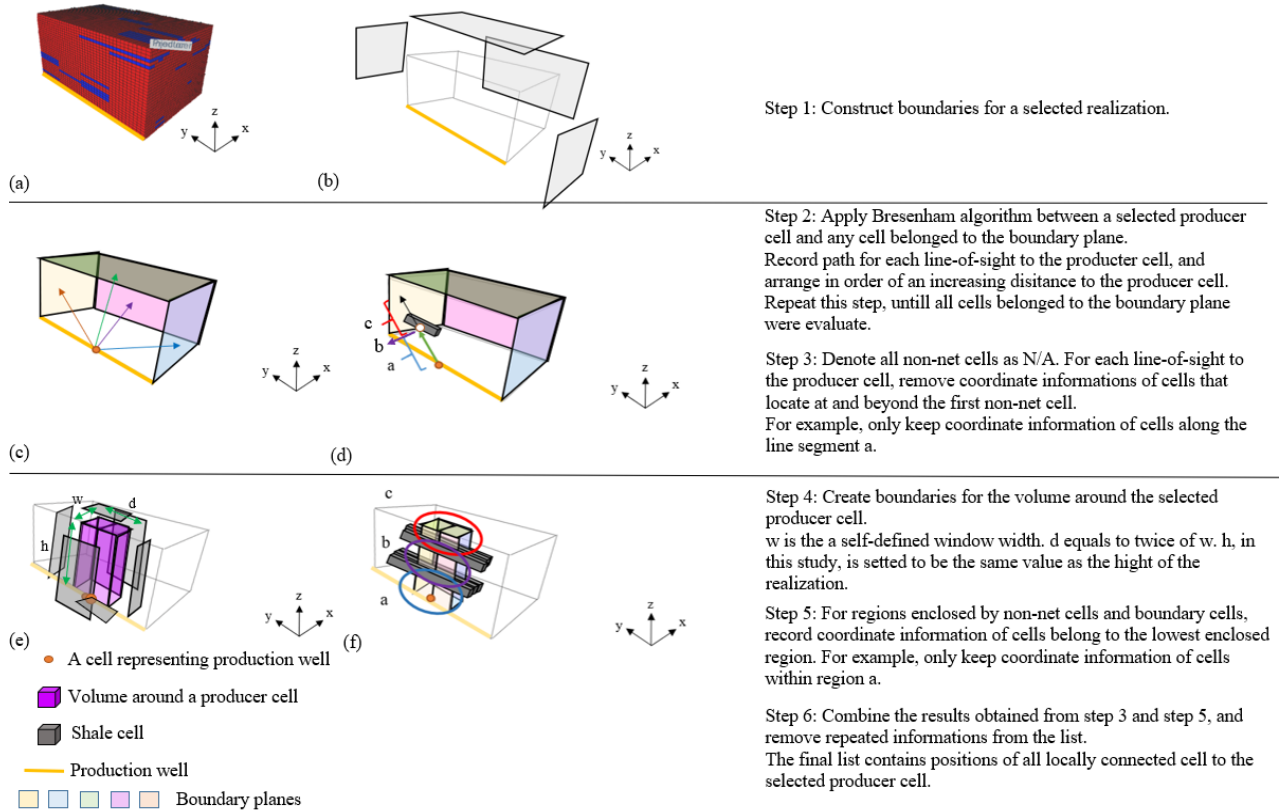
Figure 10-8. A workflow for determining all locally connected cells to a particular producer cell.

3.3.1.4 Permeability Along a Flow Path

In the SAGD extraction process, permeability is an important parameter. Usually, higher permeability along a flow path results in higher production rates; since it is easier for hydrocarbon to flow through the material with high permeability to the production well.

Figure 10-9 presents a scenario where A and B productive cells have the same geological properties. Additionally, the flow path from both cells A and B to the production well has the same

flow distance, but with different permeability along the path. With the addon permeability modifying factor, the two cases can be easily distinguished from each other; Whereas, if simply applying the CHV ranking method, the two cases would be considered to be the same.

$$f_{pj}^{l} = \left(\frac{p_j^l}{p_{max}^l} \right)^{\omega p} \quad \text{..} \quad (10\text{-}8)$$

Where p_j^l is the geometric average of the permeability of cells along a shortest flow path from a productive cell j to the well iw in a realization l. p_{max}^l is a user-specified maximum permeability and, in this study, it takes the maximum permeability value observed in a realization l. ωp is a calibration parameter and typically takes values between 0 to 2 (Wilde and Deutsch, 2012). When a flow path is not considered, ωp is set to be 0. In this study. In this work, ωp is set to be 1.
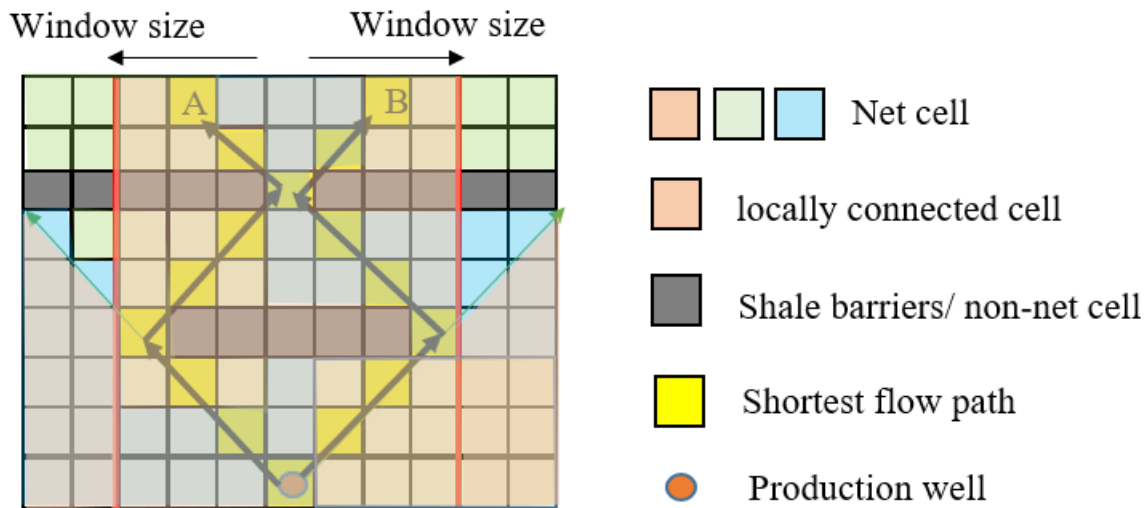
Figure 10-9. An example of permeability along a flow path from a productive cell to the production well.

3.3.1.5 Distance from a producer

The length of a flow path is also an important factor in SAGD production performance. Hydrocarbon farther from the production well is likely to flow through a more tortuous path and requires a longer time to the production well than hydrocarbon closer to the production well. A longer flow path could potentially reduce the probability of production.

Figure 10-10 illustrates the shortest flow path from a productive cell to the production well. In this example, the length of the flow path is the sum of d1, d2 and d3.

$$ f_{d_j}^{l} = \left(\frac{D_j^l}{D_{max}^l} \right)^{\omega d} $$ .... (10-9)

Where D_j^l is the shortest distance from a productive cell j to the production well iw in a realization l, D_{max}^l is the maximum distance observed in a realization l, ωd is a calibration parameter and typically takes values between 0 to 2 (Wilde and Deutsch, 2012). When a flow path is not considered, ωd is set to be 0. In this work, ωd is set to be 1.
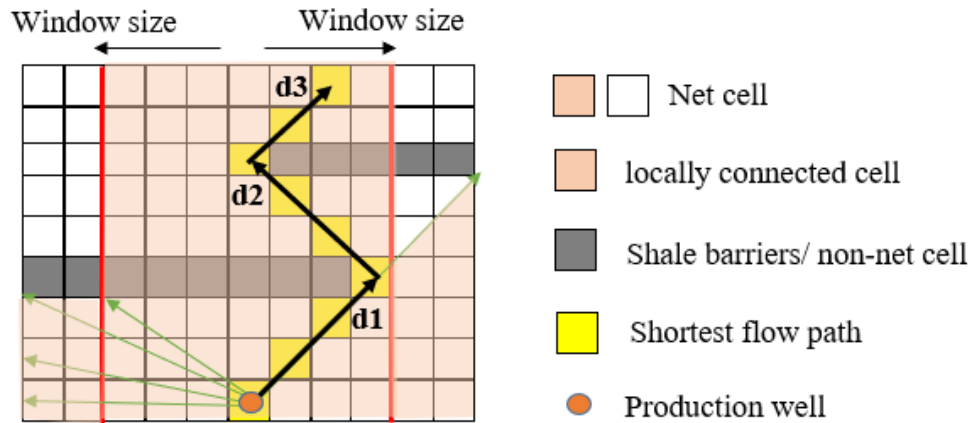
Figure 10-10. An example of a flow path from a productive cell to the production well.

3.3.1.6 Qs Workflow

Figure 10-11 shows the workflow for the static quality measure for any randomly selected realization. After importing the pertinent model parameters, use workflow described in Section 2.5.2 to create lists for each producer cell with their corresponding locally connected cells. Sequentially select an unsampled producer cell iw. Using the sampling list corresponding to the producer cell iw, an unsampled cell j in that list is sequentially selected. Then, judge whether the selected producer cell, iw, is the closest producer cell to this selected cell j. If not, using the sampling lists corresponding to those producer cells which is closer to cell j, judge whether the cell j is locally connected to any of these producer cells. If it is, select the next unsampled cell in the list and then do the same judgment. Otherwise, determine and calculate the shortest flow distance between the selected cell j to the selected producer cell iw. Also, calculate the geometric average permeability along the flow path from the cell j to the producer iw. Then, a Q_{Sj}^{l} is obtained for the locally connected cell j and the corresponding producer iw. This process is repeated until Q_{Sj}^{l} is calculated for all locally connected cells and their corresponding producer cells. The final Q_{S}^{l} value for a realization l is the sum of all Q_{Sj}^{l} calculated from previous steps.
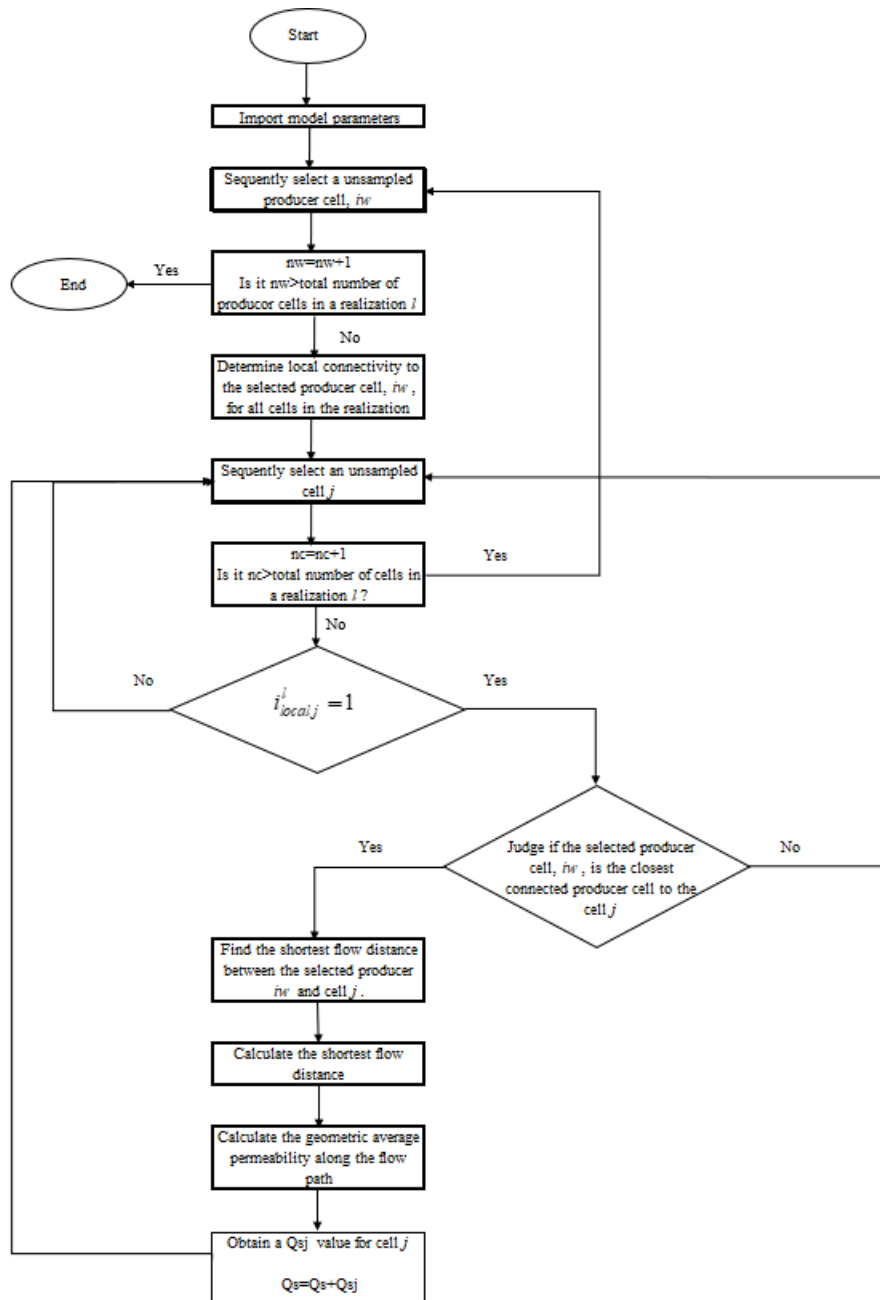
Figure 10-11. A workflow for applying the static quality ranking method.

3.3.2 Hausdorff Distance

The Hausdorff distance is applied to quantify the dissimilarity between two images according to their spatial arrangement and shape of relevant objects. If a 3D heterogeneous reservoir is

considered as an image (each grid cell is a pixel) and the shale barriers are the objects of interest, the Hausdorff distance can be used to compute a static-based distance measure. The first step is to transfer the edge pixels of all objects into a point set. For example, in reservoir A, the grid cells that are located at the boundary of any shale barrier are assembled into a point set of size p: $A=\{a_1, \ldots, a_p\}$. Similarly, another point set of size q is assembled for reservoir B: $B=\{b_1, \ldots, b_q\}$. The Hausdorff distance between the two point sets, $H_f(A,B)$, is defined as:

$$H_f(A,B) = \max(h(A,B), h(B,A)) \ldots\ldots (10\text{-}10)$$

where the directed Hausdorff distance, $h(A,B)$, that is measured from A to B is defined as:

$$h(A,B) = \max_{a \in A} \min_{b \in B} \{d(a,b)\} \ldots\ldots(10\text{-}11)$$

$d(a,b)$ refers to the Euclidean distance between any two points, a and b. An example is illustrated in Figure 10-12. It seeks to identify the shortest distances between every point of A to another point in B. In contrast to most other shape comparison methods, the Hausdorff distance focuses on quantifying proximity rather than the exact superposition (overlapping) of objects. This method evaluates the most representative partial distance between two point sets by comparing how similar the objects are, in terms of their spatial location and shape, among the two images.
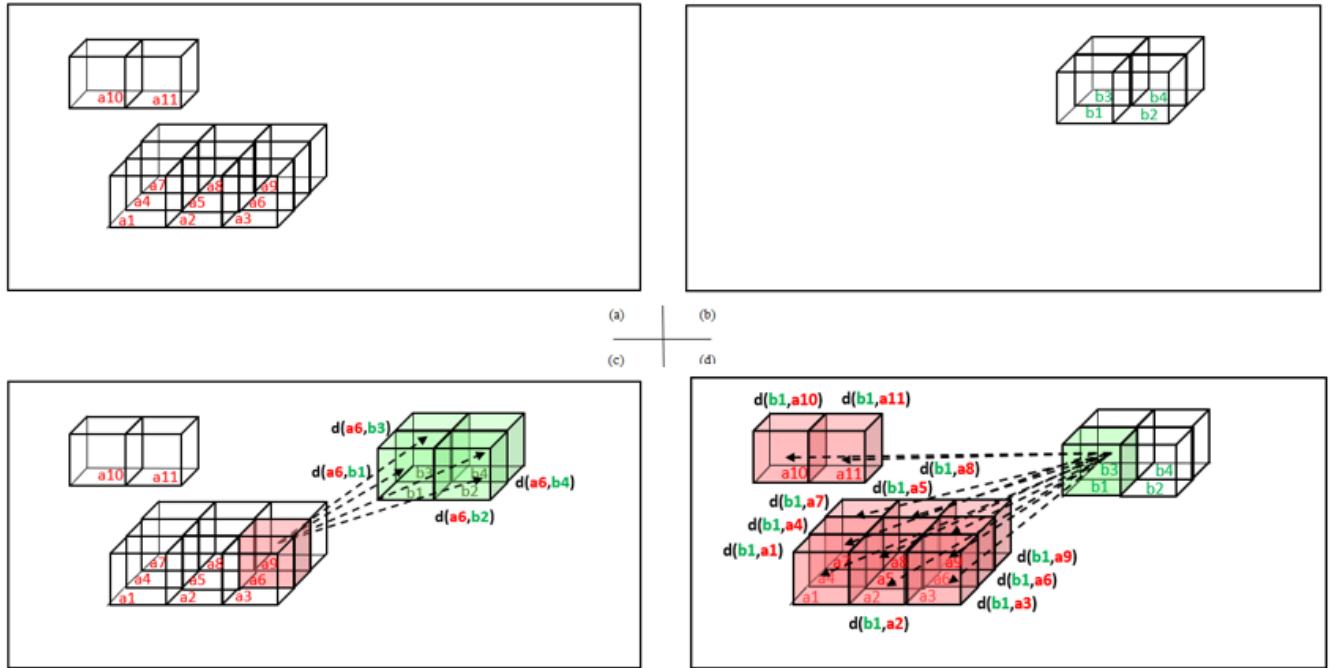
Figure 10-12. An example of the Hausdorff distance calculation: (a) – two shale barriers in realization A; (b) – a shale barrier in realization B; (c) – calculation of $d(a,b)$ for a = a6; (d) – calculation of $d(b,a)$ for b = b1.

3.4 Distance Functions for Static Quality, Hausdorff Distance and Detailed Flow Simulation

The distance function measures the distance between any two elements of a set (Arpat, 2005; Suzuki and Caers, 2008). In this study, it is used to quality the (dis)similarity between any two geological models in terms of their spatial properties or other forms which reflect the production response of a SAGD recovery process.

In this study, for static quality (Qs), the distance function, d, is formulated to evaluate the differences in the expected drainage volumes of various SAGD reservoirs. From a pair of static quality Q_S^l and $Q_S^{l^*}$, the local connectivity-based distance, d^{ll^*}, can be computed between any two realizations:

$$d^{ll^*} = (Q_S^l - Q_S^{l^*})^2 \quad \text{.. (10-12)}$$

For Hausdorff distance, the distance function, d, is formulated to measure the geometrical difference of the SAGD reservoirs. For any two SAGD reservoir models l and l^*, the static distance, d^{ll^*}, is defined as:

$$d^{ll^*} = H_f(l, l^*) \quad \text{.. (10-13)}$$

For the detailed flow simulation, the distance function, d, is formulated to capture the differences in steam chamber expansion profiles. The chamber volume at a given time level, $V_{ch}(t)$, is computed by summing the pore volume of all cells with a gas saturation value ≥ 0.3. At the end of a 10-year production period, a time series of chamber volumes can be obtained for each model. From a pair of time series of $V_{ch}^l(t)$ and $V_{ch}^{l^*}(t)$, the flow-based distance, d^{ll^*}, can be computed between any two realizations:

$$d^{ll^*} = \sum_{t=1}^{m} w(V_{ch}^l(t) - V_{ch}^{l^*}(t))^2 \quad \text{.. (10-14)}$$

where w is the weighting factor, and it is set as $1/t^2$ in this study. m refers to the numbers of the production months. This formulation is based on the observation that the development of a steam chamber is significantly impeded by any shale barriers located near the well pair, and the impacts

of these near-well shale barriers are most prominent in the early-time data. A weighting factor of $1/t^2$ would ensure the data corresponding to low values of t to be given more emphasis.

For each distance measures method, after obtaining values of the distance function between every pair of synthetic reservoir models, a size of 200×200 dissimilarity matrix, M, is computed for base model type 1 and a size of 50×50 dissimilarity matrix, M, is computed for base type model 2. Then, they are transformed into a set of 200 points for base model 1 and a set of 50 points for base model 2 in a 2D Euclidean space via MDS, where k-means clustering is applied to categorize these points into different groups/clusters.

3.5 Results and Discussions for Static Distance Measures and Detailed Flow Simulation

This section includes three sub-sections: (1) Decisions of grid cell size selection for each distance measures method (2) results and discussions for detail flow simulation; (3) results and discussions for the static quality method, as well as its comparison with the detail flow simulation; and (4) results and discussions for the Hausdorff distance method, as well as its comparison with the detail flow simulation.

3.5.1 Grid Sensitivity Analysis

3.5.1.1 Detailed Flow Simulation Resolution

According to Mccarthy (1993), for dynamic flow simulation, it is important to define how fine a grid image of a reservoir is good enough to achieve realistic fluid flow simulation. In order to select an optimal grid size for the detailed flow simulation, various grid sizes are tested. According to

section 3.2.1 and section 3.2.2, the smallest fundamental building block in base model type 1 is $4m \times 20m \times 2m$ in *x*-, *y*-, and *z*-directions, and the anisotropy of shale barriers in based model type 2 is $15m \times 40m \times 2m$ along the *x*-, *y*-, and *z*-directions, respectively. In order to capture the heterogeneity, the resolution in corresponding directions should set to be less than the dimensions mentioned above. Additionally, according to Zheng et al. (2018b), they observed that the average shale barriers thickness is 1.22 meters, and shale barriers less than 0.3 meters in thickness would not hinder steam chamber development nor affect the production performance. As a result, in other to find out the optimum balance between the model accuracy and the computational cost, a single grid block with a size of $1m \times 10m \times 1m$, $1m \times 4m \times 1m$, $1m \times 2m \times 1m$ and $1m \times 1m \times 1m$ are test in detailed flow simulation.

Figure 10-13 shows comparison results of steam chamber expansion profiles over 10 years for a randomly selected reservoir model selected from base model type 2 using different grid block sizes. Table 10-3 summarizes the runtime for each grid block size selection. Results using grid block sizes of $1m \times 2m \times 1m$ and $1m \times 1m \times 1m$ looks relatively similar. Considered the computational cost, the grid block size for this work is set as $1m \times 2m \times 1m$.
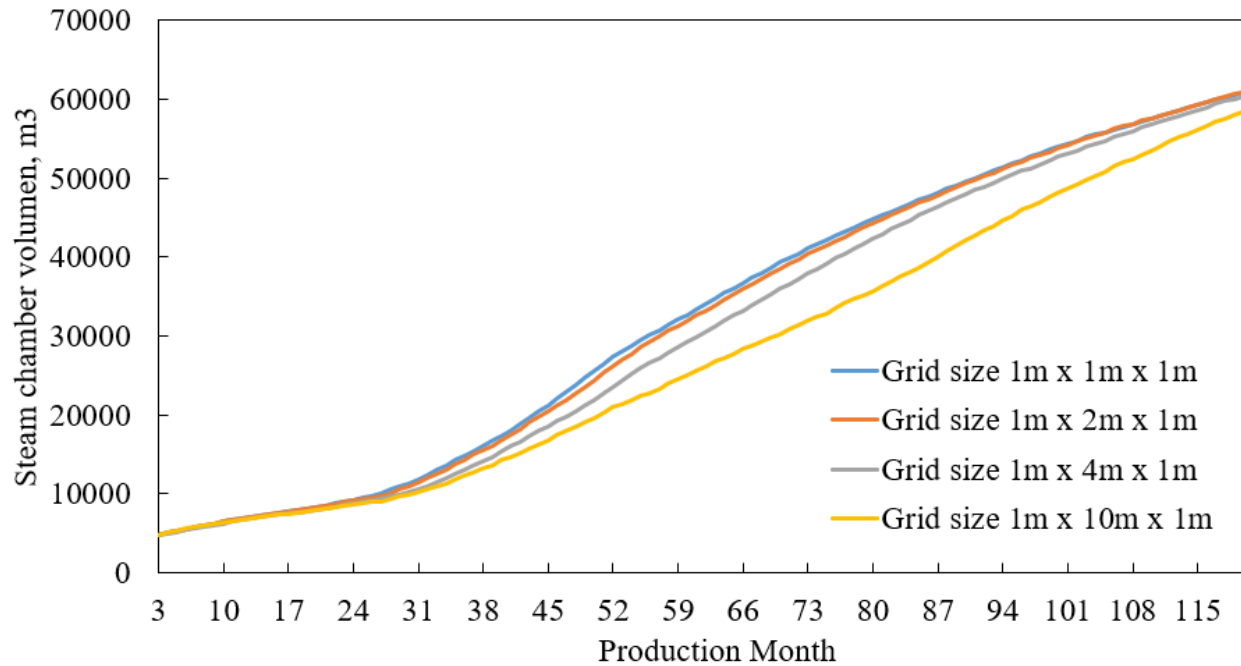
Figure 10-13. Comparison simulation results of a model from base model type 2 with different grid block sizes.

Table 10-3. Runtime of a model from base model type 2 with different grid block sizes for detailed flow simulation.

Grid cell size	1 m × 1 m × 1 m	1 m × 2 m × 1 m	1 m × 4 m × 1 m	1 m × 10 m × 1 m
Reservoir dimension	50 m × 80 m × 30 m	50 m × 80 m × 30 m	50 m × 80 m × 30 m	50 m × 80 m × 30 m
Total number of grid cells	120,000	60,000	30,000	120,00
Simulation time per case	38 hours	8 hours	6 hours	2 hours

3.5.1.2 Static Geological measures Resolution

Different from the dynamic flow simulations, static geological measures are not sensitive to the choice of the grid cell size. For Hausdorff distance, it evaluates the distance between shale barriers of a pair of reservoir models. For static quality (Qs), it measures the local connectivity hydrocarbon volume within a local window size and along line-of-sights to the production well, as well as the distance and permeability along a flow path. Neither of these factors would dramatically change if

using a slightly different simulation grid cell size. In this work, for both Hausdorff distance and Qs calculation, the grid cell size is selected as $1m \times 1m \times 1m$.

3.5.2 Detailed Flow Simulation Results

3.5.2.1 Result for Base Model Type 1

Figure 10-14 presents the MDS and clustering results. Six randomly selected heterogeneous realizations from different clusters are shown in Figure 10-15; and, the steam chamber evolution profiles for these cases over the initial 8 production years are presented in Figure 10-16 to Figure 10-21.

Three groups are identified for the flow simulation. Each of the three clusters exhibits different steam chamber development characters. Cluster 1 consists of cases with little shale barriers influence in the near-well region (zone 1 and 2). For cases in cluster 1, as shown in Figure 10-16 to Figure 10-17, the steam chamber can develop relatively efficiently away from the well pair with little influence of shale barriers in the near well region. As presented in Figure 10-15, cases identified in this cluster (cases 120 and 158) are with good communication between the well pair in all 4 segments along the well length. Additionally, the proportion of areas with low permeability due to the influence of shale barriers in the near-well region is very small. Both clusters 2 and 3 consists of cases with some shale barriers influence in the near-well region. For cases in these clusters, according to Figure 10-15 and Figure 10-18 to Figure 10-21, the steam chamber is somewhat impeded due to a mix of factors: the present of large proportion of area with low permeability (due to the influence of shale barriers) in the near-well region, and/or the present of shale barriers that locates either in between the well pair or in close proximity to the wells. The

main difference between clusters 2 and 3, however, is that, in cluster 3, shale barriers influence in the near-well region has severe impacts on chamber development.

As mentions in Section 3.2.1, for base model type 1, instead of physical shales, arbitrary shale barriers with different sizes and shapes to represent the sum of individual impacts caused by a set of small shale. While modeling in flow simulator, such zones with low permeability value are considered as big chunks of shale barriers, and they significantly impede the overall steam chamber development during the simulation. Additionally, it makes the reservoir model not geologically reasonable. To solve this issue, a new base model (base model type 2) is constructed and used for further comparison.
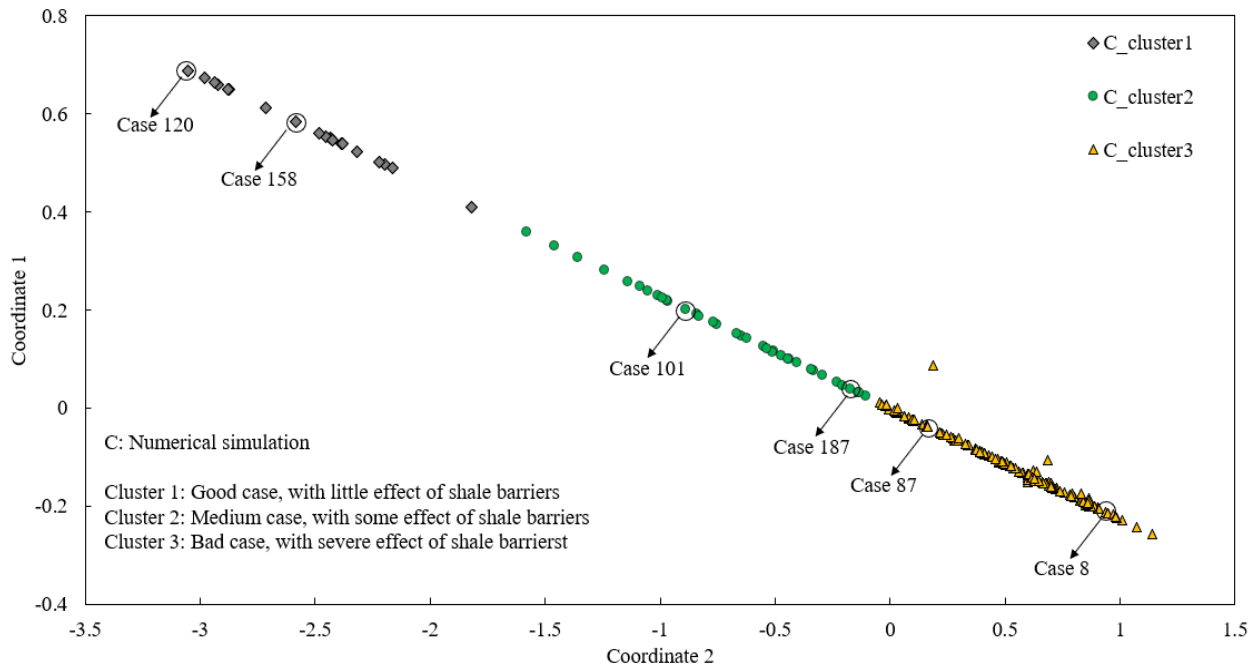
Figure 10-14. MDS and clustering results based on the flow simulations for base model type 1.
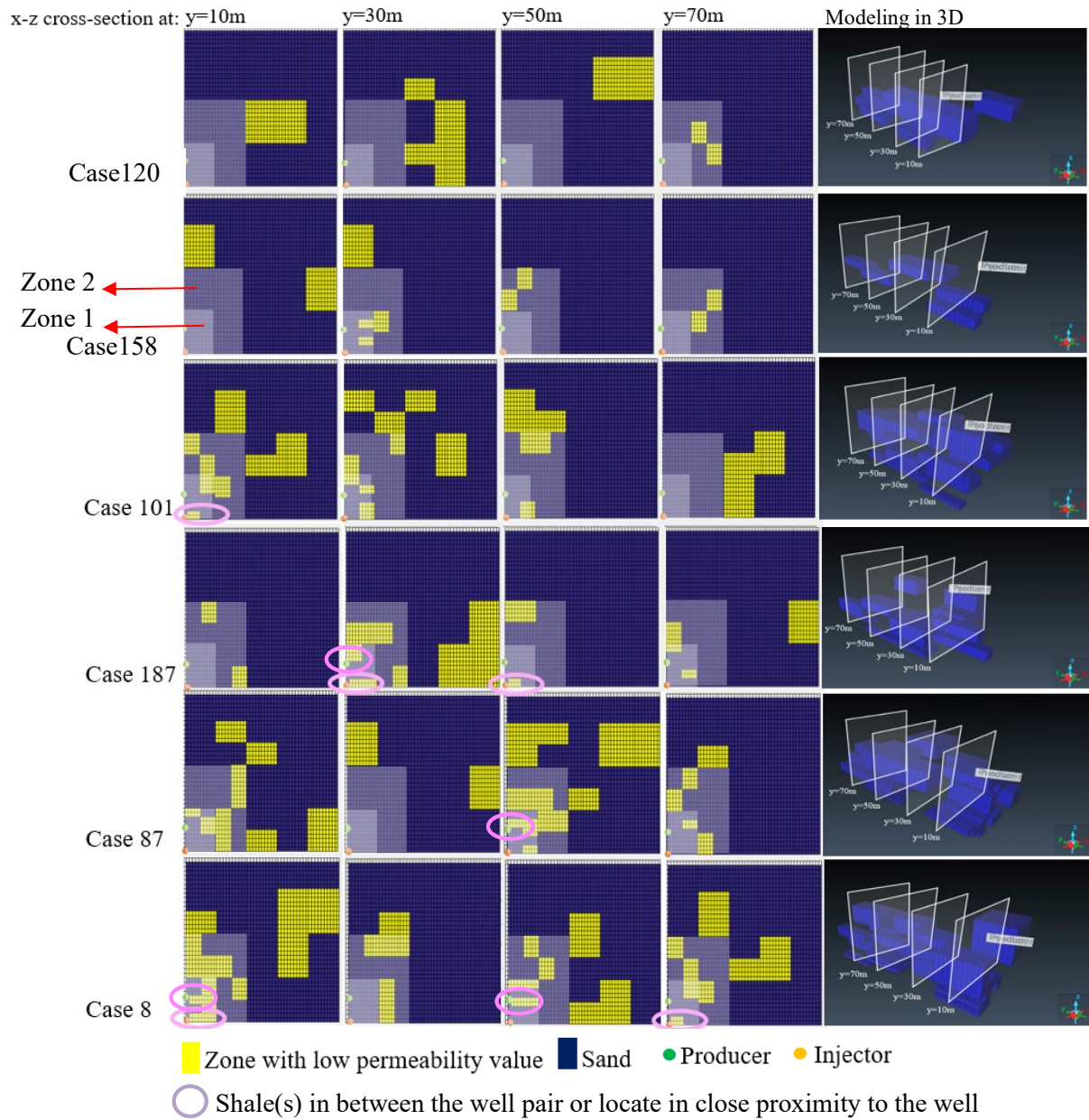
Figure 10-15. Six selected heterogeneous realizations from base model type 1: the first four columns correspond to the four segments along the *y*-axis, and the last column illustrates the shale barrier configuration in 3D.
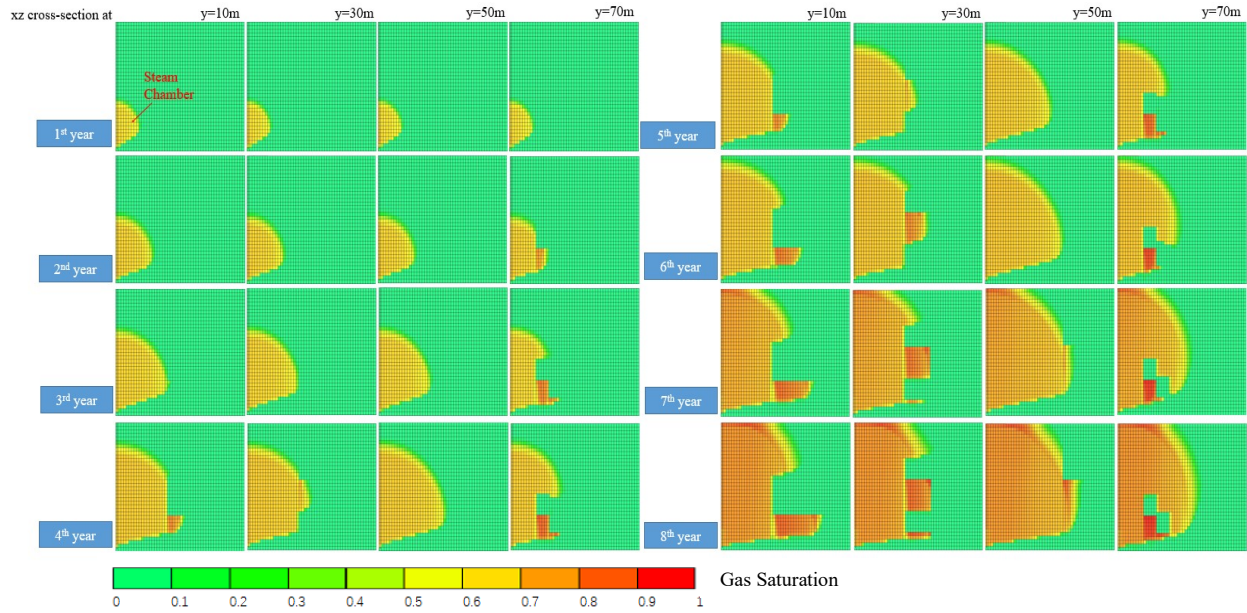
Figure 10-16. Steam chamber evolution over the initial 8-year period corresponding to the heterogeneous model Case 120 identified in cluster 1 for base model type 1.
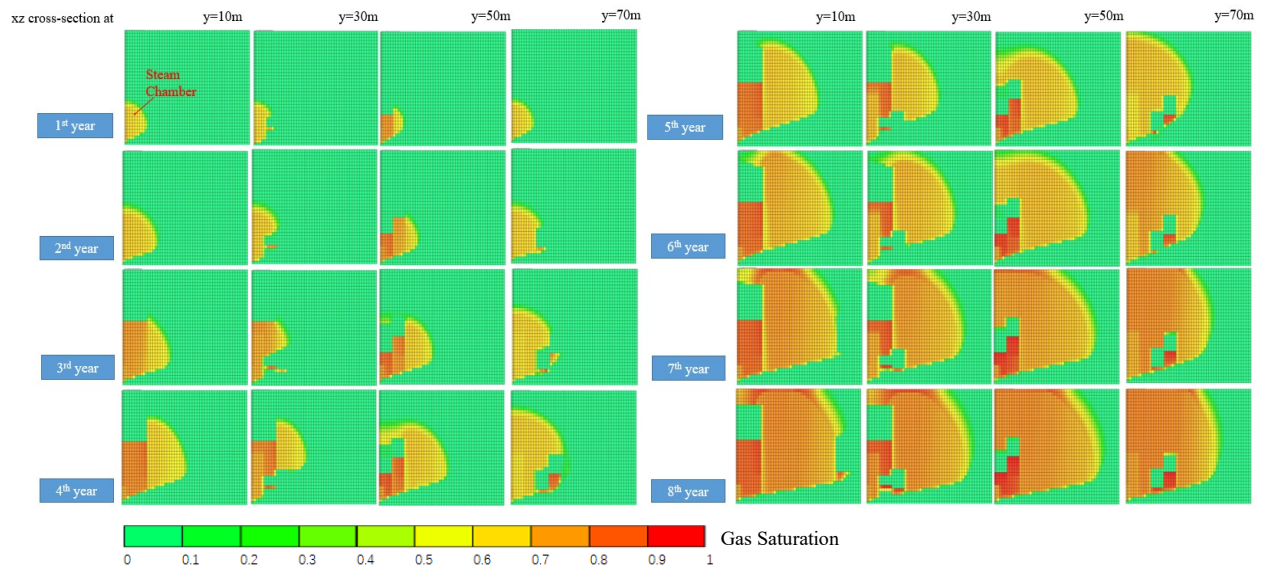
Figure 10-17. Steam chamber evolution over the initial 8-year period corresponding to the heterogeneous model Case 158 identified in cluster 1 for base model type 1.
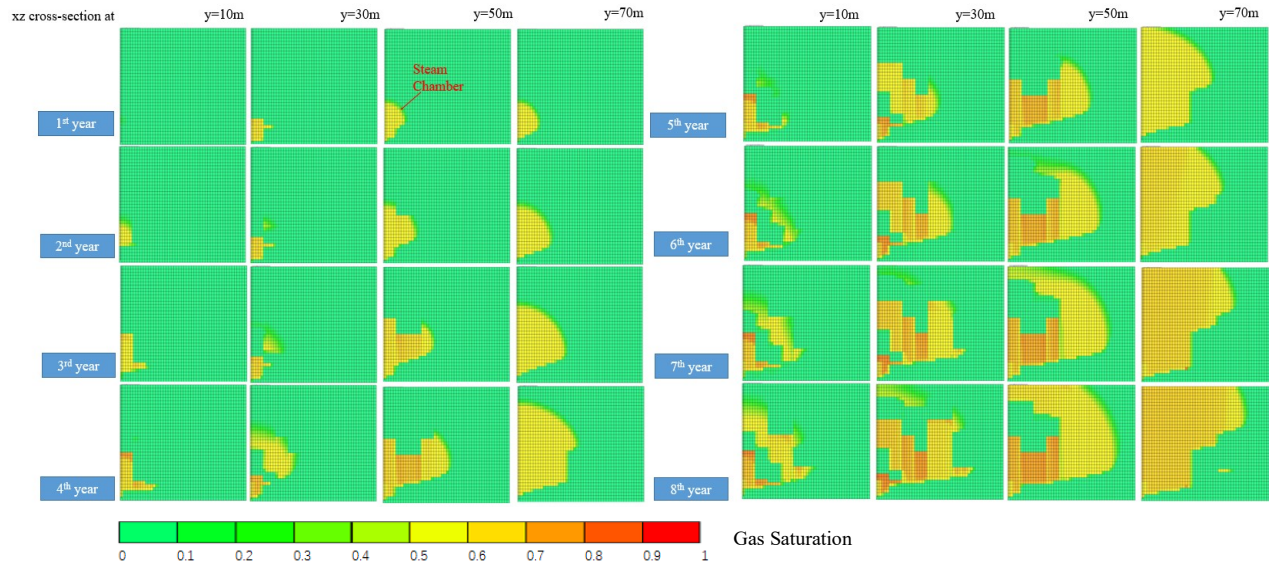
Figure 10-18. Steam chamber evolution over the initial 8-year period corresponding to the heterogeneous model Case 101 identified in cluster 2 for base model type 1.
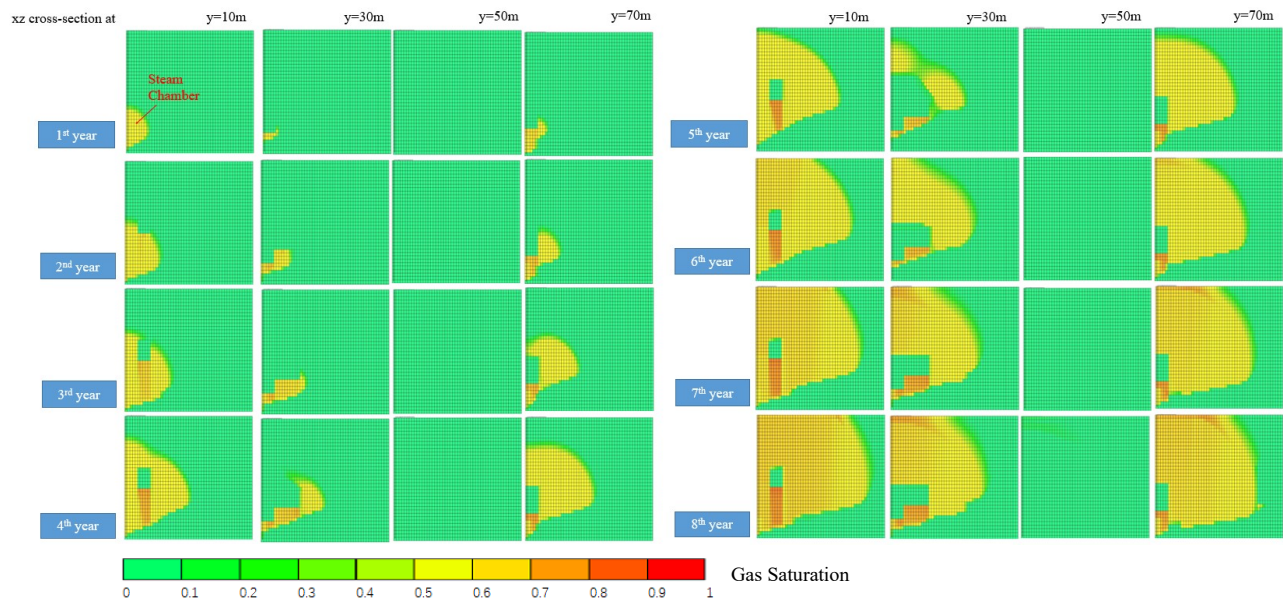
Figure 10-19. Steam chamber evolution over the initial 8-year period corresponding to the heterogeneous model Case 187 identified in cluster 2 for base model type 1.
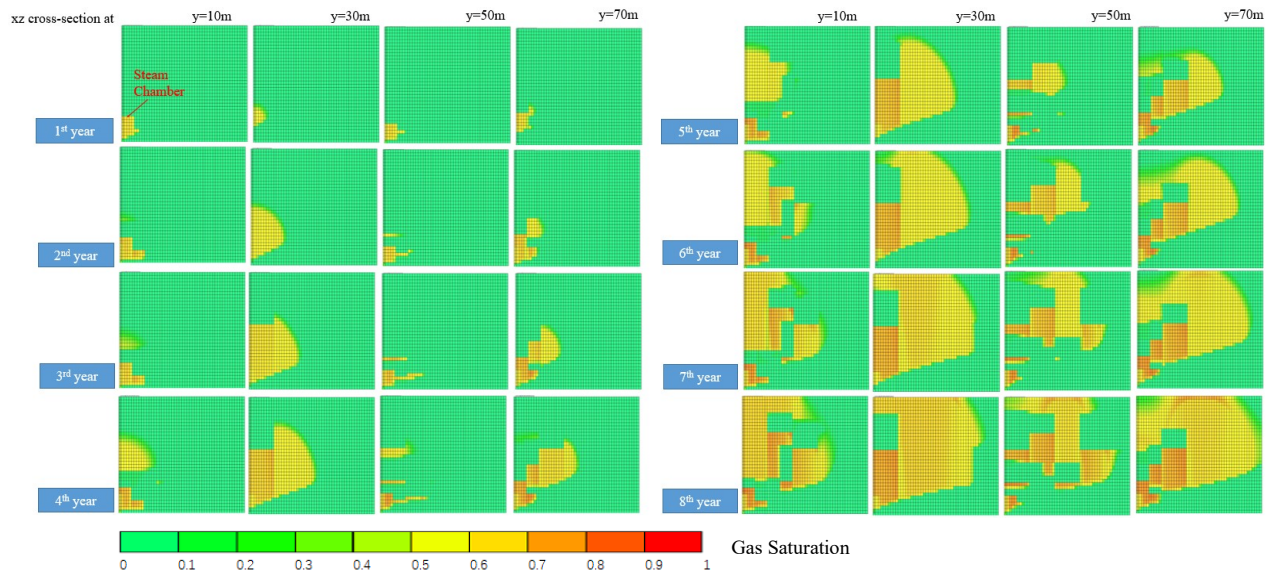
Figure 10-20. Steam chamber evolution over the initial 8-year period corresponding to the heterogeneous model Case 87 identified in cluster 3 for base model type 1.
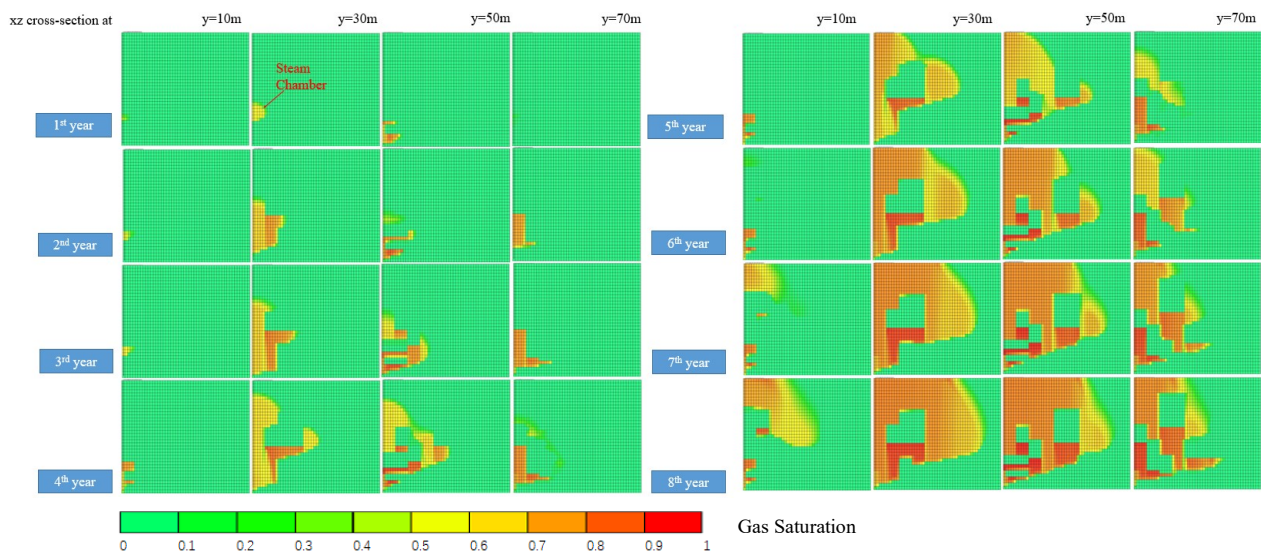
Figure 10-21. Steam chamber evolution over the initial 8-year period corresponding to the heterogeneous model Case 8 identified in cluster 3 for base model type 1.

3.5.2.2 Result for Base Model Type 2

Figure 10-22 presents the MDS and clustering results. All heterogeneous realizations from different clusters are shown in Figure 10-23 to Figure 10-25. A randomly selected heterogeneous realization from different clusters and their corresponding steam chamber evolution profiles over the initial 8 production years are presented in Figure 10-26 to Figure 10-28.

Three groups are identified for the flow simulation. Cluster 1 consists of cases where the effects of shale barriers in the near-well region are minimal. As shown in Figure 10-23 and Figure 10-26, there is good communication between the injector and producer (no shale barrier is observed in between the well pair) in all 4 segments along the well length. According to Figure 10-24 and Figure 10-25, as well as Figure 10-27 and Figure 10-28, both clusters 2 and 3 include scenarios where there is presence of shale barriers located in between a well pair or sit right next to the well (injector/producer). Such shale barriers, even when small and discontinuous, pronouncedly inhibit the communication between the well pair. Due to the operational constrain -a constant pressure constrain, this result little/no steam injection in those segments and locally limits the steam chamber development. The main difference between clusters 2 and 3, however, is that, in cluster 3, shale barriers in the near-well region has introduced severe impacts on the chamber development. In cluster 3, there are shale barriers located in between the well pair and result limit communication between the well pair for at least two of the segments (half of the well length).
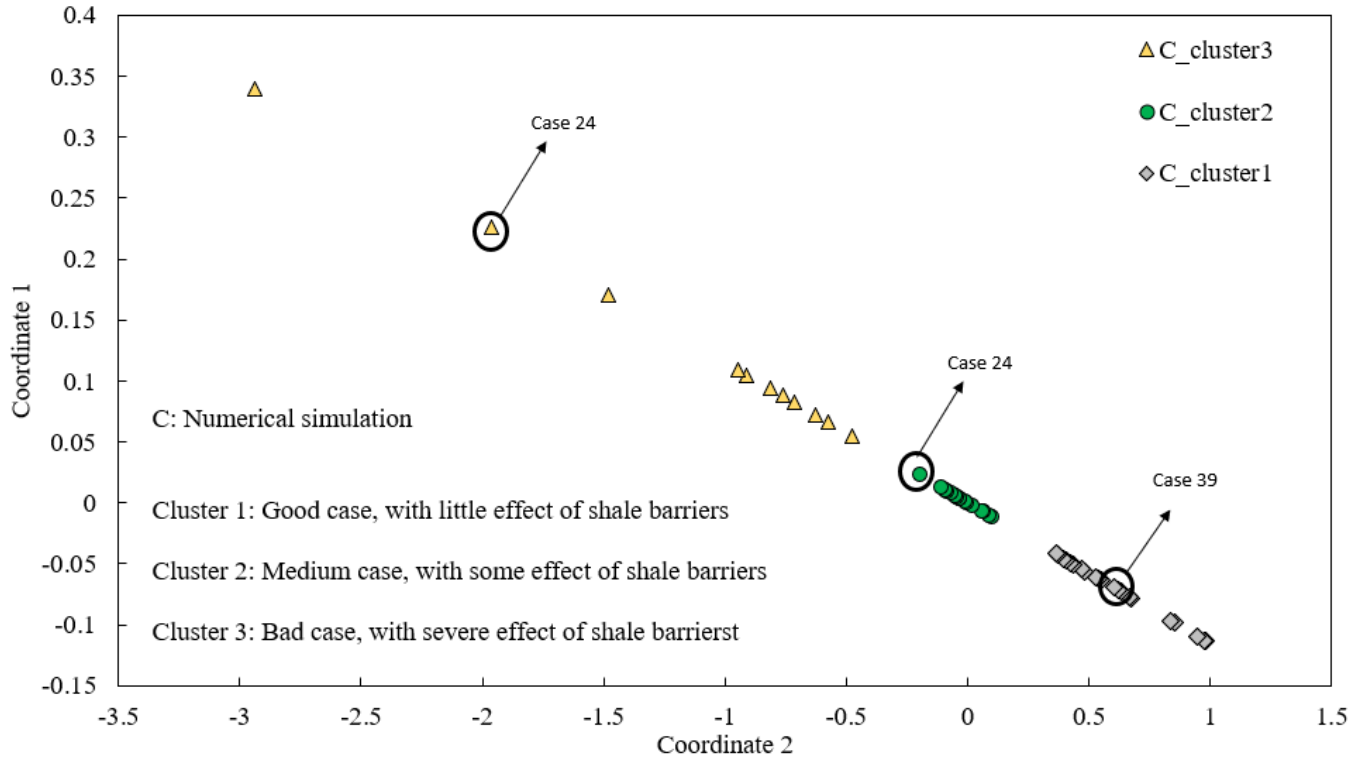
Figure 10-22. MDS and clustering results based on the flow simulations for base model type 2.

x-z cross-section at: y=10m   y=30m   y=50m   y=70m

Case2
Case3
Case6
Case8
Case9
Case11
Case12
Case13

Producer   Injector   Sand   Shale

x-z cross-section at: y=10m   y=30m   y=50m   y=70m

Case14

Case17

Case20

Case26

Case28

Case29

Case30

Case33

Producer   Injector   Sand   Shale
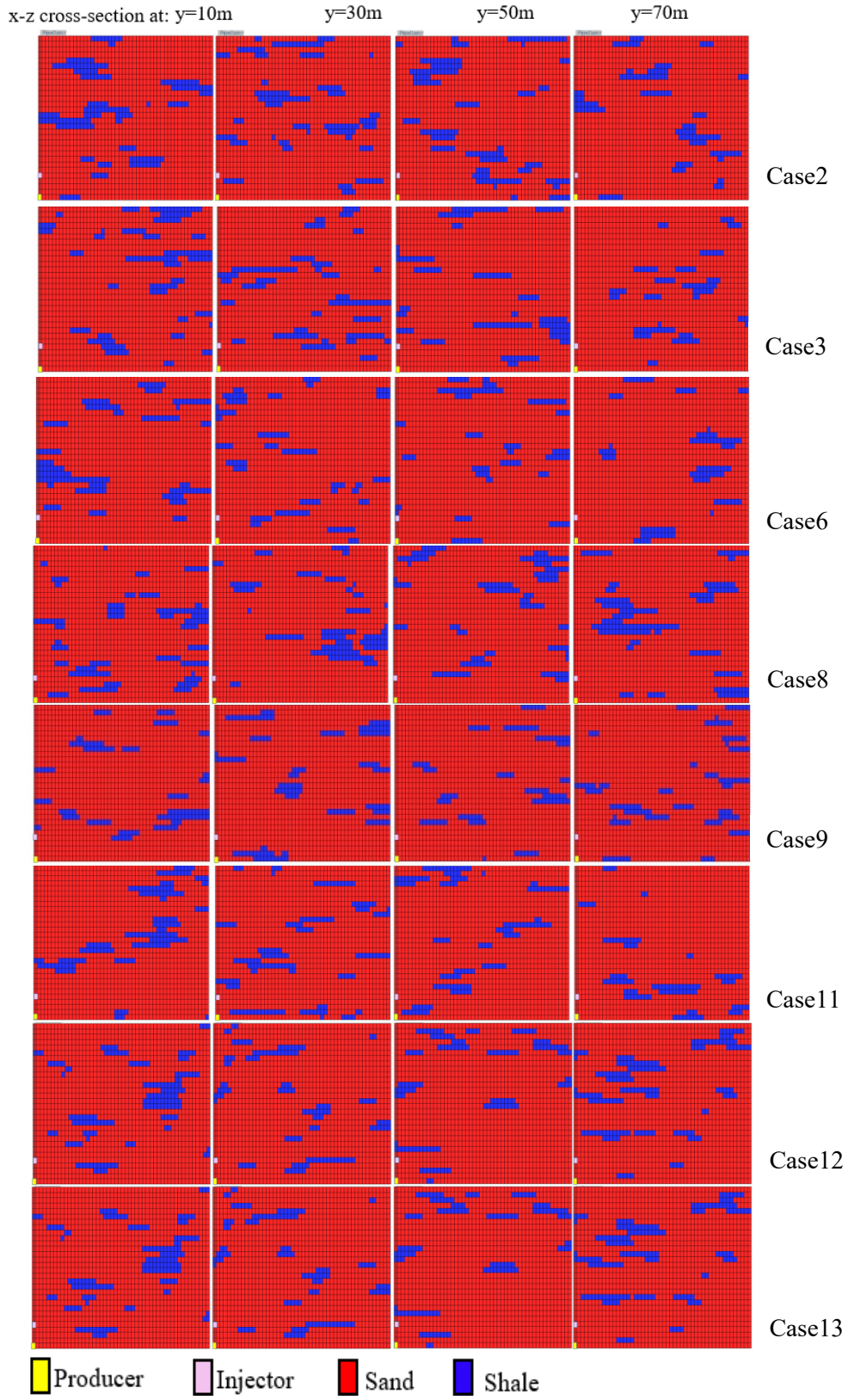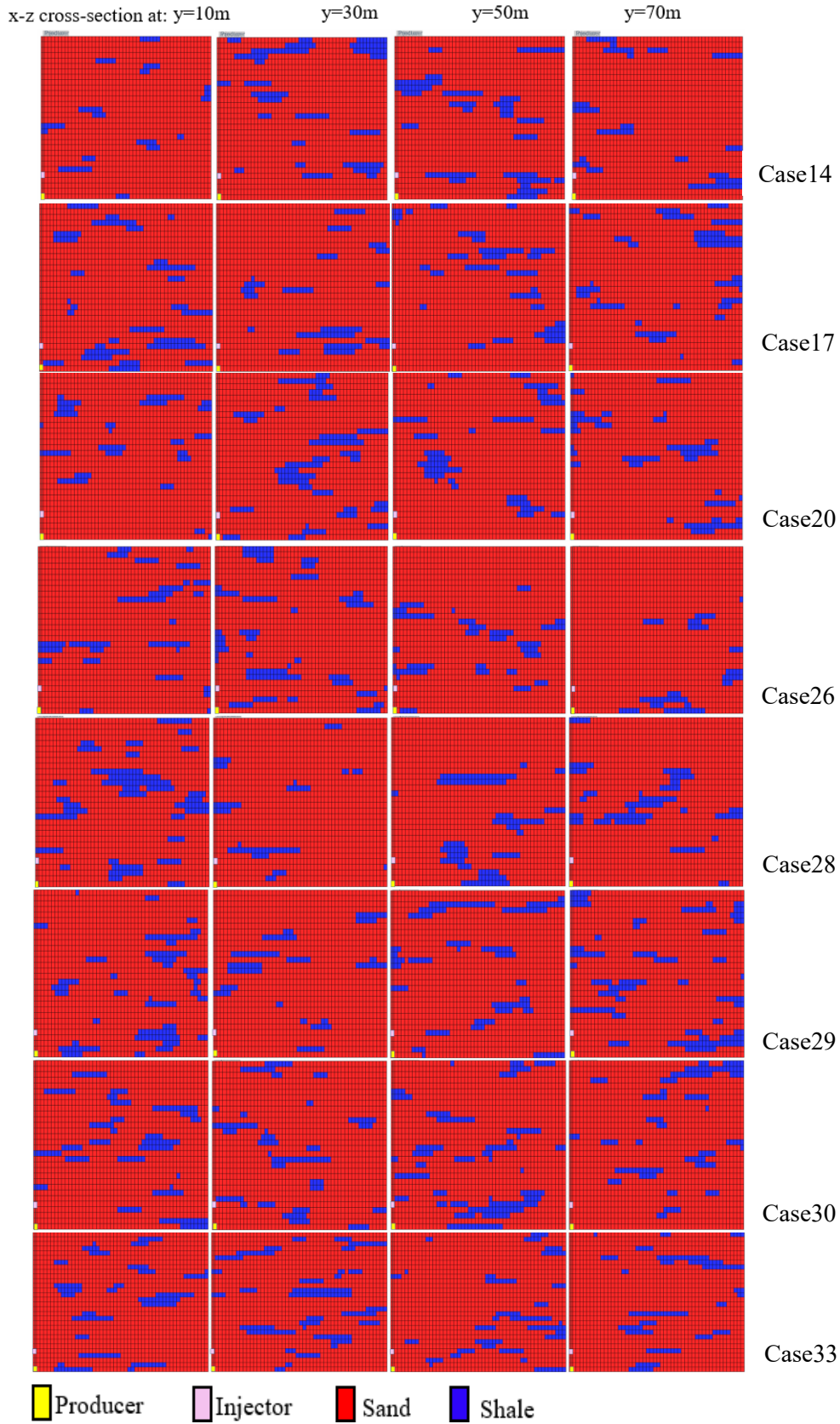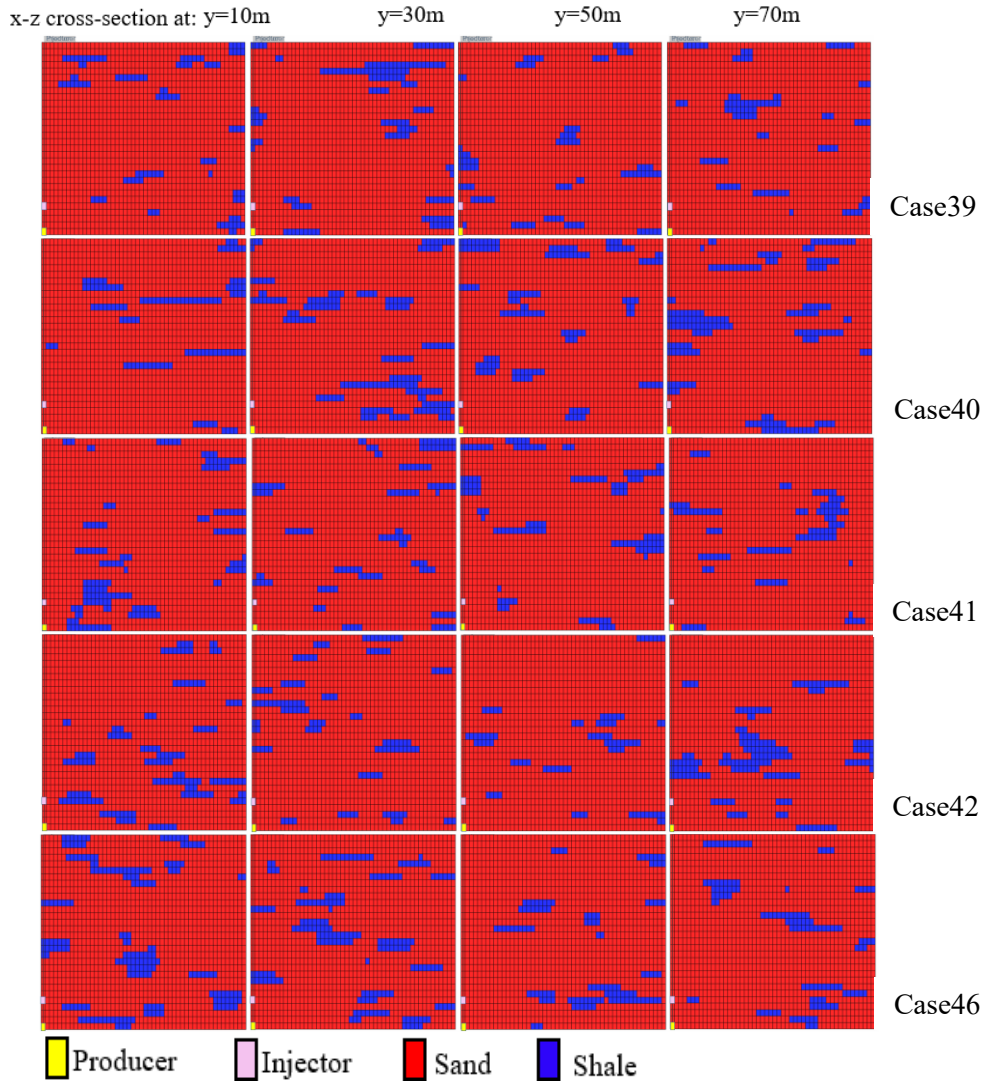
Figure 10-23. All heterogeneous realizations in cluster 1 for base model type 2: the four columns correspond to the four segments along the *y*-axis.

x-z cross-section at: y=10m   y=30m   y=50m   y=70m

Case1

Case4

Case5

Case7

Case16

Case18

Case21

■ Producer   ■ Injector   ■ Sand   ■ Shale   ◯ Shale(s) in between the well pair

◯ Shale(s) right next to the injection well

x-z cross-section at: y=10m   y=30m   y=50m   y=70m

Case22

Case23

Case24

Case31

Case34

Case36

Case35

Producer   Injector   Sand   Shale   ◯ Shale(s) in between the well pair
◯ Shale(s) right next to the injection well
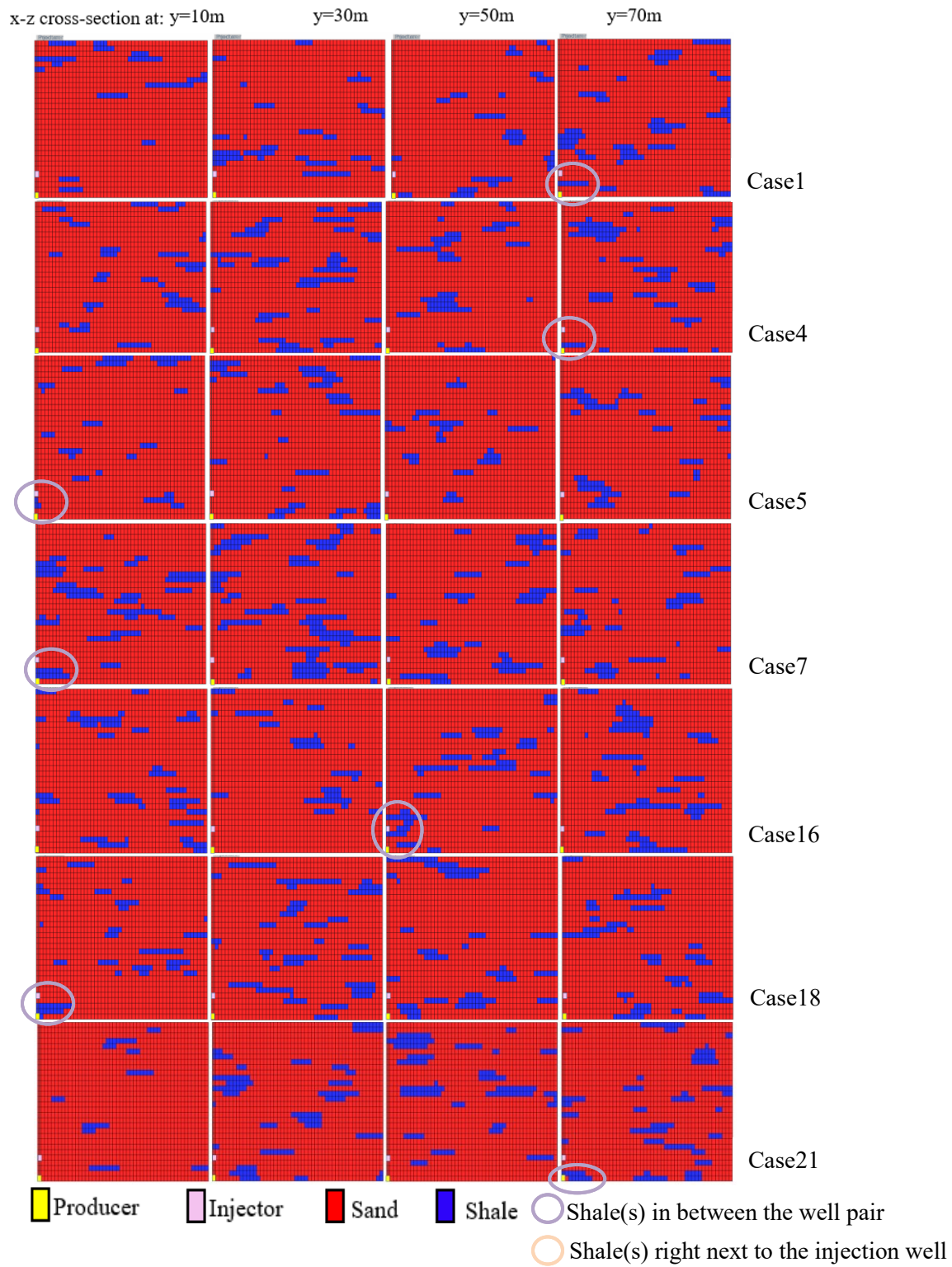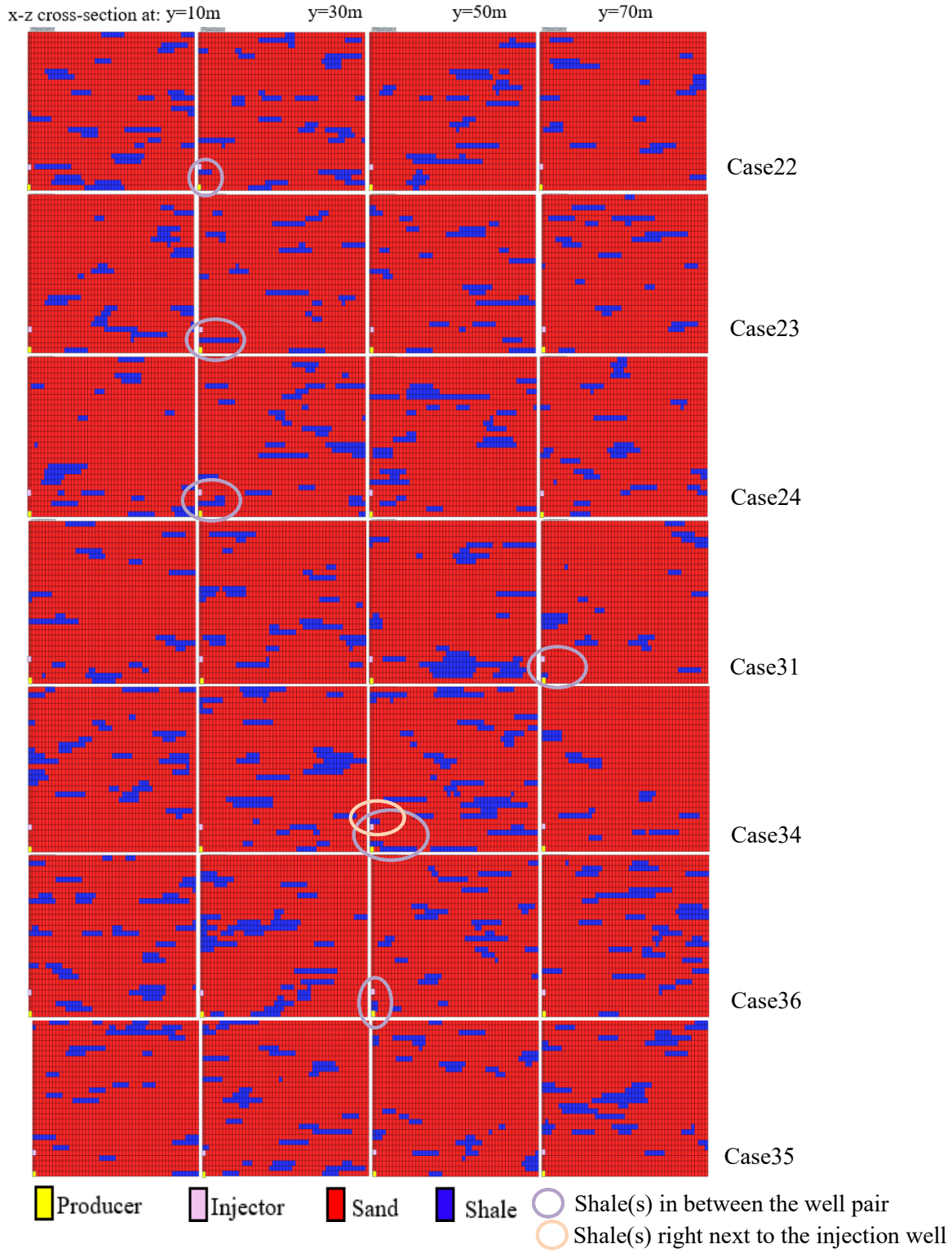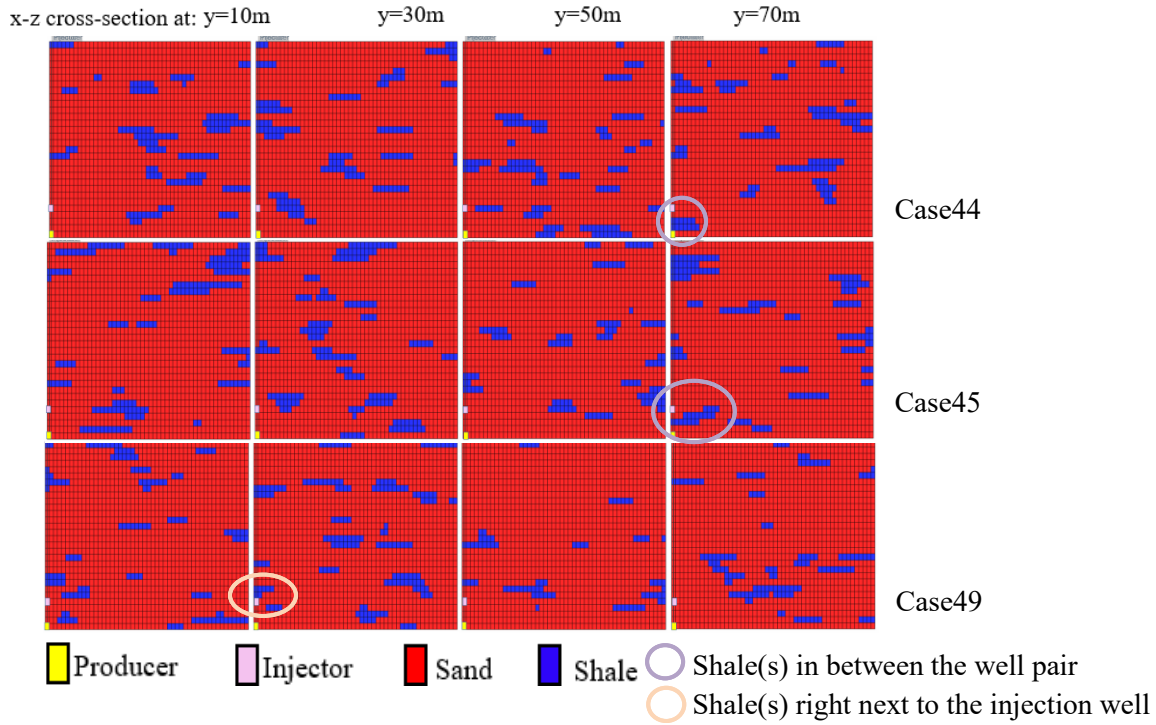
Figure 10-24. All heterogeneous realizations in cluster 2 for base model type 2: the four columns correspond to the four segments along the *y*-axis.

x-z cross-section at: y=10m   y=30m   y=50m   y=70m

Case10
Case15
Case19
Case25
Case27
Case32
Case38

Producer   Injector   Sand   Shale   ◯ Shale(s) in between the well pair

◯ Shale(s) right next to the injection well
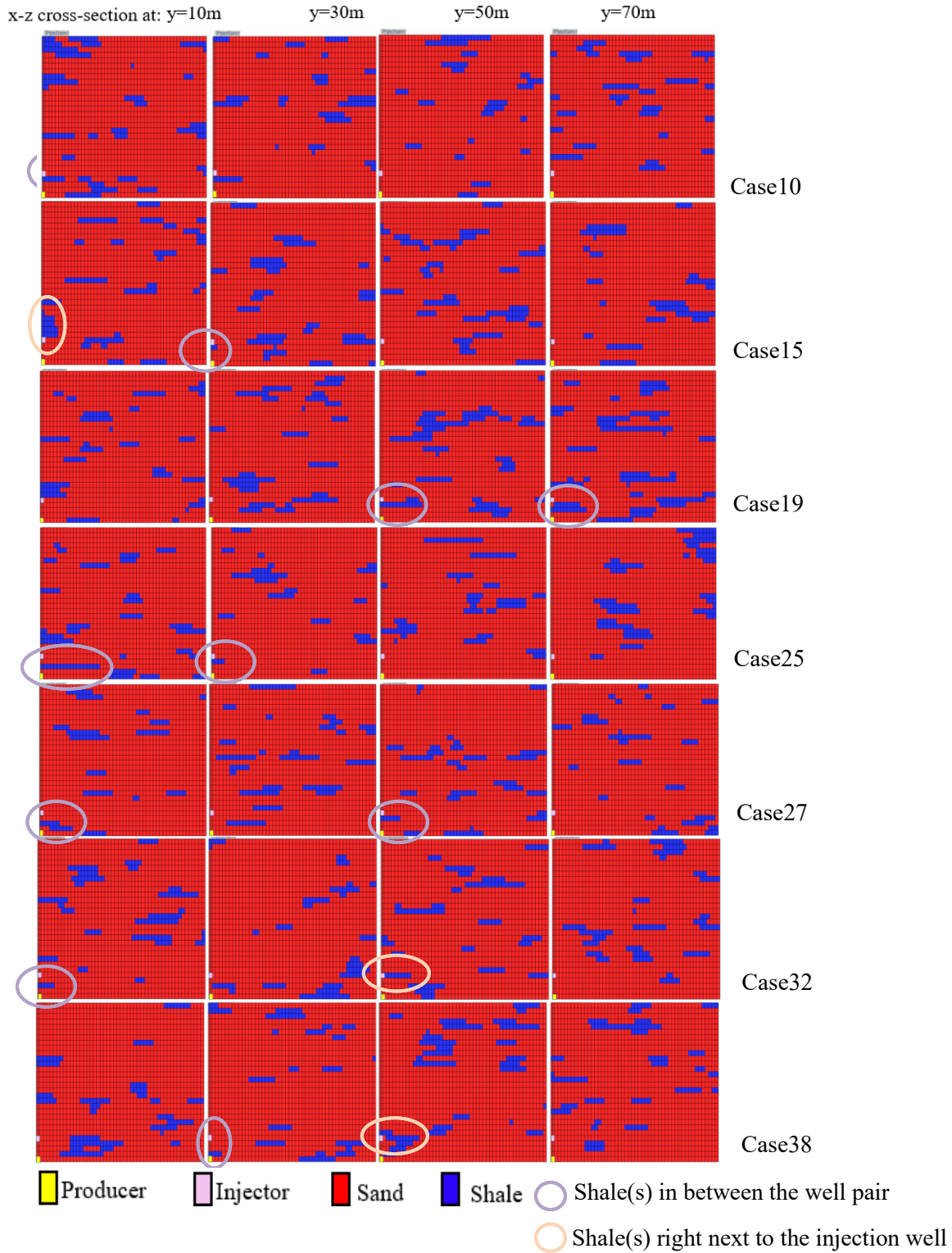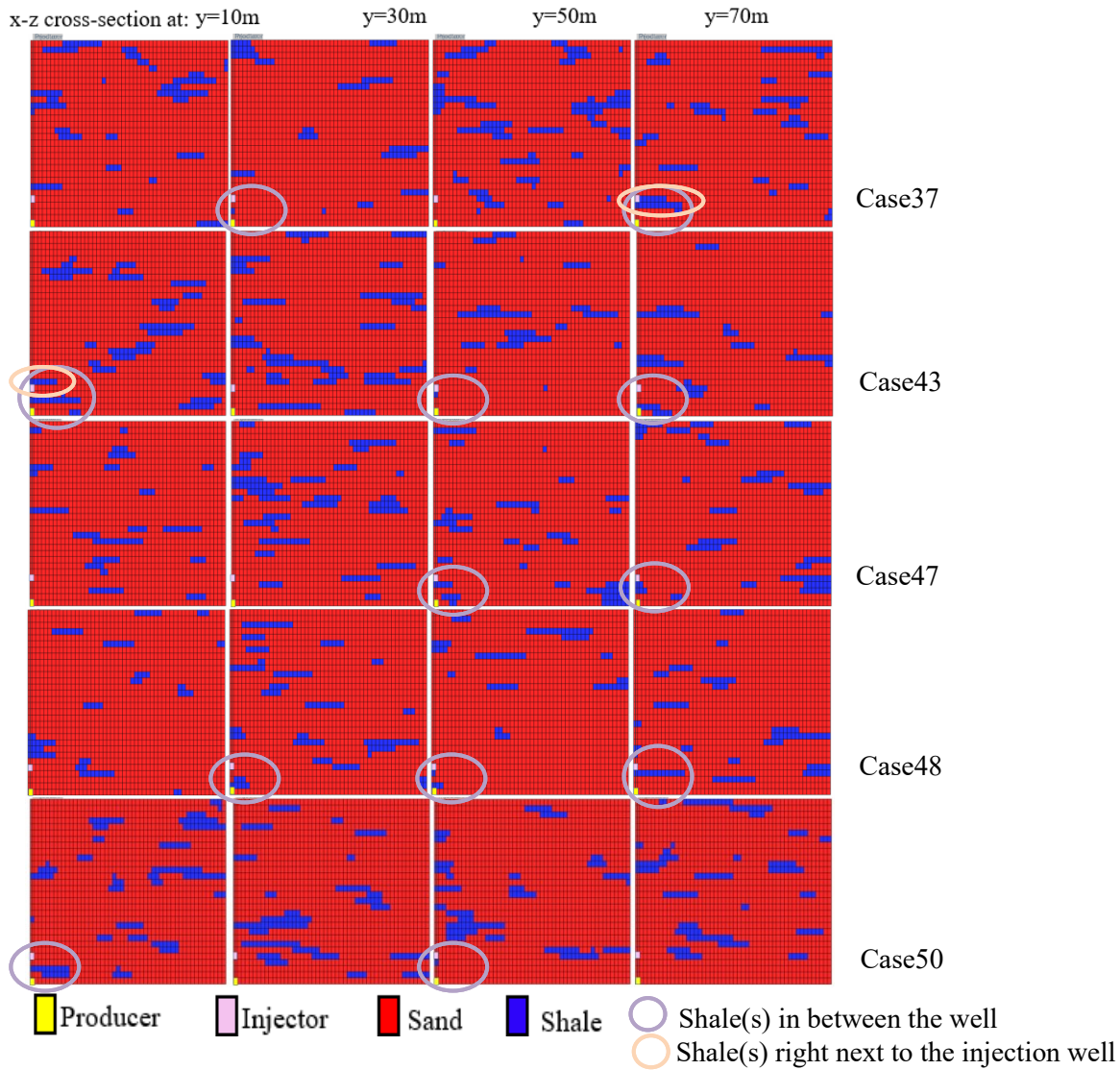
Figure 10-25. All heterogeneous realizations in cluster 3 for base model type 2: the four columns correspond to the four segments along the *y*-axis.
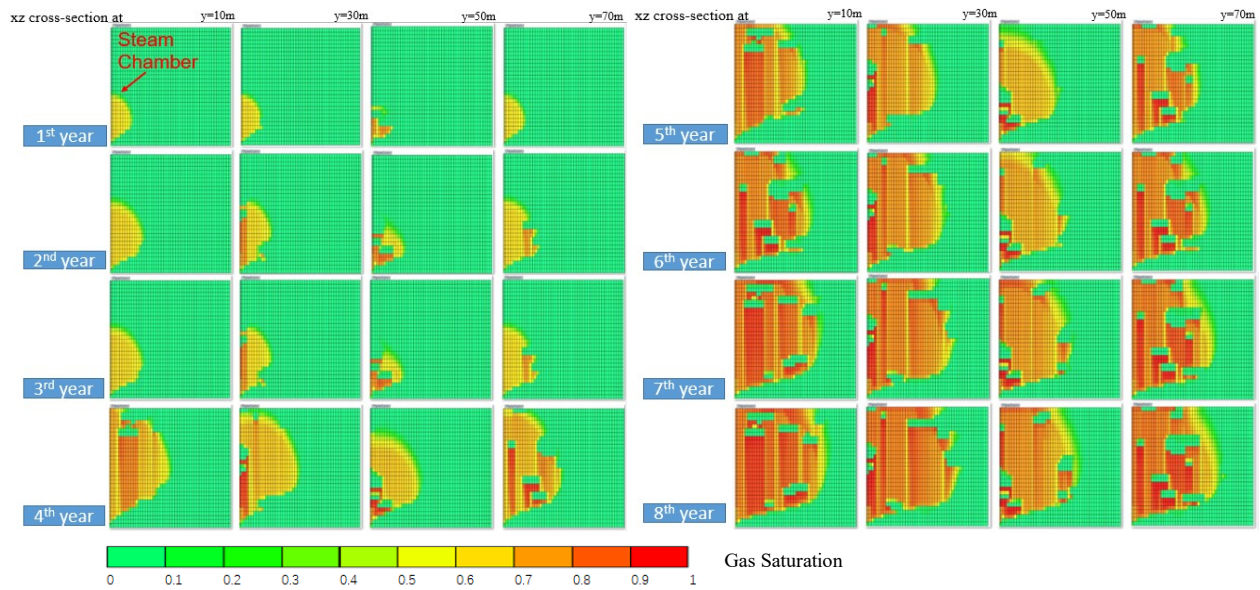
Figure 10-26. Steam chamber evolution over the initial 8-year period corresponding to the heterogeneous model Case 39 identified in cluster 1 for base model type 2.
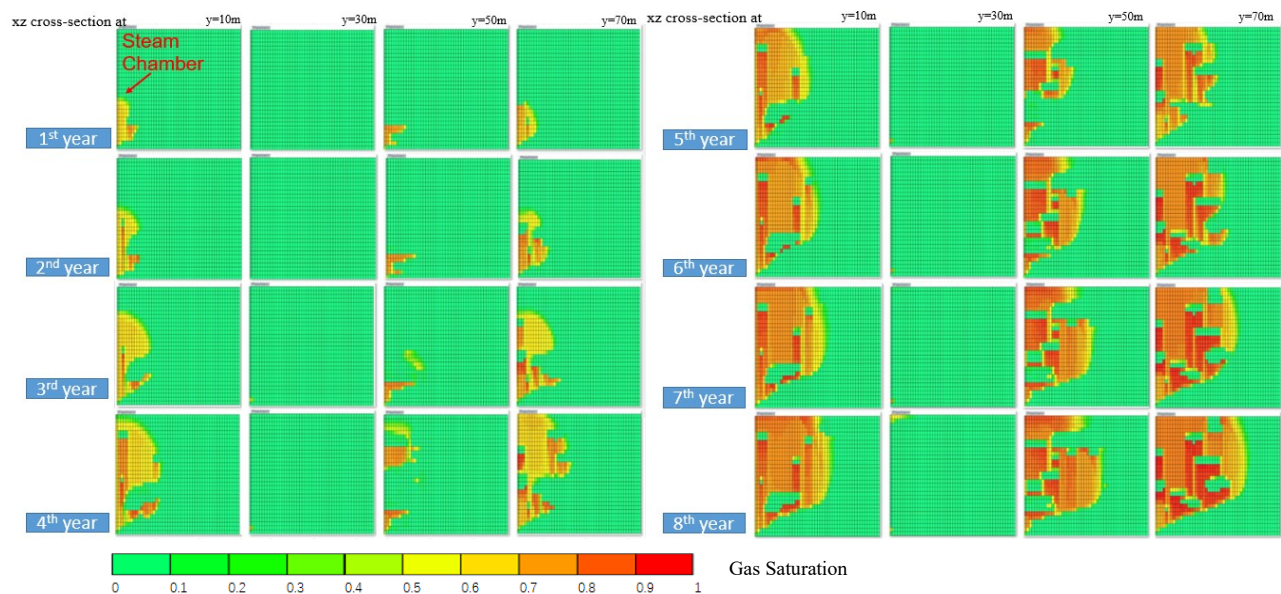
Figure 10-27. Steam chamber evolution over the initial 8-year period corresponding to the heterogeneous model Case 24 identified in cluster 2 for base model type 2.
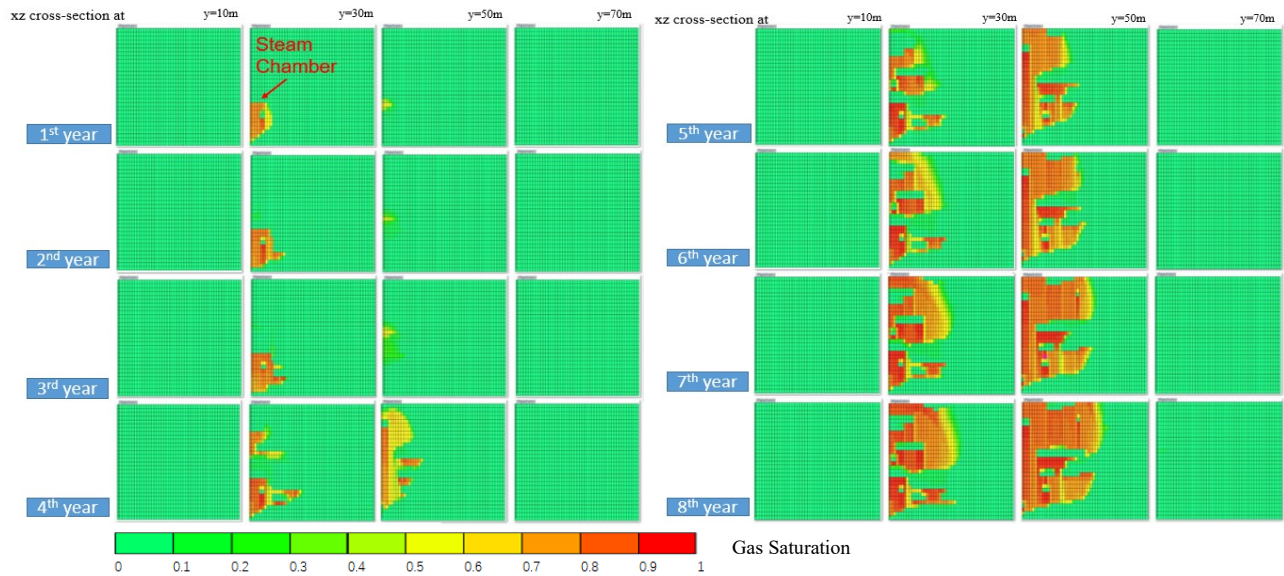
Figure 10-28. Steam chamber evolution over the initial 8-year period corresponding to the heterogeneous model Case 43 identified in cluster 3 for base model type 2.

3.5.3 Static Quality (Qs) Results

The Static quality (Qs) calculations are implemented in MATLAB® (MathWorks, R2019B). For base model type 2, a 50 × 50 dissimilarity matrix is obtained and mapped onto a 2D Euclidean space after applying MDS; finally, k-means is used to classify these 50 heterogeneous realizations into three clusters. In Table 10-5, the model set-up and execution run time for the static quality calculation are compared with those from the flow simulation. The average execution time for the static quality measure is about 48 times shorter than that for the numerical simulation.

Table 10-4. Set-up of the numerical simulation and static quality measure for base model type 2.

Parameters	Numerical Simulation	Static Quality Measure
Reservoir dimension	50 m × 80 m × 30 m	50 m × 80 m × 30 m
Grid cell size	1 m × 2 m × 1 m	1 m × 1 m × 1 m
Total number of grid cells	600,00	120,000
Simulation time per case	480 minutes	10 minutes

Similar to the flow simulation, three clusters are identified for the static quality results: Cluster 1 consists of cases with little effect of shale barriers in the near-well region. For the Qs calculation, all shale barriers located relatively far from the production well. Clusters 2 and 3 consists of cases with some effect of the shale barriers in the near-well region. The main difference between clusters 2 and 3 is that, in cluster 3, shale barriers in the near-well region have noticeable impacts on the production performance. In cluster 3, there is a presence of a large proportion of long and continuous shale barriers located in close proximity to the production well.

The MDS and clustering results corresponding to the Qs with window sizes of 5 meters, 15 meters, and 25 meters are presented in Figure 10-29 to Figure 10-31, respectively. Randomly selected cases from each cluster and their corresponding static quality at different window sizes are shown in Figure 10-32 to Figure 10-34. The yellow grid cells in Figure 10-32 to Figure 10-34 are the locations that are locally connected to the production well. The regions highlight in yellow represents the expected steam chamber drainage volume. As presented in Figure 10-32 to Figure 10-34, regardless of the window size selection, the production performance is always sensitive to the proportion of the shale barriers in the vicinity of the producer. For cases with small window size, the expected drainage volume mainly depends on the locally connected hydrocarbon volume on line-of-sight; and hence, their production performance is more sensitive to the relative location of shale barriers to the producer, and the volume or continuity of the shale barriers in the near-well region: as the relative distance between a shale barrier (even if it is small and discontinuous) to the producer decreases, or as the volume or continuity of a shale barriers locate proximity to the producer increases, the amount of locally connected hydrocarbon on line-of-sight decreases and the overall expected drainage volume decreases. As window size increasing, the expected drainage volume depends more on the locally connected hydrocarbon volume within a local window.

Therefore, for cases with large window size, their production performance is more sensitive to the presence of extensive and continuous shale barriers located right above the producer: as the distance between the long and continuous shale barrier located right above the producer and the producer decreases, locally connected hydrocarbon volume within the window size decreases and the overall expected drainage volume decreases.

According to Figure 10-29 to Figure 10-31, there is a high degree of correspondence between the two sets of clustering results when window size (expected drainage volume size) is 5 meters. This is because the clusters identified by the flow simulation mainly depends on how many/which portions of the well length are with good communication between the injection-production well pair. Clustering results from the flow simulation show that the most determinate factor to the production performance is the shale barriers located in between the well pair, regardless of their size and continuity. Similarly, during the Qs calculation, the Qs method weighs the relative distance between a shale barrier to the producer heavier for a small window size; whereas, the Qs method weighs the size and continuity of shale barriers located right above the producer heavier as window size increasing. When the window size is 5 meters, for cluster 1, most of the cases identified in this cluster using the Qs would correspond to the same cluster using the flow simulation. These are cases where the steam chamber is expected to develop relatively far away from the producer and has a large chamber size. As shown in Figure 10-32, for cases 14, 15, and 37 belong to cluster 1 based on Qs method, the overall expected drainage volume is largest compared to cases belong to other clusters. For cases in this cluster, the overall shale barriers' relative location to the producer is far. What is more, the proportion and size of shale barriers in the near-well region are small. As for cluster 2, half of the cases identified in this cluster based on the Qs method would correspond to either clusters 1 or 2 based on flow simulation. Similarly, for

59

cluster 3, half of the cases identified in this cluster based on the Qs results would correspond to either clusters 2 or 3 based on flow simulation. This observation indicates that, with a well choosing window size, the Qs ranking measure can generally capture some influences of shale barriers on the steam chamber development, such as the proportion of shale barriers in near-well region or the overall shale barriers' relative location to the well; but it represents their influences differently than the flow simulation. This discrepancy is reasonable, considering that the calculation of Qs does not incorporate any physics. Additionally, only the location of the producer is considered in the Qs calculation. According to the literature review in Section 2.2, it is observed that production performance is highly sensitive to any shale barriers located in between the well pair. However, in the Qs calculation, the location of the injection well is not taken into account. If a moderately-sized shale barrier presents right above the producer, the Qs measure believe that the steam chamber evolution is partially impeded in the upward direction and it would expand sideways away from the production well (Figure 10-32 to Figure 10-34). On the other hand, the flow simulation would predict a reduced oil production, which leads to low steam injection for a constant pressure constraint.
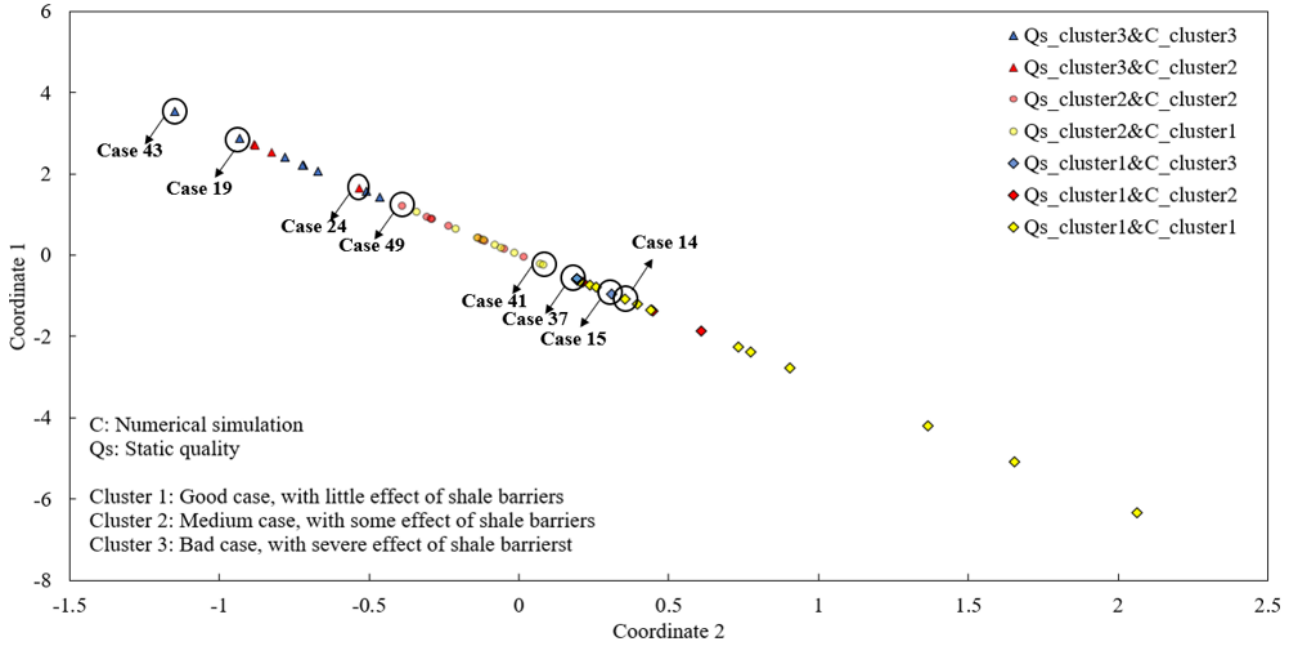
Figure 10-29. MDS and clustering results corresponding to the static quality (Qs) with a window size of 5m for base model type 2 – clustering results for the flow simulations are compared; noticeable differences are noted comparing the two methods.
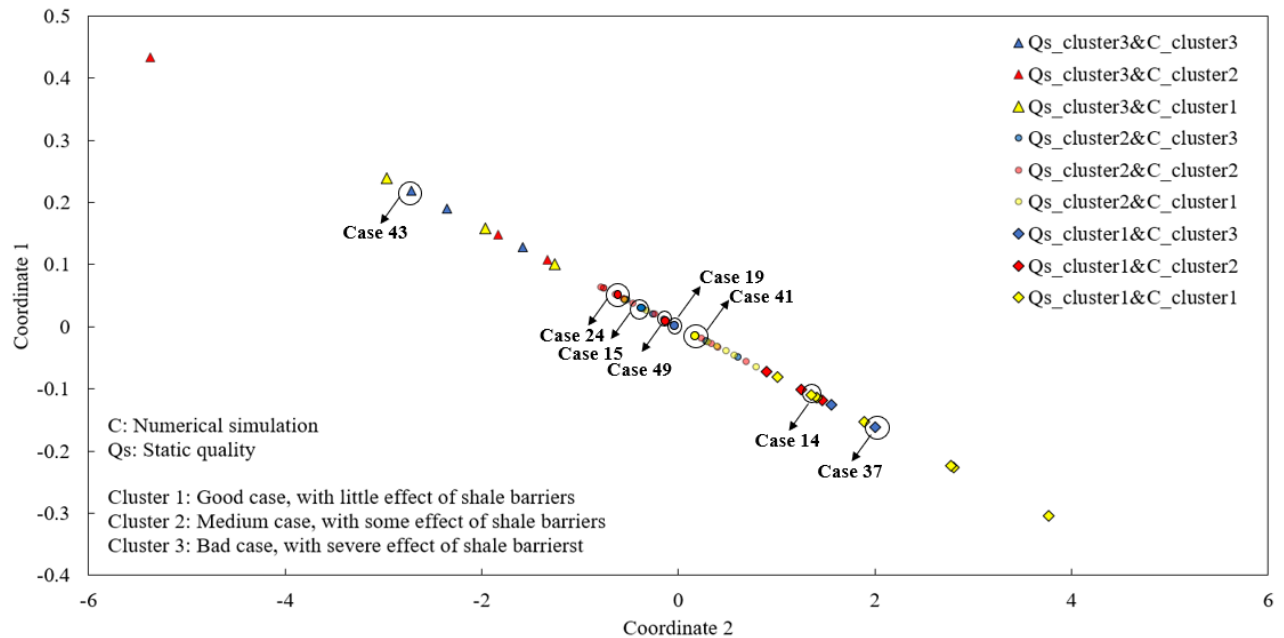
Figure 10-30. MDS and clustering results corresponding to the static quality (Qs) with a window size of 15m for base model type 2 – clustering results for the flow simulations are compared; noticeable differences are noted comparing the two methods.
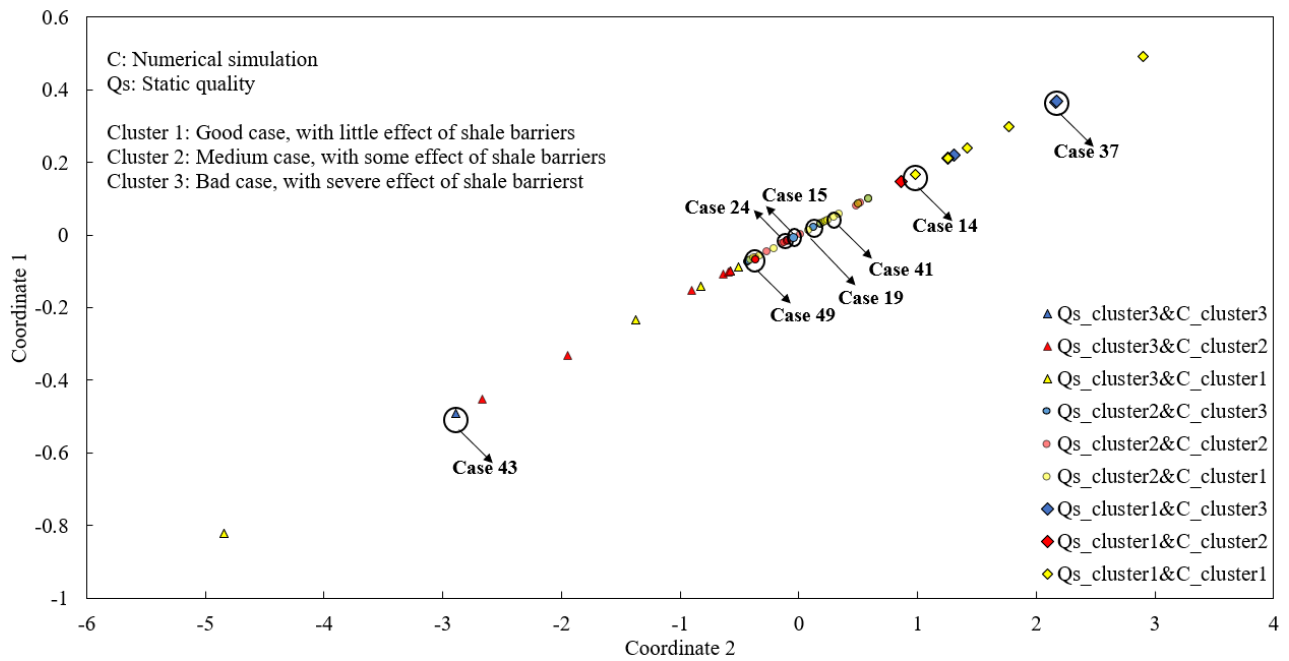
Figure 10-31. **MDS and clustering results corresponding to the static quality (Qs) with a window size of 25m for base model type 2 – clustering results for the flow simulations are compared; noticeable differences are noted comparing the two methods.**
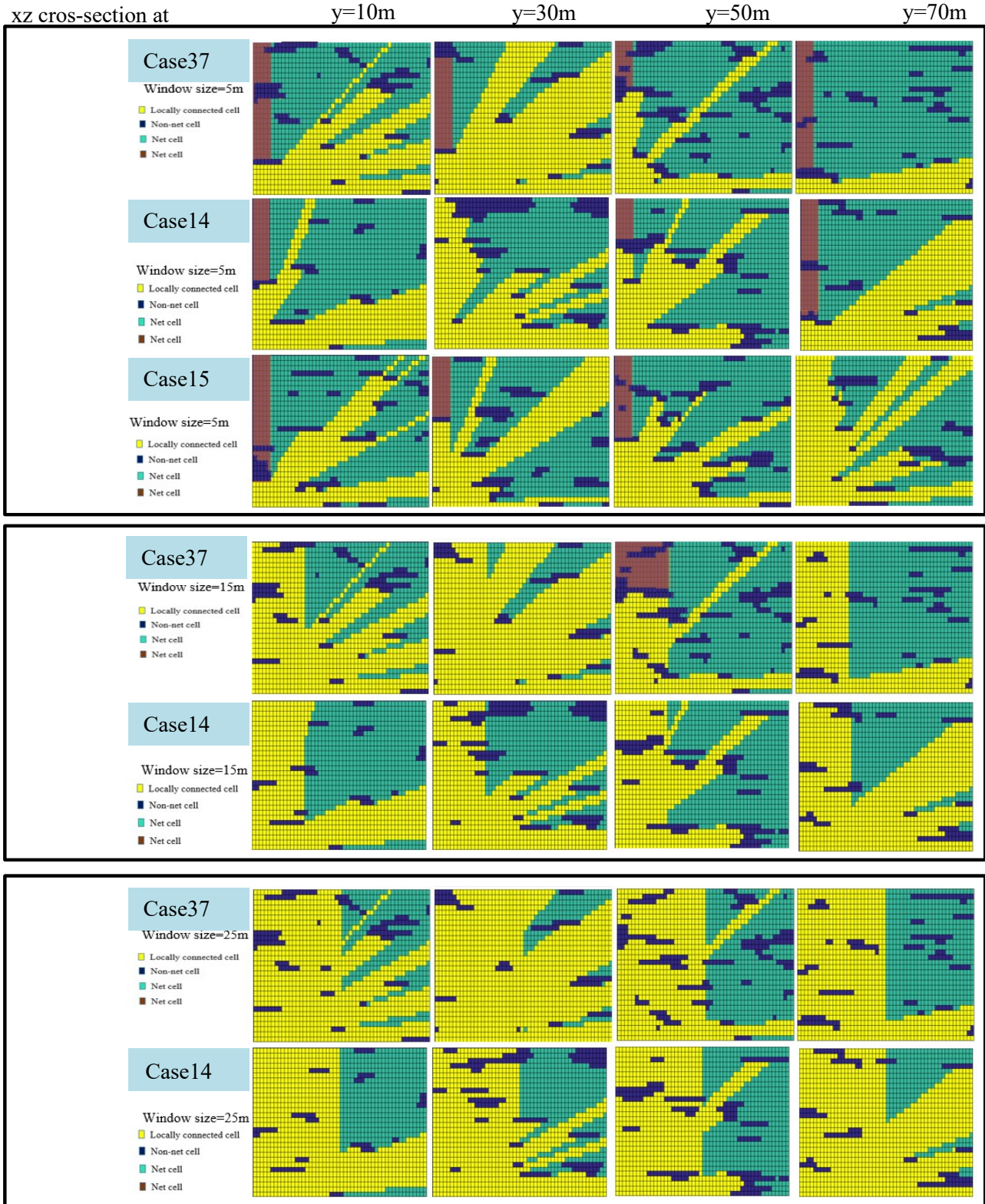
Figure 10-32. Case(s) identified in cluster 1 based on Qs with different window sizes for base model type 2.

xz cros-section at   y=10m   y=30m   y=50m   y=70m

Window size=5m
☐ Locally connected cell
■ Non-net cell
■ Net cell
■ Net cell

Case49

Case41

Window size=5m
☐ Locally connected cell
■ Non-net cell
■ Net cell
■ Net cell

Window size=15m
☐ Locally connected cell
■ Non-net cell
■ Net cell
■ Net cell

Case49

Case41

Window size=15m
☐ Locally connected cell
■ Non-net cell
■ Net cell
■ Net cell

Case24

Window size=15m
☐ Locally connected cell
■ Non-net cell
■ Net cell
■ Net cell

Case19

Window size=15m
☐ Locally connected cell
■ Non-net cell
■ Net cell
■ Net cell

Case15

Window size=15m
☐ Locally connected cell
■ Non-net cell
■ Net cell
■ Net cell

xz cros-section at   y=10m   y=30m   y=50m   y=70m

Figure 10-33. Case(s) identified in cluster 2 based on Qs with different window sizes for base model type 2.
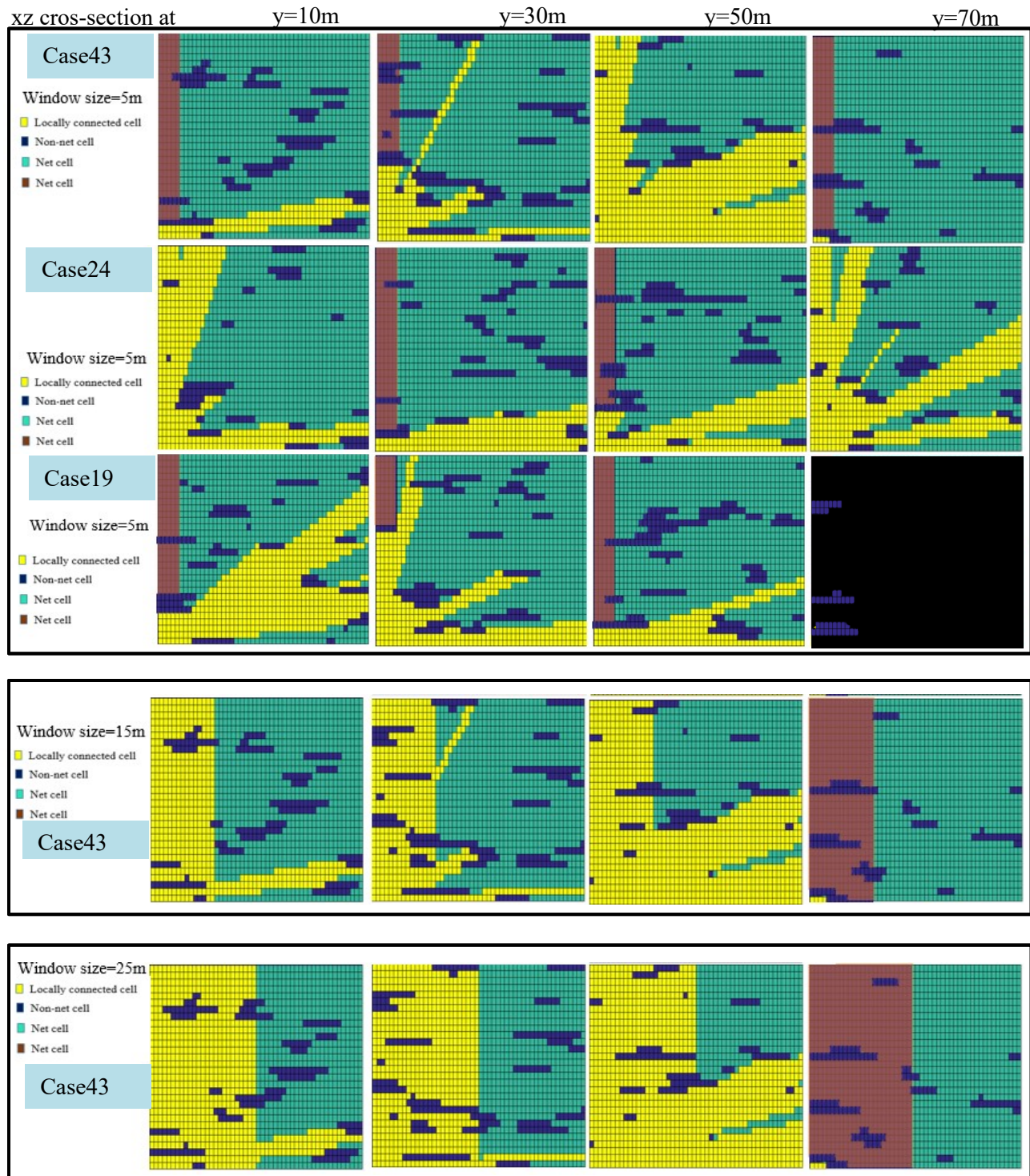
Figure 10-34. Case(s) identified in cluster 3 based on Qs with different window sizes for base model type 2.

3.5.4 Hausdorff Distance Results

The Hausdorff distance calculations are implemented in MATLAB® (MathWorks, R2019B). Table 5 compares its calculation set-up and execution run time with those from the flow simulation. A 50 × 50 dissimilarity matrix is obtained for base model type 2 and it is mapped onto a 2D Euclidean space after applying MDS; finally, k-means clustering analysis is used to classify these 50 heterogeneous realizations into three clusters.

Table 10-5. Set-up of the numerical simulation and Hausdorff distance methods for base model type 2.

Parameters	Numerical Simulation	Hausdorff Distance Model
Reservoir dimension	50 m × 80 m × 30 m	50 m × 80 m × 30 m
Grid cell size	1 m × 2 m × 1 m	1 m × 1 m × 1 m
Total number of grid cells	600,00	120,000
Simulation time per case	480 minutes	1 minute

The MDS and clustering results are presented in Figure 10-35. Three realizations from each cluster are shown in Figure 10-36 to Figure 10-38. No obvious clustering patterns can be detected from Figure 10-35, indicating that the features captured by the Hausdorff distance measure appear to be similar. Inspecting the shale barrier configurations in Figure 10-36 to Figure 10-38, it is clear that the geometries, as well as the approximate positions, of various shale barriers among the same cluster are similar. However, differences among different clusters are not overly pronounced. The issue seems to be that the Hausdorff distance measures the similarity, in terms of the shapes and positions of various objects, between a set of images. For this particular application, two images may appear similar (in terms of the spatial distribution of shale barriers), but the corresponding steam chamber evolution profiles could be markedly different, depending on the precise locations of certain shale barriers in relation to the well pair. The results confirm that flow-based proxy and

distance measures are often needed to capture the essential features associated with the underlying physical mechanisms. Thus, as shown in Figure 10-35, the clusters identified based on the Hausdorff distance do not correspond well with those based on flow simulations.
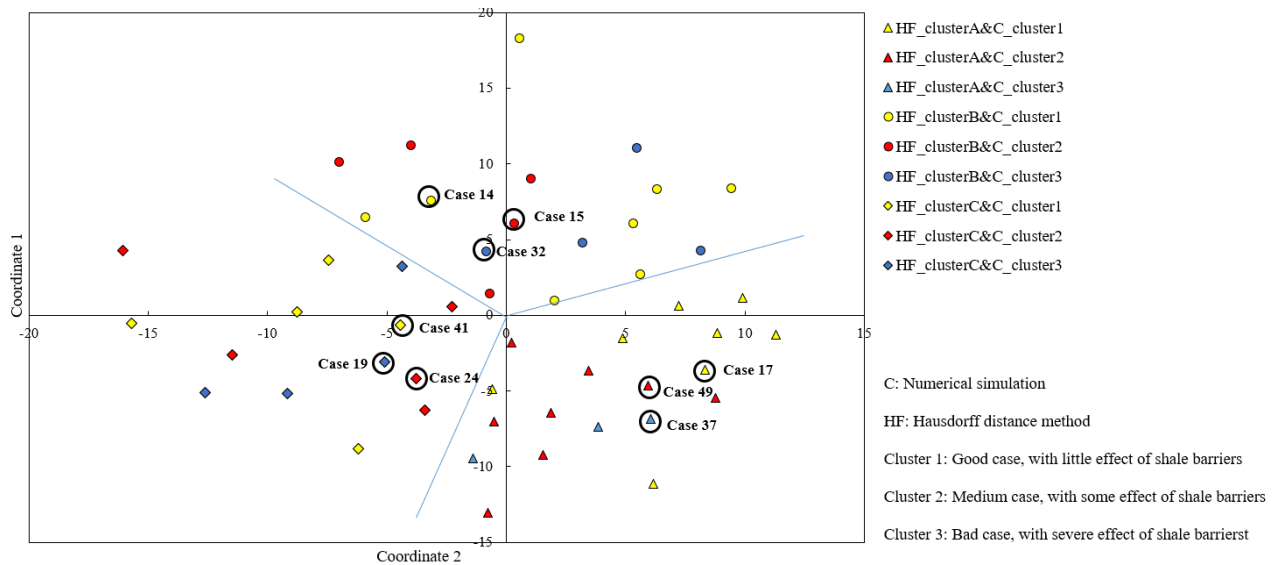
Figure 10-35. MDS and clustering results corresponding to the Hausdorff distance for base model type 2 – clustering results for the flow simulations are compared; noticeable differences are noted comparing the two methods.

xz cross-section at y=10m xz cross-section at y=30m xz cross-section at y=50m xz cross-section at y=70m Modeling in 3D

Producer   Injector   Sand   Shale
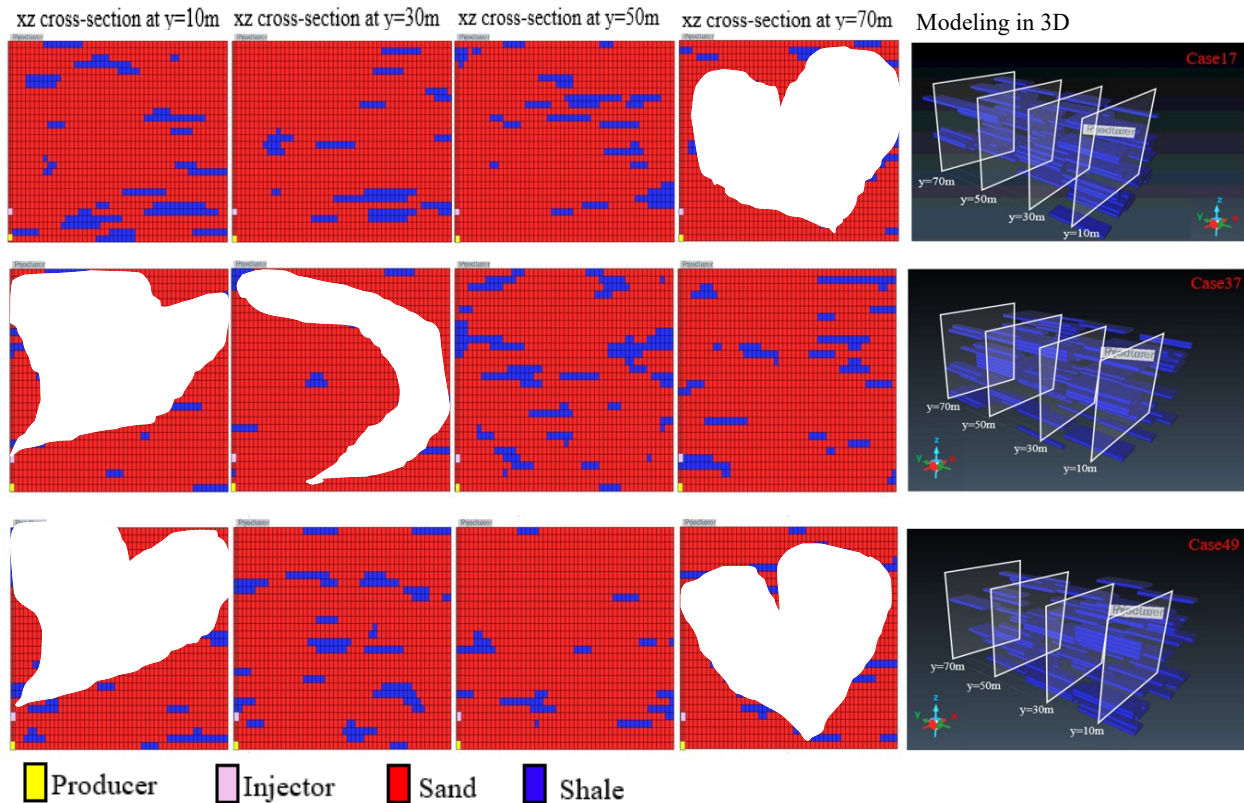
Figure 10-36. Three selected heterogeneous realizations from cluster A for base model type 2 using the Hausdorff distance algorithm: the first four columns correspond to the four segments along the *y*-axis, and the last column illustrates the shale barrier configuration in 3D.
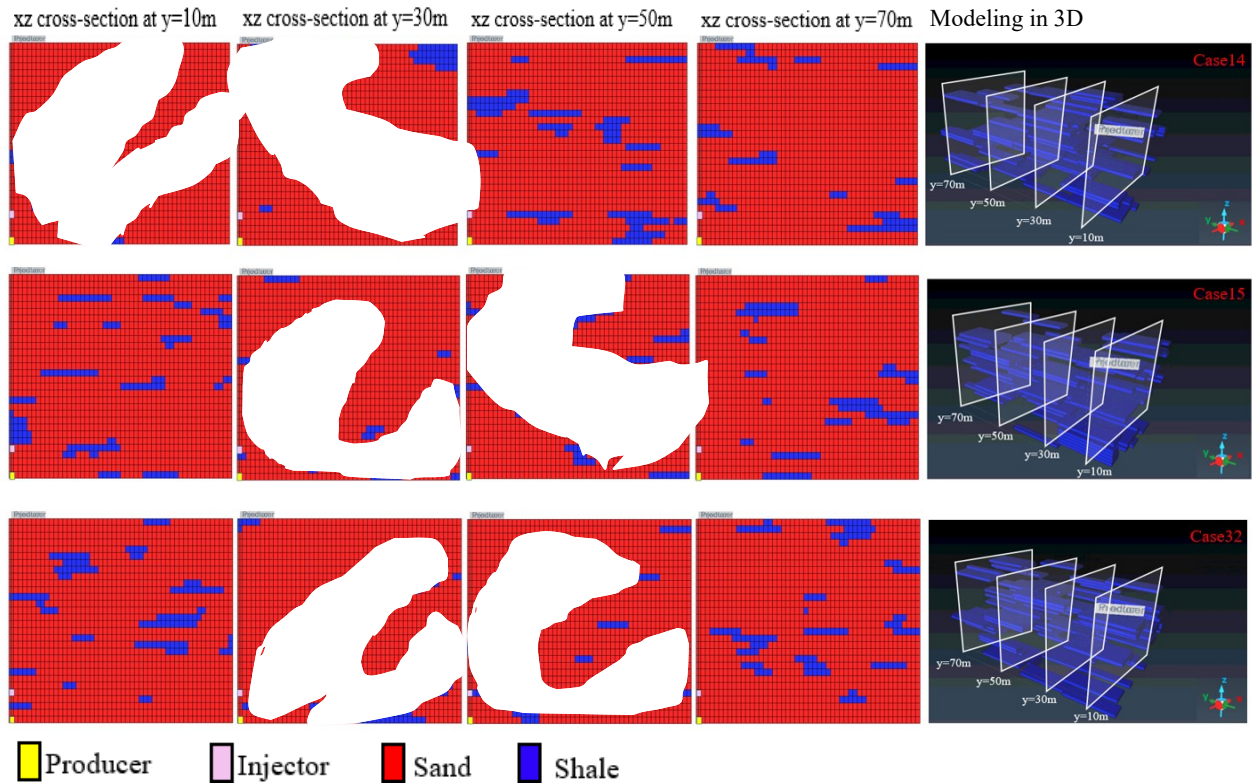
Figure 10-37. Three selected heterogeneous realizations from cluster B for base model type 2 using the Hausdorff distance algorithm: the first four columns correspond to the four segments along the *y*-axis, and the last column illustrates the shale barrier configurations in 3D.

xz cross-section at y=10m | xz cross-section at y=30m | xz cross-section at y=50m | xz cross-section at y=70m | Modeling in 3D

Producer   Injector   Sand   Shale
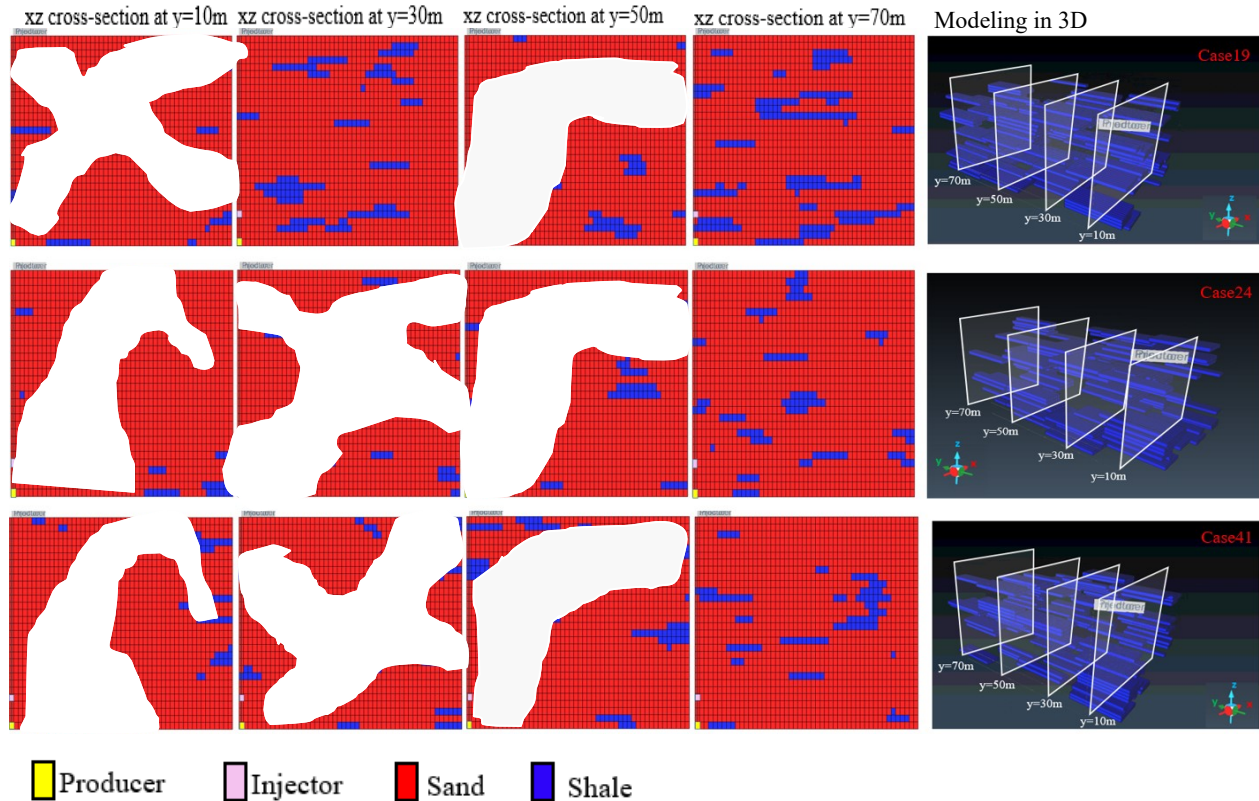
Figure 10-38. Three selected heterogeneous realizations from cluster C for base model type 2 using the Hausdorff distance algorithm: the first four columns correspond to the four segments along the *y*-axis, and the last column illustrates the shale barrier configurations in 3D.

3.5.5 Detailed Examination of the Clustering Result obtained from detailed numerical simulations vs. Hausdorff Distance, and Static Quality

In this section, a more detailed examination of the clustering results is presented. The comparison between the Hausdorff distance and flow simulation results is shown in Figure 10-39. As discussed in section 3.5.4, the static measure computed based on the Hausdorff distance is not effective in capturing the key impacts of shale barriers on the dynamic evolution of the steam chamber. In the Hausdorff distance formulation, all objects, irrespective of their locations relative to the well pair,

are weighted equally. Future studies should propose an alternative static distance measure that incorporates a weighting factor based on the relative positions of these shale barriers.

The comparison between the static quality (Qs) calculation with a window size of 5 meters and flow simulation results is shown in Figure 10-39. For cluster 1, half of the cases identified in this cluster using the flow simulation would correspond to either clusters 1 or 2 based on the Qs calculation. As for cluster 2, half of the cases identified in this cluster based on the flow simulation would correspond to the same cluster based on the Qs calculation. For the remaining 44% of the cases, half of these cases would correspond to either cluster 1 or cluster 3 based on the flow simulation. 73% of the cases identified in cluster 3 following the flow simulation would correspond to the same clusters based on the Qs calculation results. The remaining 27% of cases, which belong to cluster 3 based on the flow simulation analysis, are misclassified as cluster 2 following the Qs calculation. All the misidentified cases are due to presences of shale barrier(s) in between the well pair. According to the literature review in section 2.2 and observation in section 3.5.2.2, shale barriers located in between the well pair are the most detrimental factor to the production performance. Such shale barriers hinder the communication between well pair, results in little/no steam injection in those segments and causes locally limited steam chamber expansion. As explained in section 3.5.3, the Qs method does not take the injection well's location into account. The absence of the injector in Qs calculation eventually results in the discrepancy between the two sets of clustering results. What is more, the Qs measures just simply estimates the potential recoverable reserves, without any physic implemented in. Different from the flow simulation, without the operational constrains (e.g., a constant pressure constrain), the Qs method assumes that, if a steam chamber is impeded in a particular direction, it could always expand sideways and advanced beyond the shale barriers. Generally speaking, Qs calculation somewhat offers an

alternative to show some minor influences of shale barriers on steam chamber development. For the key influence factor to the production performance, which is the presence of the shale barriers in between the well pair, the Qs method is not able to inform. Future studies should propose an alternative static distance measure that includes the connectivity between the well pair.

Cluster 1 – little effect of shale barriers, good connectivity between the well;
Cluster 2 – limited effect of shale barriers, limited connectivity between the well pair in some segments along the well length
Cluster 3 – most noticeable impacts of shale barriers, limited connectivity between the well pair in most segments along the well length
Cluster a – little effect of shale barriers, the amount and the size of shale barriers in near-well region is small
Cluster b – limited effect of shale barriers, some shale barriers in near-well region
Cluster c – most noticeable impacts of shale barriers, laterally-extensive shale barriers in close proximity to the production well

Figure 10-39. Comparison of the clustering results obtained from detailed numerical simulations vs. particle tracking modeling and the Hausdorff distance method, as well as the static quality calculation.

CHAPTER 4: Particle-Tracking Algorithm

Due to the limitations of existing static geological measures, simple dynamic flow simulations could be applied as an alternative approach to quantifying the (dis)similarity among a set of reservoir models. In this chapter, a particle-tracking method is developed to track the movement of steam particles and to approximate the steam chamber development in a three-dimensional heterogeneous reservoir. A preliminary formulation was presented in an earlier publication (Gao et al., 2019), and several key modifications and improvements have since been implemented. For example, in addition to the production period, a preheating period is also modeled.

The key steps can be described as follow: first, a large number of steam particles are injected, but to avoid fracturing the formation, the number of steam particles launched is adjusted according to the grid cell's capacity. The transition probability of a particle from its current location to the nearby cells are computed according to Darcy's law (momentum balance) and energy balance: the transition direction is related to the transmissibility between two cells (which is computed according to their intrinsic permeabilities), while the cold bitumen is heated by the energy released by the condensing steam particles. Next, the temperatures of neighboring cells are computed after each time interval (i.e., one month in this study). The above process is repeated to model a continuous injection: new steam particles are launched at the beginning of the next time step. The locations visited by the steam particles are tracked over time to analyze the chamber development.

---

[2] The content in Chapter 4 of this thesis is derived from the following paper:

Gao, C., Ma, Z., & Leung, J.Y. (2018). A novel particle-tracking based proxy for capturing SAGD production features under reservoir heterogeneity, Paper presented at *SPE Western Regional Meeting*, San Jose, California, USA.

Gao, C., & Leung, J.Y. (2020). Techniques for fast screening of 3D heterogeneous shale barrier configurations and their impacts on SAGD production behavior, Paper presented at *SPE Canada Heavy Oil Technical Conference*, Calgary, AB, Canada.

4.1   Main assumptions

In an SGAD process there includes 2 major physics: displacement of fluids and energy transfer. Since the focus of this work is to predict the chamber development, instead of oil production. In the proposed model, a major assumption is that only energy transfer is considered. This proposed model only incorporates energy balance to mimics how the energy of steam particles delivered from one cell to another. It should be noted that explicit fluid displacements (fluid movement between cells) are not modeled here; in other words, the heated bitumen and condensed steam particles become immobile, and they would remain the cells instead of flowing towards the producer (no steam particles are taken out of the reservoir models). It is further assumed that fluid mobility (e.g., mobile/immobile water/gas pockets) would not affect the steam injectivity. It is undoubtedly a significant assumption, considering that steam chamber growth depends strongly on both heat transfer and fluid mobility, as more steam would come in contact with the cold bitumen if more fluids are draining down to the producer. However, it must be noted that the proposed method captures only the latent heat transfer from the steam particles to the in-situ bitumen; therefore, these steam particles are analogous to exothermic tracers. To partially account for the effects of fluid flows, a preheating period is simulated first to assess the connectivity between the well pair along different segments over the entire well length. In section 3, potential errors or implications from neglecting any fluid displacements are examined.

4.2   Preheating – Connectivity Assessment

When the steam particles are launched at the injector, their movements would not be affected by any shale barriers located below the injector (i.e., in between the well pair), since fluid productions

cannot be captured in this particle-tracking method. Figure 11-1 (a) and (b) illustrate two such scenarios. For case (a), no oil production would be observed due to the presence of a laterally-extensive shale barrier in between the injector and producer; however, when the steam particles are launched at the injector, this shale barrier would have no effect on the chamber development. For case (b), a shorter shale barrier is present in between the well pair; in principle, the steam particles can travel around this shale barrier and be able to reach the producer; however, due to the presence of a laterally-extensive shale barrier located right above the injector, oil production and vertical expansion of the steam chamber are still impeded. These examples illustrate that since fluid flows are not directly modeled, by launching the particles at the injector would not guarantee that the connections between the well pair and with the rest of the domain are sufficiently represented. Another scenario where flow to the producer is blocked are shown in Figure 11-1 (c) and (d); for both cases, detailed flow simulation results would reveal that no steam can be injected, as no oil can be produced due to the presence of a small shale barrier located right next to the producer, assuming that the well pair is operated under pressure constraint.

For all cases in Figure 11-1, there is either limited connectivity between the well pair or flow is impeded due to the presence of a shale barrier located in close proximity to the wells, resulting in little to no steam injection, as continually injecting steam with no oil production can fracture the formation. Therefore, it would not be reasonable to keep launching steam particles in these cases. Unfortunately, the lack of connectivity in the near-well region may not be reflected when steam particles are launched at the injector. Therefore, each model should be screened for connectivity prior to the particle-tracking modeling. A preheating period is proposed in this study to assess this connectivity.

A preheating period is a merely short duration where steam particles are launched and their breakthrough behavior at each of the producer cells is analyzed. Steam particles are continuously injected and travel through the domain following the description in the rest of section 2. For example, no steam particles are observed at the producer cell for all cases in Figure 11-1 at the end of the preheating period. If no injected particles have reached a particular producer cell, it is concluded that there is no communication between the well pair for that particular y-location, and no steam particles would be dispatched from the injector cell at that particular y-location during the production period. Otherwise, steam particles are launched at the injector at the start of the production period.

To mimic continuous injection, during both the preheating and production periods, new steam particles are launched at cells along the chamber edge that have already reached the injected steam temperature (in the first time step, particles are launched at the injector). By launching the steam particles directly at the chamber edge would imply that injectivity is not affected by fluid mobility – all particles could travel easily to the interface and be in direct contact with the cold bitumen. This process is illustrated in Figure 11-2.
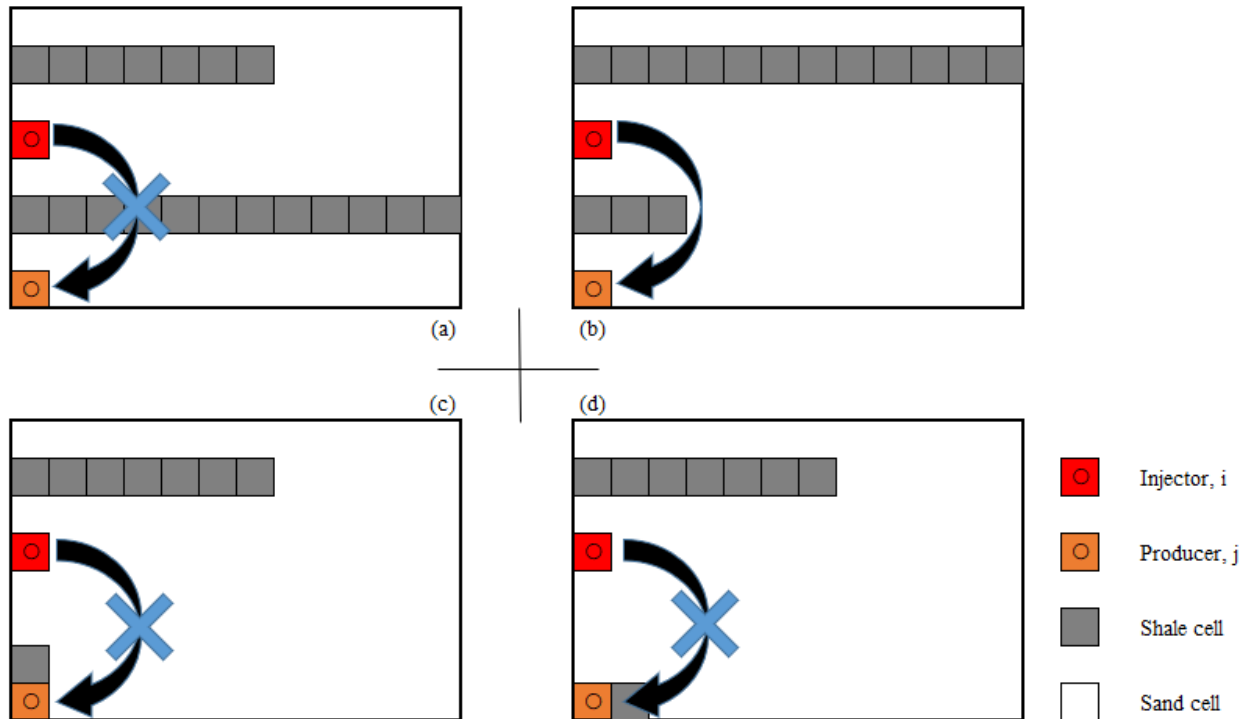
Figure 11-1. Four scenarios where shale barriers are located in the near-well region (*x-z* plane): (a) – A laterally-extensive shale barrier is located in between the well pair; (b) – A shale barrier limited in length is located in between the well pair; (c) – A shale barrier is located right above the producer; (d) – A shale barrier is located right next to the producer.
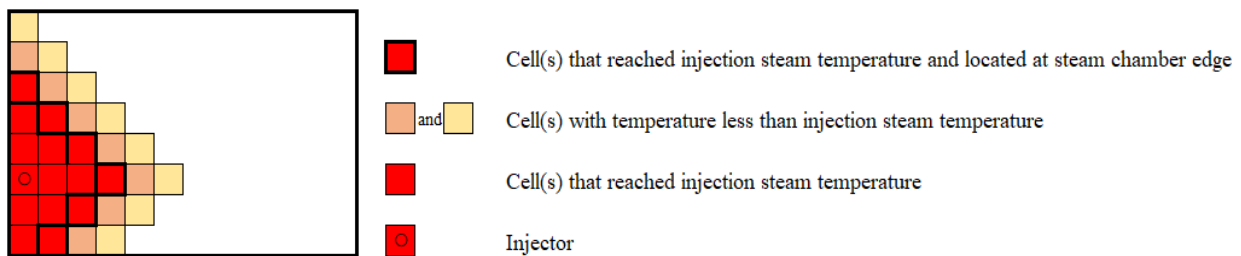
Figure 11-2. An illustration of continuous injection (*x-z* plane): new particles are launched at cells along the chamber edge that are at the injected steam temperature.

4.3   Transition Probability for Particle Movement

Eq. 4-1 shows the transition probability of a particle, P_{ij}^n, traveling from its current location, cell i, to one of its 6 neighbors, cell j, at time level n. T_{ij}^n is the transmissibility between the two cells, and it is computed according to Eq. 4-2, which is related to Darcy's law for single-phase flow, where A_{ij} is the cross-sectional area, L_{ij} is the distance between the centers of two cells; k_{ij} is the harmonically averaged absolute permeability, and μ_{gi}^{n-1} is steam viscosity at a cell i for time level $(n-1)$.

$$P_{ij}^n = \frac{\widehat{T_{ij}^n}}{\sum\limits_{j=1}^{j=6} \widehat{T_{ij}^n}} \quad\quad\quad\quad\quad\quad\quad\quad\quad\quad\quad\quad\quad\quad\quad\quad\quad\quad\quad\quad\quad\quad\quad\quad\quad (11\text{-}1)$$

$$\widehat{T_{ij}^n} = \frac{I k_{ij} A_{ij}}{\mu_{gi}^{n-1} L_{ij}} \quad\quad\quad\quad\quad\quad\quad\quad\quad\quad\quad\quad\quad\quad\quad\quad\quad\quad\quad\quad\quad\quad\quad (11\text{-}2)$$

Certain criteria must be satisfied to ensure the steam particles in cell i are capable of transferring the energy to its neighbor and cell j has the capacity to accept this energy: (1) the temperature at cell i at time level n, T_i^n, must be equal to the injected steam temperature, T_{inj}; (2) the temperature at cell j at time level $(n-1)$, T_j^{n-1}, is lower than the injected steam temperature. This criterion is imposed by introducing a binary temperature index, I, in transmissibility calculation: $I = 1$, if $T_i^n = T_{inj}$ and $T_j^{n-1} < T_{inj}$; otherwise, $I = 0$.

4.4   Energy Balance – Temperature Updating

Neither phase change or fluid displacements is modeled in this particle-tracking formulation; in other words, oil and water volumes in the cells are not updated. Eqs. 4-3 to Eqs. 4-4 represent the energy balance of a control volume (i.e., a grid cell): the energy accumulated by the cell is equal to the energy released from the steam particles arriving at the cell.

Energy balance of a cell j;

$$In = Accumulation \dots\dots\dots\dots (11\text{-}3)$$

The heat released from steam particles to cell j:

$$In = N_j^n H_{inj} \dots\dots\dots\dots (11\text{-}4)$$

If cell j contains oil sand, the accumulation term is formulated as:

$$Accumulation_{os} = C_{p_o} V_{o_{os}} \rho_o (T_j^n - T_j^{n-1}) + C_{p_r} V_{r_{os}} (T_j^n - T_j^{n-1}) + V_{w_{os}} (C_{p_w}^n T_j^n \rho_w^n - C_{p_{wi}}^n T_i^n \rho_{wi}^n) \dots\dots (11\text{-}5)$$

If cell j contains shale, the accumulation term is formulated as:

$$Accumulation_{sh} = C_{p_o} V_{o_{sh}} \rho_o (T_j^n - T_j^{n-1}) + C_{p_r} V_{r_{sh}} (T_j^n - T_j^{n-1}) + V_{w_{sh}} (C_{p_w}^n T_j^n \rho_w^n - C_{p_{wi}}^n T_i^n \rho_{wi}^n) \dots\dots (11\text{-}6)$$

where the subscripts o, os, r, sh and w represent oil, oil sand, rock, shale, and water, respectively. H_{inj} is the enthalpy per kilogram of the steam particles. C_p and ρ denote the specific isobaric heat

capacity and density. V is the volume of a certain phase within the cell. N_j^n is the total mass of steam particles entering cell j at time level n. An example is illustrated in Figure 11-3 Cell #2 may receive particles from only one source (i.e., the injector cell located right next to it); its corresponding N_j^n is computed by multiplying the total number of particles exiting cell i by P_{ij}^n. Cell #5, on the other hand, may receive particles from multiple sources (it is located in between two injection points along the horizontal trajectory); its corresponding N_j^n is the summation of all arriving particles arriving.

The only unknown is the temperature at cell j at time level n, T_j^n. Eqs. 4-3 to Eqs. 4-4 are solved together with either Eqs. 4-5 or Eqs. 4-6, depending on whether cell j contains oil sand or shale (V_o and V_r are different for these two rock types). Since C_{p_w} and ρ_w are coupled with the solution of T_j^n, a look-up table of N_j versus T_j, C_{p_w}, and ρ_w is set up for each cell j, according to Eqs. 4-3 to Eqs. 4-6, to facilitate the solution of T_j^n. Fluid properties are defined using the IAPWS IF97 standard formulation (Wagner et al., 2000).
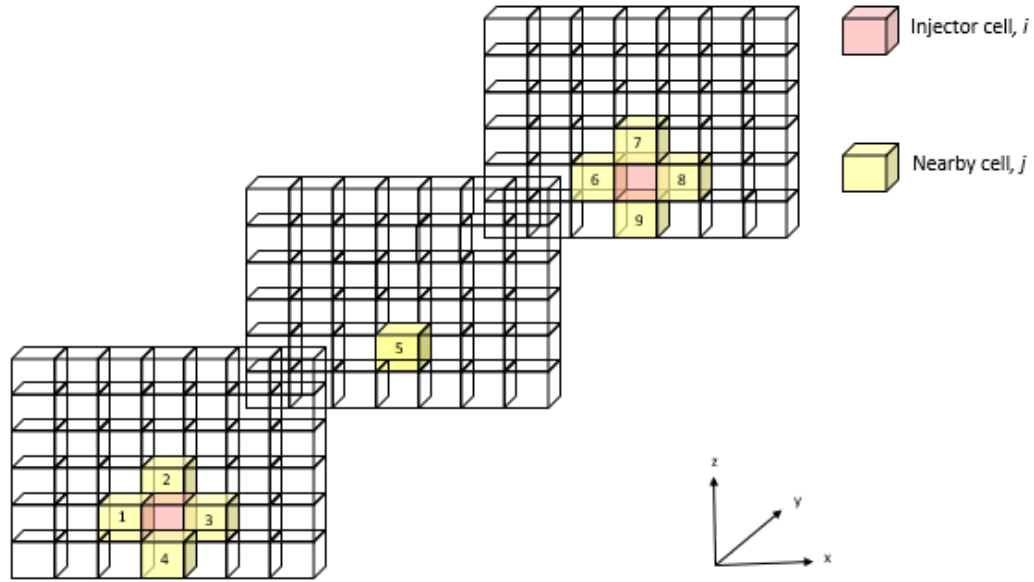
Figure 11-3. A schematic of steam particle transitions from the injector cell, *i*, to the neighboring cell(s), *j*.

4.5   Computation of Total Injection Mass

There should be a limit on how many additional steam particles are allowed to enter cell j, and this maximum allowable incremental mass ($N_{j,\max}^{n}$) is defined as follow:

If cell j contains oil sand:

$$N_{j,\max-os}^{n} = \frac{C_{p_o} V_{o_{os}} \rho_o (T_{inj} - T^0) + C_{p_r} V_{r_{os}} (T_{inj} - T^0) + V_{w_{os}} (C_{p_w}^n T_{inj} \rho_w^n - C_{p_{wi}}^0 T_i^0 \rho_{wi}^0)}{H_{inj}} - N_{osj}^{n-1} \quad \ldots\ldots\ldots(11\text{-}7)$$

If cell j contains shale:

$$N_{j,\max-sh}^n = \frac{C_{p_o}V_{o_{sh}}\rho_o(T_{inj}-T^0)+C_{p_r}V_{r_{sh}}(T_{inj}-T^0)+V_{w_{sh}}(C_{p_w}^n T_{inj}\rho_w^n - C_{p_{wi}}^0 T_i^0 \rho_{wi}^0)}{H_{inj}} - N_{shj}^{n-1} \quad\ldots\ldots\ldots\ldots(11\text{-}8)$$

The superscript "0" denotes the initial reservoir temperature. The following steps are implemented to ensure that this limit is honored:

- The total mass of new steam particles, N_{total}^n, being launched at the beginning of time level n is adjusted according to Eq. 4-9. As stated in section 4.2, new steam particles are added at cells currently at T_{inj} along the chamber edge. N_{total}^n is the summation of all $N_{j,\max}^n$ values along the chamber edge that have already reached T_{inj}.

$$N_{total}^n = \sum_{j\in edge}(N_{j,\max-os}^n + N_{j,\max-sh}^n) \quad\ldots\ldots\ldots\ldots\ldots\ldots\ldots\ldots\ldots\ldots\ldots\ldots\ldots\ldots\ldots\ldots\ldots\ldots\ldots\ldots\ldots\ldots\ldots\ldots\ldots\ldots(11\text{-}9)$$

- If $N_j^n > N_{j,\max}^n$, cell j would temporarily accept the excess steam particles and pass them onto its neighboring cells with a temperature below T_{inj} immediately in the next time level $(n+1)$.

Figure 11-4 illustrates the steam particle movements from the injector cell(s), i, to the neighboring cells, j during the initial time steps for a homogeneous domain and a heterogeneous domain. As an example, N_{total}^n would be the summation of $N_{j,\max}^n$ over all 6 yellow cells for case (a), 15 yellow cells for case (b), 6 yellow cells for case (c) and 12 yellow cells for case (d). The main difference between (b) and (d) is that there is a shale barrier in cell #12 in case (d), which did not receive enough steam particles during time step 2 (i.e., its temperature is below T_{inj} and it is not part of the chamber edge), so no new particles can be launched there at time step 3.
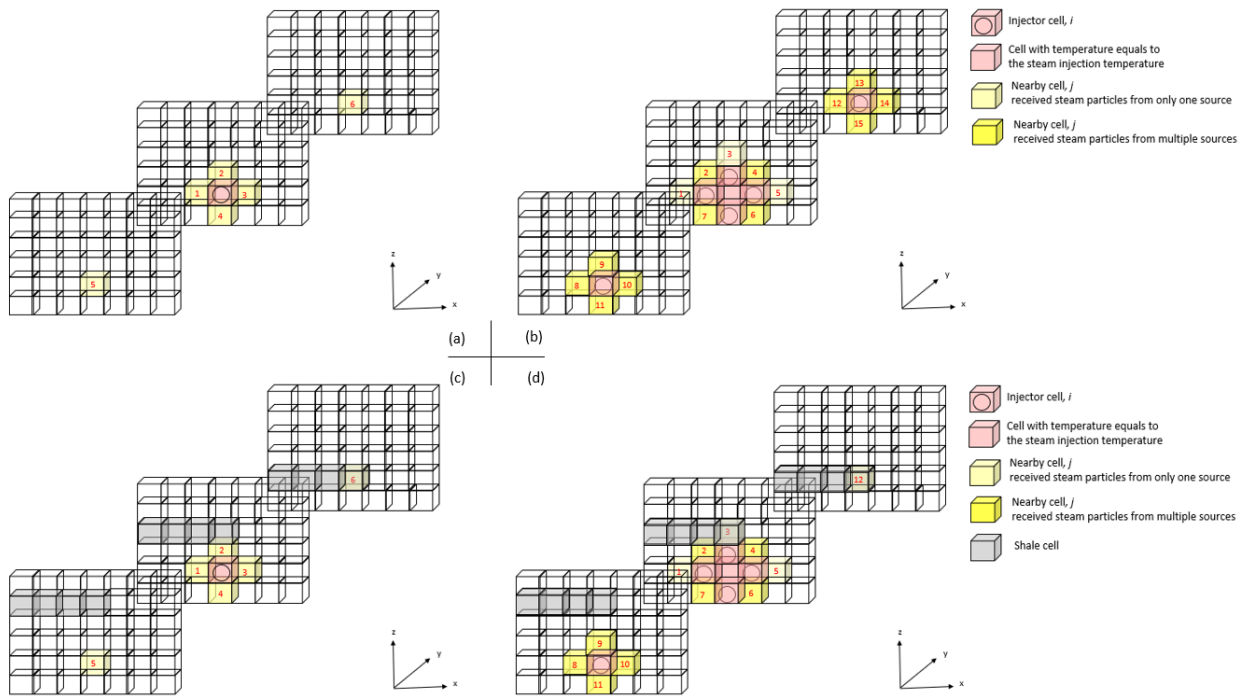
Figure 11-4. An illustration of steam particle transitions from injectors, *i*, to neighboring cells, *j*: (a) homogeneous reservoir at time step 2; (b) homogeneous reservoir at time step 3; (c) heterogeneous reservoir at time step 2; (d) heterogeneous reservoir at time step 3.

4.6   Particle-Tracking Workflow

Figure 11-5 shows the workflow for the particle-tracking method, which is applied for both the preheating and production periods. First, after importing the pertinent model parameters, steam particles are dispatched from the injector cells; for subsequent time steps, steam particles are added to cell(s) along the chamber edge that has/have reached the injected steam temperature (sections 2.2.1 and 2.2.4). Next, steam particles would move to the neighboring cell(s) (sections 2.2.2 and 2.2.4). Finally, temperature and other cell properties are updated (section 2.2.3). In this study, a total of 7 and 113 time levels are used for preheating and producing periods, respectively.

Start

Import model parameters

Lauch particles at the injector cells

Calculate total mass of steam particles to be launched, using Eqs. 5.1, 5.2 and 6

Calculate mass of steam particles newly launched to cell j, N_j^n

$N_j^n < N_{j,max}^n$

Yes

No

Update the neighbouring cell(s)' temperature, as well as the cell properties

Exceed amount is put aside and will be distributed to the neighbouring cell(s) in next time step $(n+1)$

n=n+1
Is it n < maximum time step?

No

End

Yes

Launch new particles along chamber edge that have already reached the injected steam temperature

For each injector cell, compute :
$$T_j^n = \frac{I k_{ij} A_{ij}}{\mu_{g_i}^{n-1} L_{ij}}$$

Let I=0 for cell(s) :
$T_j^{n-1} \geqslant T_{inj}$
$T_i^n < T_{inj}$

Let I=1 for cell(s) :
$T_j^{n-1} < T_{inj}$
$T_i^n = T_{inj}$

Calculate transition probability

Figure 11-5. A workflow for applying the particle-tracking model.

CHAPTER 5: Results and Discussions for Particle-Tracking Modeling

This chapter contains results and discussion of the proposed particle-tracking model, as well as comparison with the detailed flow simulation. The particle-tracking method is implemented in MATLAB® (MathWorks, R2019B) to estimate the steam chamber development for two sets of 3D heterogeneous reservoir models. To establish a baseline for comparison, all models are also subjected to flow simulation for 10 production years using STARS (CMG 2019).

5.1   Distance Functions for Particle-Tracking Modeling

After subjecting a total of 50 heterogeneous models based on model type 2 to the particle-tracking and flow simulations, it is important to visualize and compare the steam chamber development characteristics among these different models. Following the work of Zheng et al. (2018a), multidimensional scaling method (MDS) and k-means clustering are employed to categorize the results for all 50 realizations into several groups.

For the particle-tracking model, the chamber volume at a given time level, $V_{ch}(t)$, is calculated by summing the pore volume of all cells that have been visited by the steam particles with $T^n \geq T_{inj}$. At the end of a 10-year production period, a time series of chamber volumes can be obtained for each model. From a pair of time series of $V_{ch}^l(t)$ and $V_{ch}^{l^*}(t)$, the following flow-based distance, d^{ll^*}, can be computed between any two realizations:

---

[3] The content in Chapter 5 of this thesis is derived from the following paper:

Gao, C., & Leung, J.Y. (2020). Techniques for fast screening of 3D heterogeneous shale barrier configurations and their impacts on SAGD production behavior, Paper presented at *SPE Canada Heavy Oil Technical Conference*, Calgary, AB, Canada.

$$d^{ll^*} = \sum_{t=1}^{m} w(V_{ch}^l(t) - V_{ch}^{l^*}(t))^2 \quad \text{..} \quad (12\text{-}1)$$

where w is the weighting factor, and it is assumed to be $1/t^2$ in this study. m refers to the numbers of the production months. This formulation is based on the observation that the development of a steam chamber is significantly impeded by any shale barriers located near the well pair, and the impacts of these near-well shale barriers are most prominent in the early-time data. A weighting factor of $1/t^2$ would ensure the data corresponding to low values of t to be given more emphasis. As discussed in section 4.2, for the particle-tracking simulation, t refers to the traveling time level, instead of physical time. Due to this arbitrary traveling time definition, as well as the lack of explicit treatment of gravity and pressure effects, the steam chamber development as predicted by the particle-tracking model tends to be more uniform for all cases, irrespective of the heterogeneity distribution. Therefore, only the data corresponding to the first two production years are included in the flow-based distance calculation. This assumption is justified considering that the late time data is typically given much lesser weight. A dissimilarity matrix is computed based on the distance measures for all 50 modified time series. Then, they are transformed into a set of 50 points in a 2D Euclidean space via MDS, where k-means clustering is applied to categorize these points into three groups.

5.2   Simulation Resolution for Particle-Tracking Modeling

In order to select an optimal grid size for the detailed flow simulation, various grid sizes are tested. Table 12-1 summarizes the runtime for each grid block size selection. The comparison result of steam chamber expansion profiles of a randomly selected reservoir model from base model type 2

using different grid block sizes is presented in Figure 12-1.

Since the minimum thickness of a shale barrier is 0.3 meters, and the average shale barrier thickness is 1.22 meters (Zheng et al., 2018b). Also, considered that, compared to the detailed flow simulator, the overall computational cost of the proposed model is low. A slightly smaller grid cell size can be selected for the proposed particle-tracking model. In this study, a set of grid block sizes with $1m \times 1m \times 1m$, $0.5m \times 0.5m \times 0.5m$ and $0.3m \times 0.3m \times 0.3m$ are tested.

As presented in Figure 12-1, the discrepancy between the simulation results over the initial 2-year period using different grid sizes is small. According to Table 12-1, as the grid cell size decreases, the executive time dramatically increases. To balance both computational cost and the computational accuracy, the grid block size for this work is set as $1m \times 1m \times 1m$.
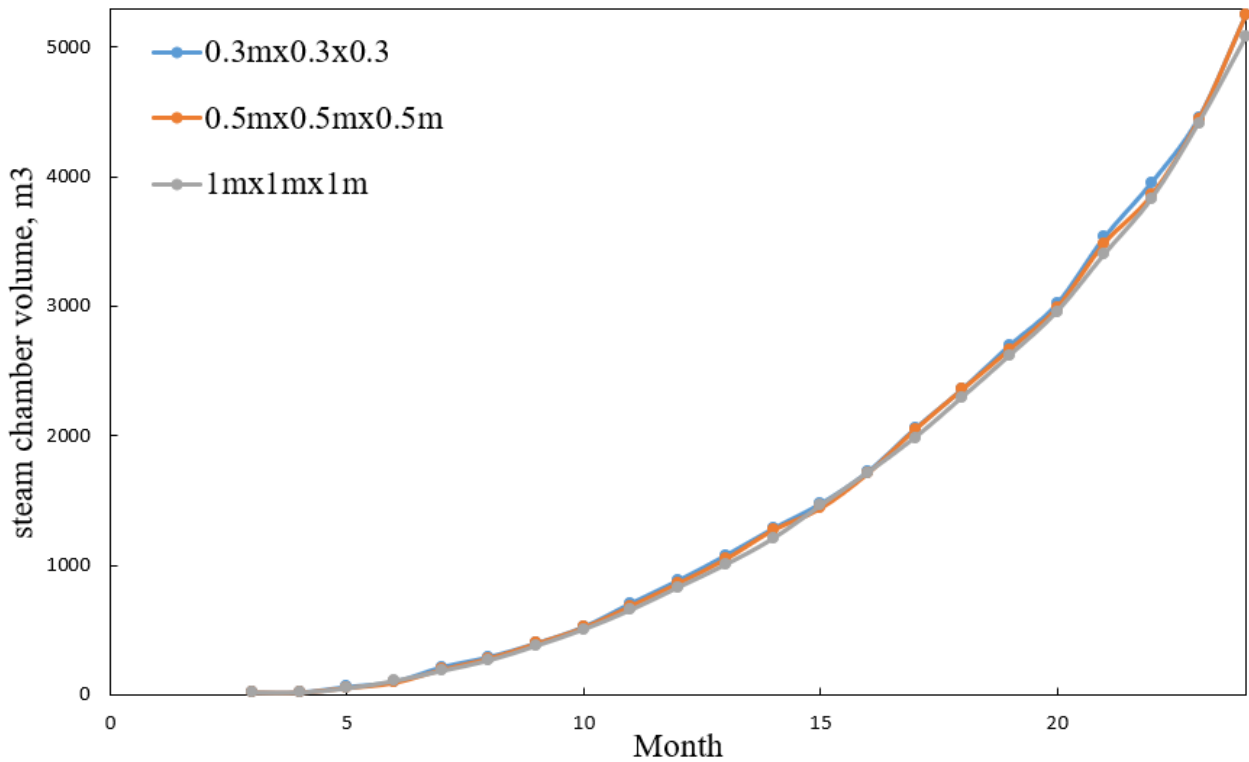
Figure 12-1. Comparison simulation results of a steam chamber expansion for a randomly selected model from base model type 2 with different grid block sizes.

Table 12-1. Runtime of a model from base model type 2 with different grid block sizes for the particle-tracking modeling.

Grid cell size	1 m × 1 m × 1 m	0.5 m × 0.5 m × 0.5 m	0.3 m × 0.3 m × 0.3 m
Reservoir dimension	50 m × 80 m × 30 m	50 m × 80 m × 30 m	50 m × 80 m × 30 m
Total number of grid cells	120,000	960,000	4,444,444
Simulation time per case	6 minutes	78 minutes	5 hours

5.3   Particle-Tracking Modeling Results

The model set-up for two simulation techniques are compared in Table 12-2. The particle-tracking simulation execution time is 80 times shorter than that for the numerical simulation. In fact, a slightly coarser grid (along the *y*-direction) has been used for the numerical simulation to reduce the computing time. In the numerical simulation model, and additional constraint is imposed such that the maximum allowable injection rate is 120 m^3/day to avoid fracturing the formation. Other model parameters are listed in Table 10-2.

Table 12-2. Set-up of the numerical simulation and particle-tracking models for base model 2.

Parameters	Numerical Simulation	Particle-Tracking Proxy Model
Reservoir dimension	50 m × 80 m × 30 m	50 m × 80 m × 30 m
Grid cell size	1 m × 2 m × 1 m	1 m × 1 m × 1 m
Total number of grid cells	600,00	120,000
Injection pressure	1500 kPa (maximum allowable rate is 120 m^3/day)	1500 kPa
Simulation time per case	480 minutes	6 minutes

Three groups are identified for both the flow simulation and particle-tracking results. Each cluster exhibits certain unique characteristics. Cluster 1 consists of cases where the effects of shale barriers in the near-well region are minimal. For both flow and particle-tracking simulations, there is good communication between the injector and producer in all 4 segments along the well length. Clusters 2 and 3 include scenarios where no connectivity can be detected during the preheating period (so no steam particles are injected in those segments). The main difference between clusters 2 and 3, however, is that, in cluster 3, shale barriers in the near-well region has introduced severe impacts on the chamber development. In cluster 3, there is no communication between the well pair for at least two of the segments (half of the well length). The MDS and clustering results for the particle-tracking modeling and flow simulation are presented in Figure 12-2 and Figure 12-3.

Six randomly selected heterogeneous realizations from different clusters are shown in Figure 12-4; and the steam chamber evolution profiles for these six cases over the initial 4-year period and next 4-year period are presented in Figure 12-5 to Figure 12-10 and Figure 12-11 to Figure 12-16, respectively.

As presented in Figure 12-2, there is a perfect agreement between the clustering results inferred for the two periods. This observation indicates that the chamber evolution during the production period, as predicted by the particle-tracking method, strongly depends on how many/which portions of the well length are subjected to steam injection. The results in Figure 12-3 show that, despite the many assumptions and simplifications invoked in the particle-tracking method, there remains a high degree of correspondence between the two sets of clustering results. In fact, discrepancies are more noticeable along the cluster boundaries (e.g., cases 37 and 49). As shown in Figure 12-4, for case 49, there is reasonable connectivity between the well pair along the entire well length (all four segments); hence, this case is classified as cluster 1 according to the particle-tracking results.

However, further inspection of segment 1, there are several shale barriers near the injector and one moderate shale barrier sits right above the injector, which has led to some negative impacts on the chamber evolution and being classified as cluster 2 according to the flow simulation results. Similarly, for case 37, there is one small shale barrier located in between the injector and the producer in segment 2 and some more laterally-extensive ones in segment 4; therefore, it is classified as cluster 3 based on flow simulation results. However, the particle-tracking simulation predicts that the steam chamber would eventually advance beyond the shale barrier in zone 2, such that this case is classified as cluster 2. As shown in Figure 12-5 and 42, for cases 20 and 39 from cluster 1, there are little differences in the steam chamber development over the initial 4-year period according to the two methods. For clusters 2 and 3 (Figure 12-6, Figure 12-7, Figure 12-9, and Figure 12-10), the steam chamber evolution profiles obtained from the particle-tracking method begin to deviate from those predicted by flow simulation as the production continues. Similar explanation for case 37 can be offered here. Flow simulation generally predicts limited chamber development in section(s) with little/no communication between the well pair; however, some level of chamber development is often predicted by the particle-tracking method as the production continues. This discrepancy can be attributed to the inability of the particle-tracking method to model fluid flows and drainage explicitly, where injectivity is controlled solely based on the connectivity assessment during the preheating period. Therefore, this discrepancy tends to grow with time. Furthermore, comparing case 24 from cluster 2 (Figure 12-12) with case 43 from cluster 3 (Figure 12-15), it is noted that their particle-tracking results are similar, while their flow simulated profiles are noticeably different. In reality, due to the gravity effect, the chamber would tend to advance upwards, whereas in the particle-tracking model, the chamber would grow based

on the transmissibility between the two neighboring grid cells; in other words, it tends to expand sideways away from the well pair.
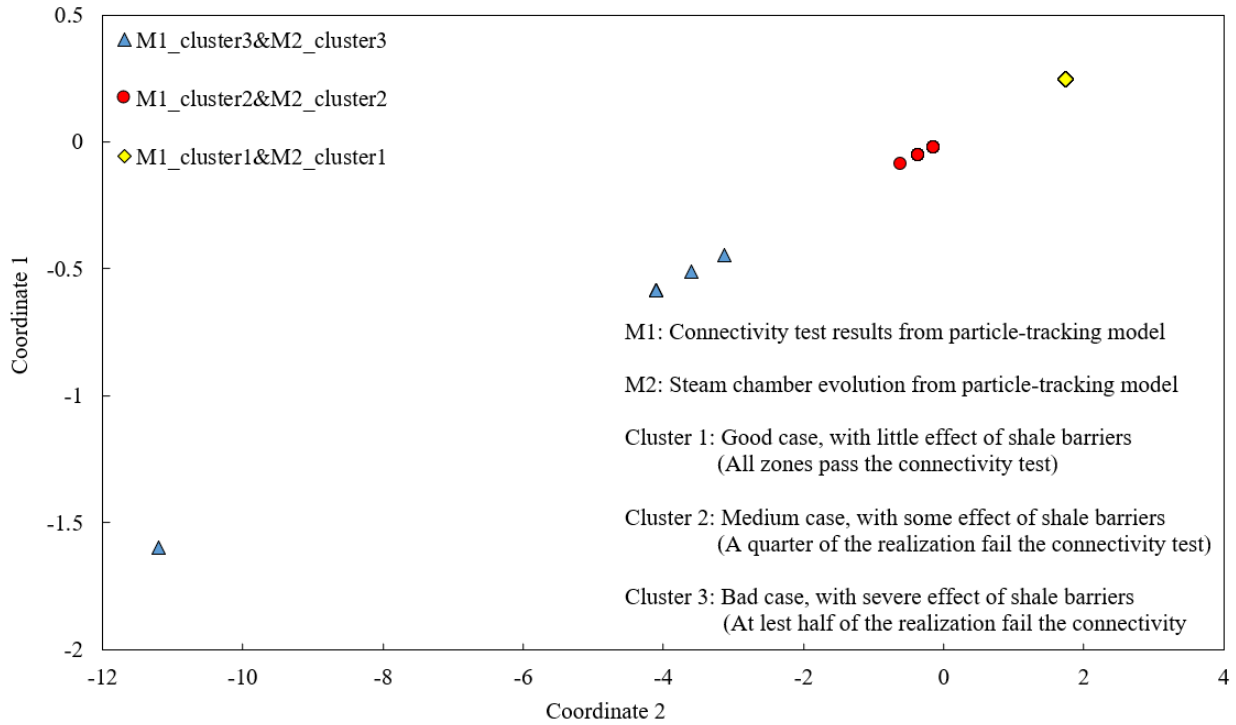
Figure 12-2. MDS and clustering results corresponding to the particle-tracking simulation for the preheating period – clustering results based on the production period are compared, demonstrating a significant correlation between the results for the two periods.
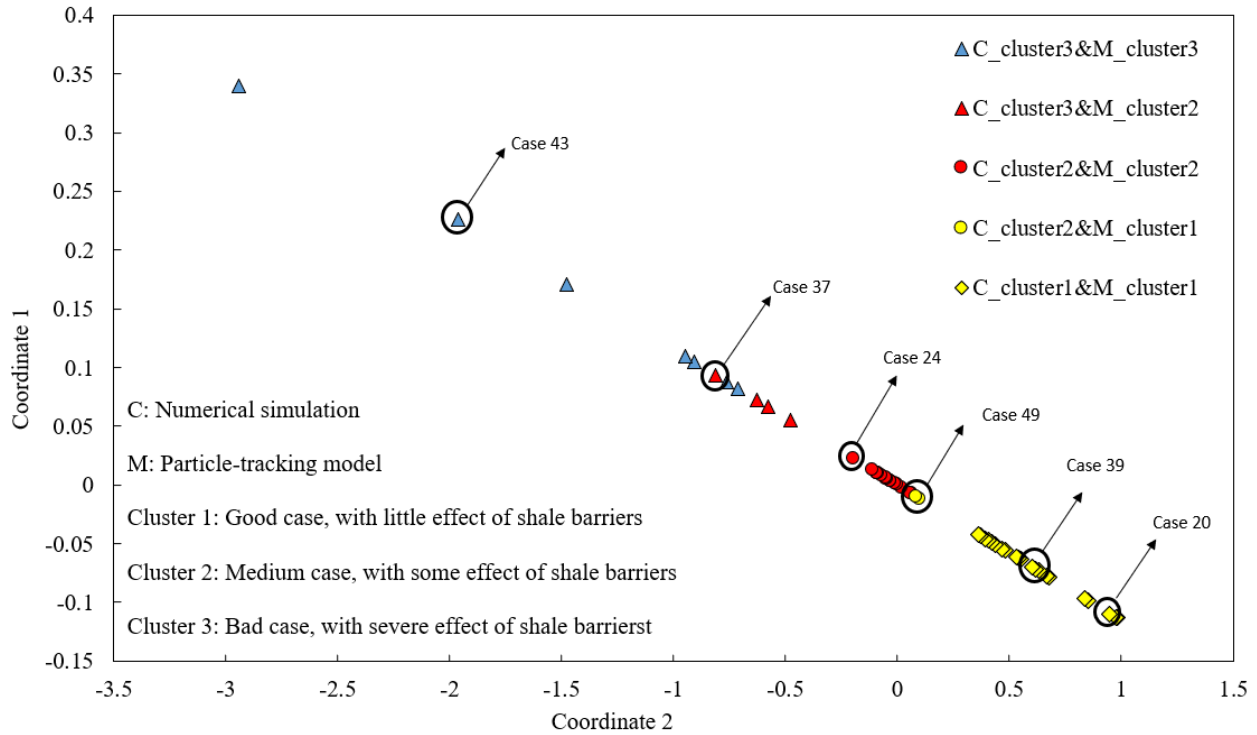
Figure 12-3. MDS and clustering results corresponding to the particle-tracking simulation for the production period – clustering results based on the flow simulations are compared, demonstrating a significant correlation between the two methods.
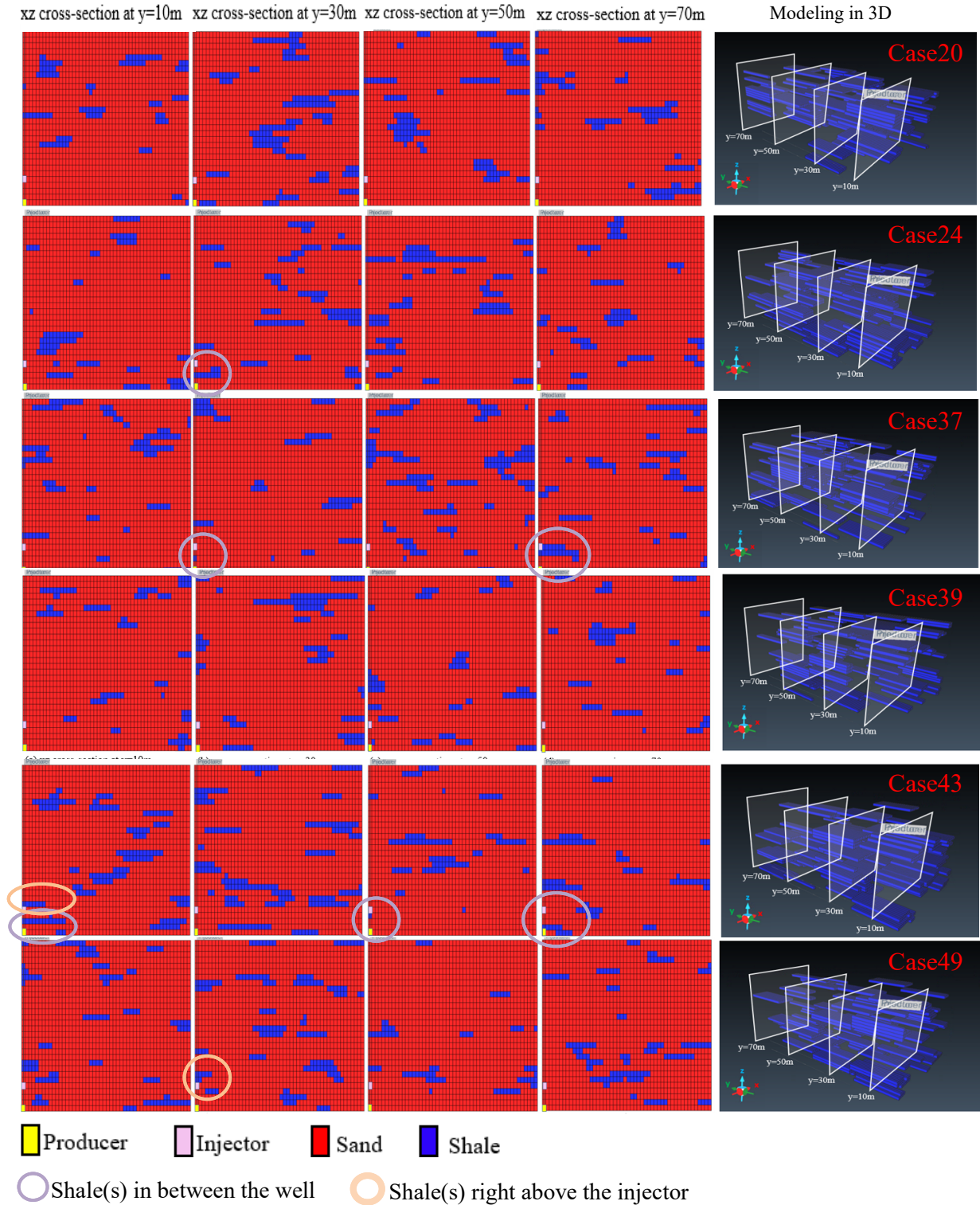
Figure 12-4. Six selected heterogeneous realizations: the first four columns correspond to the four segments along the *y*-axis, and the last column illustrates the shale barrier configuration in 3D.
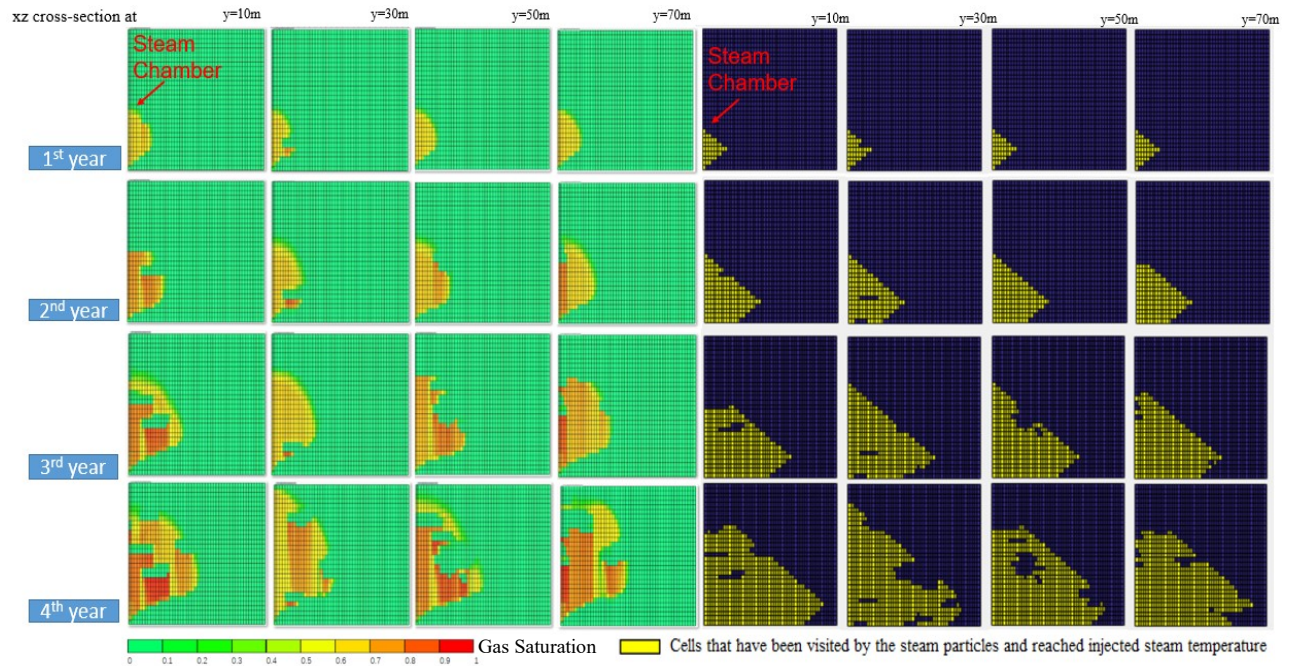
Figure 12-5. Steam chamber evolution over the initial 4-year period corresponding to the heterogeneous model Case 20.
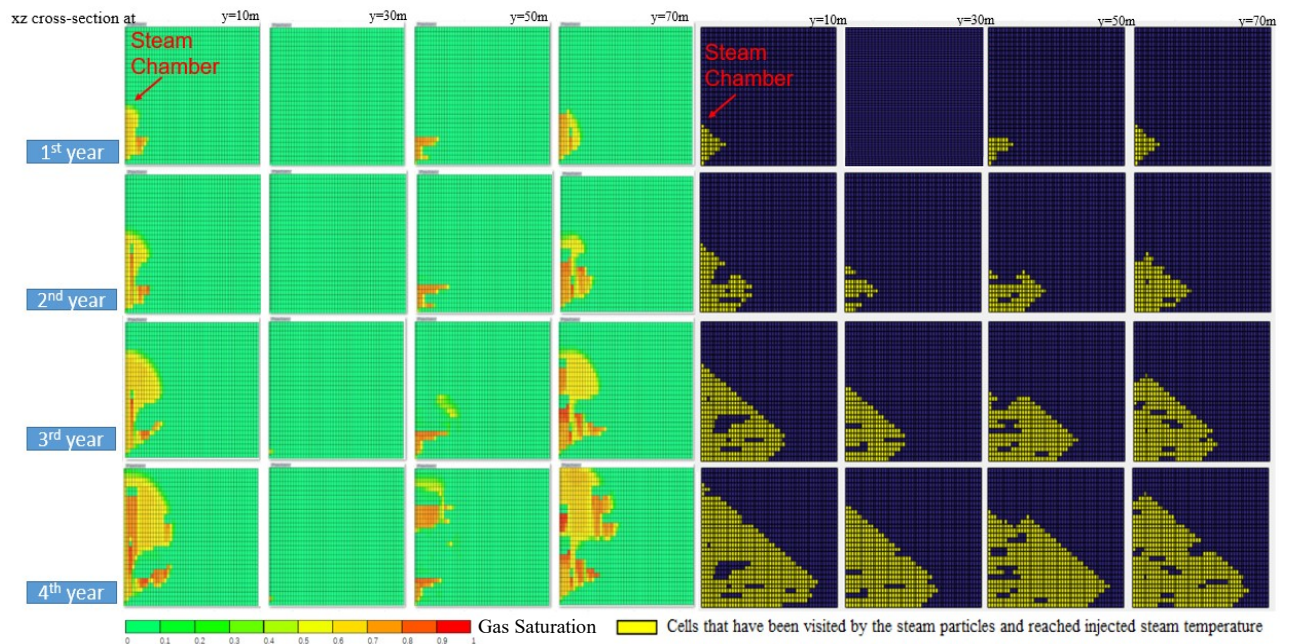
Figure 12-6. Steam chamber evolution over the initial 4-year period corresponding to the heterogeneous model Case 24.
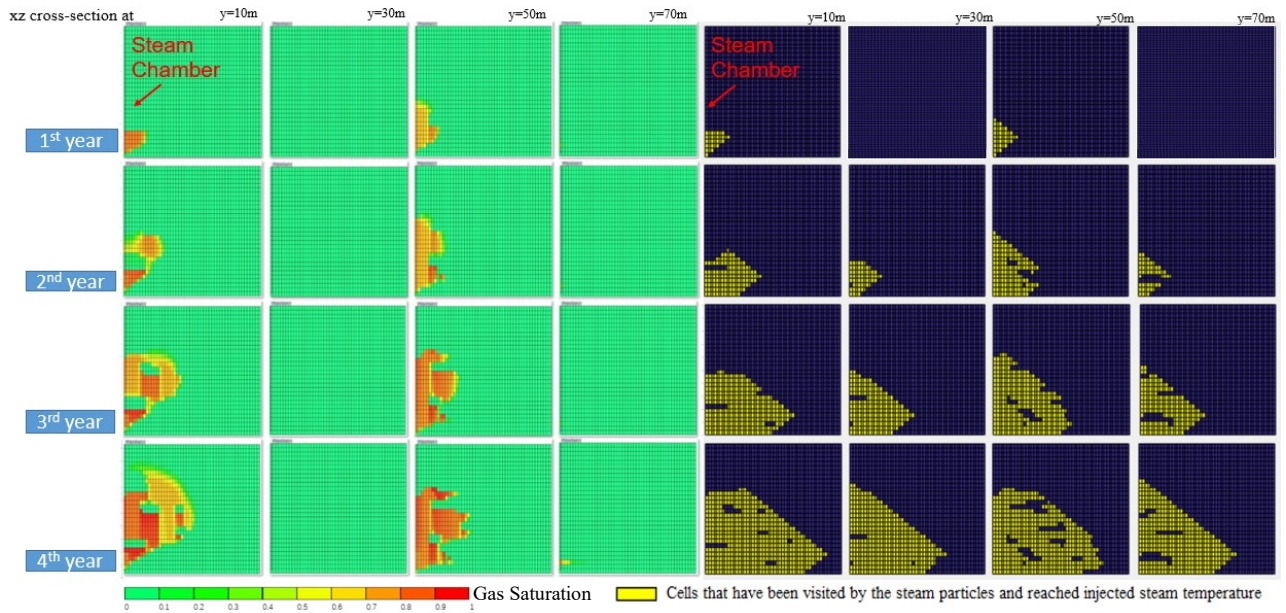
Figure 12-7. Steam chamber evolution over the initial 4-year period corresponding to the heterogeneous model Case 37.
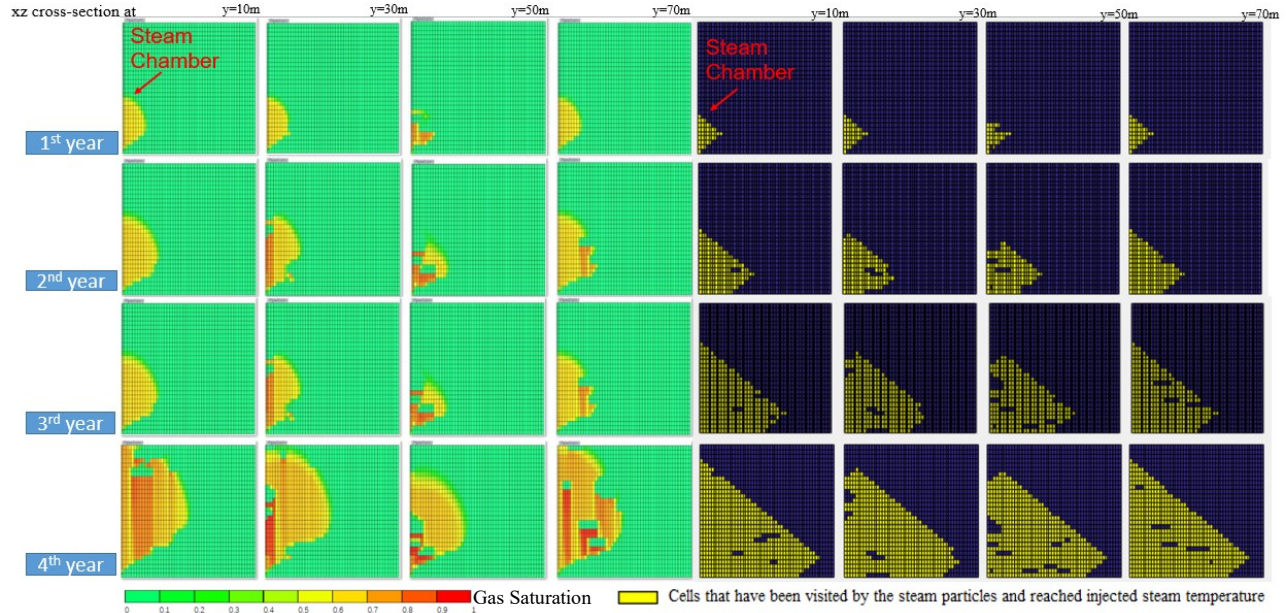
Figure 12-8. Steam chamber evolution over the initial 4-year period corresponding to the heterogeneous model Case 39.
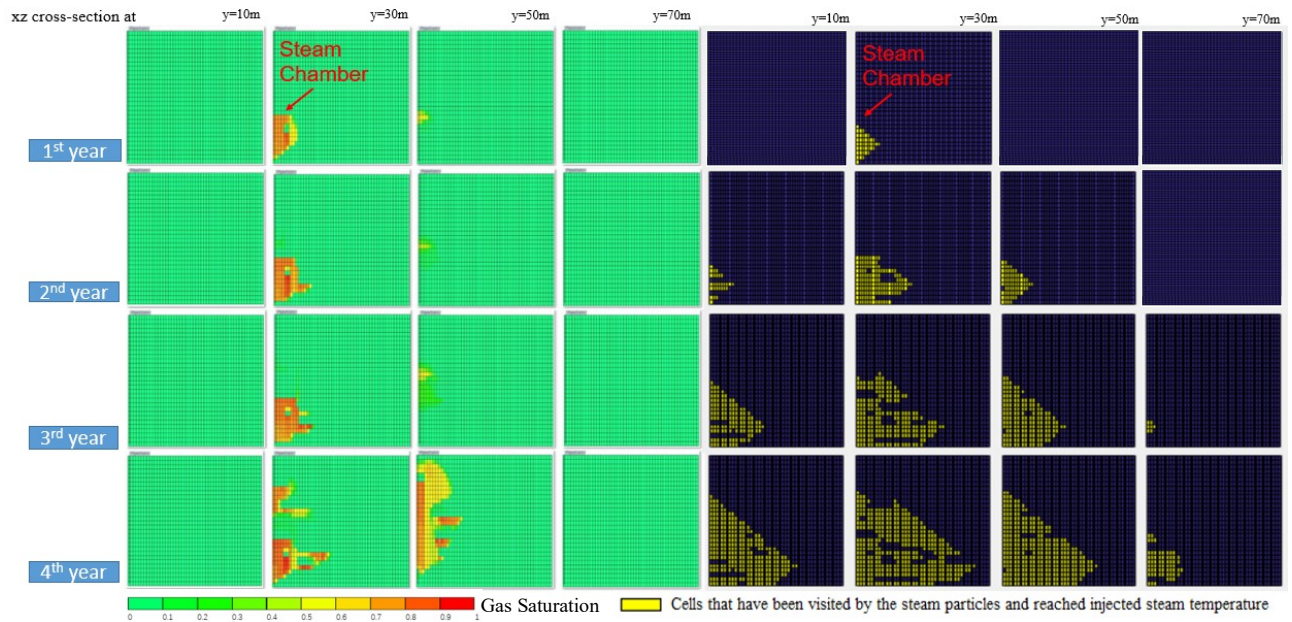
Figure 12-9. Steam chamber evolution over the initial 4-year period corresponding to the heterogeneous model Case 43.
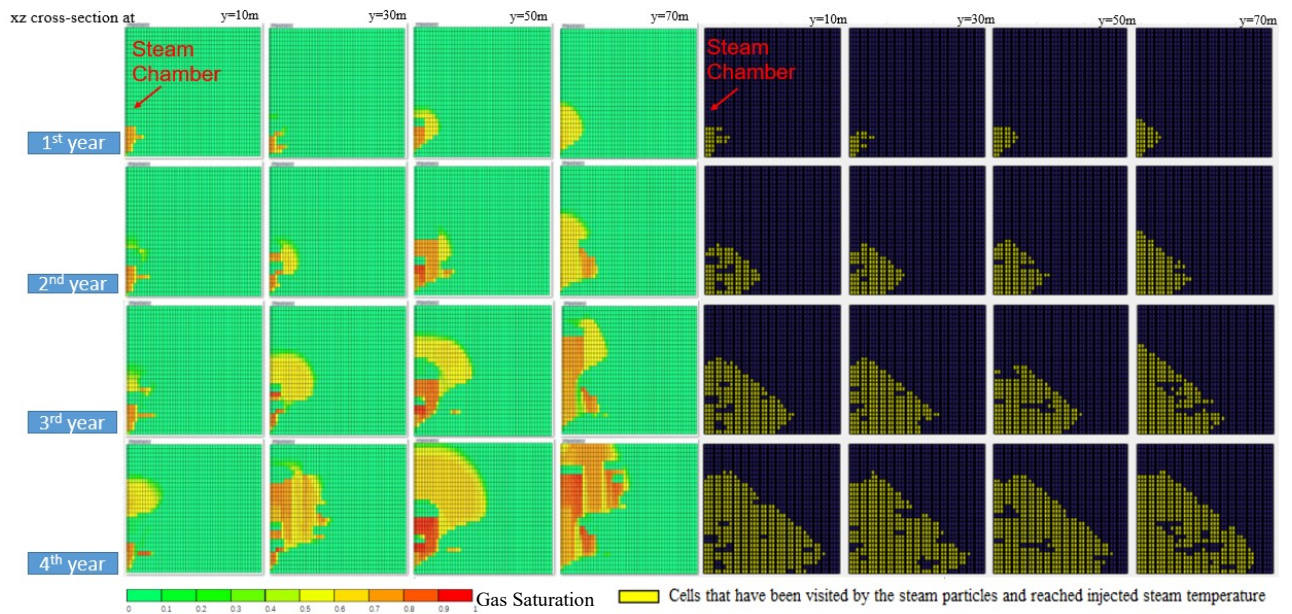
Figure 12-10. Steam chamber evolution over the initial 4-year period corresponding to the heterogeneous model Case 49.
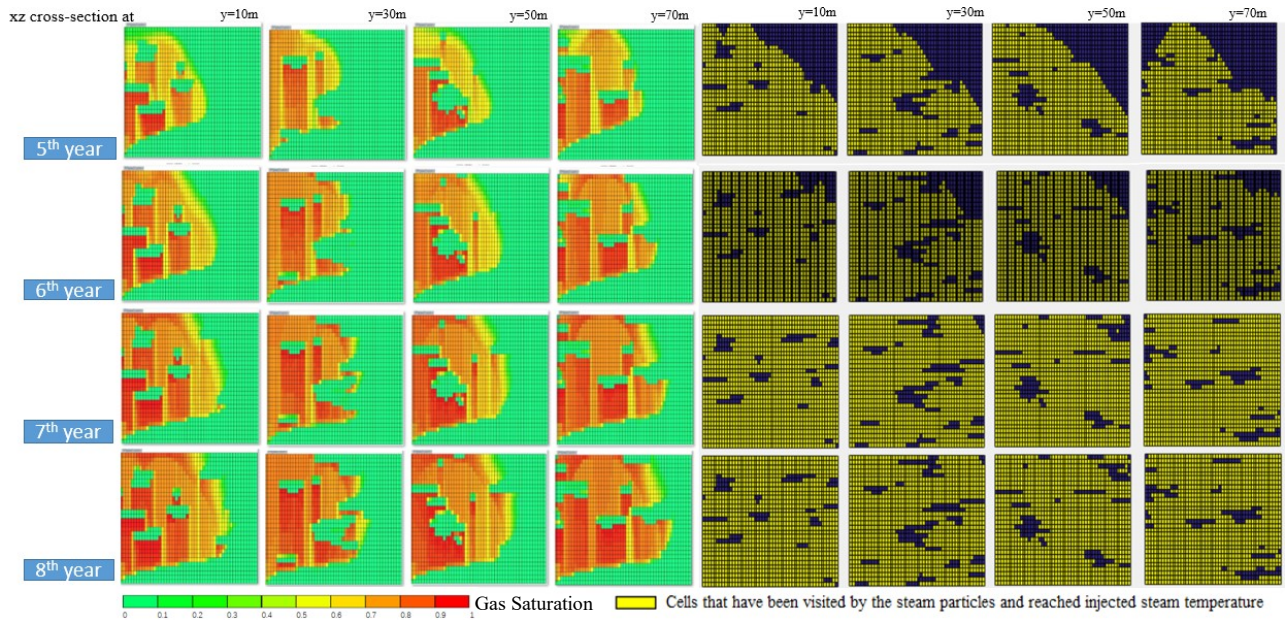
Figure 12-11. Steam chamber evolution over the 5th to 8th year corresponding to the heterogeneous model Case 20.
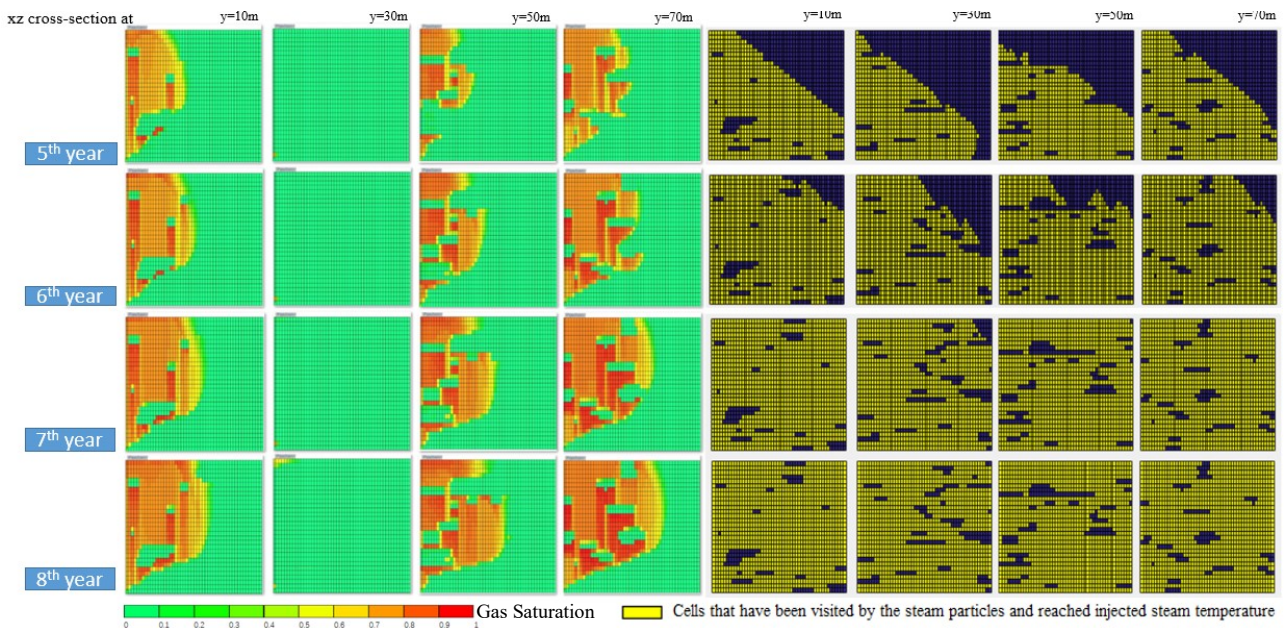
Figure 12-12. Steam chamber evolution over the 5th to 8th year corresponding to the heterogeneous model Case 24.
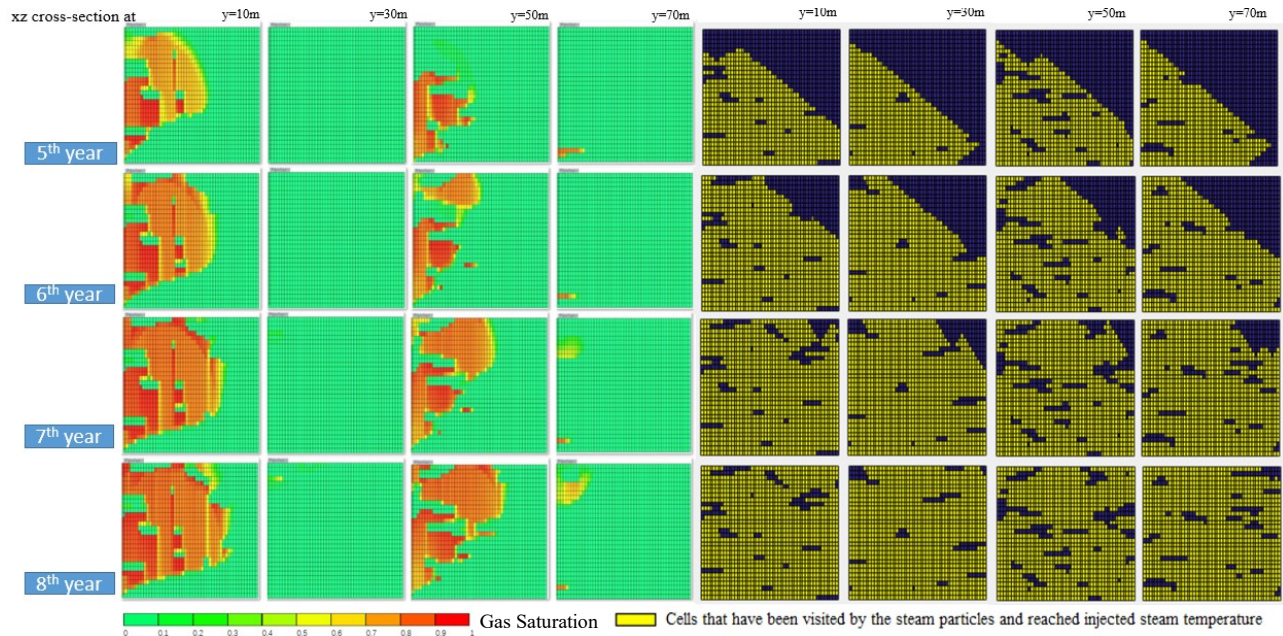
Figure 12-13. Steam chamber evolution over the 5ᵗʰ to 8ᵗʰ year corresponding to the heterogeneous model Case 37.
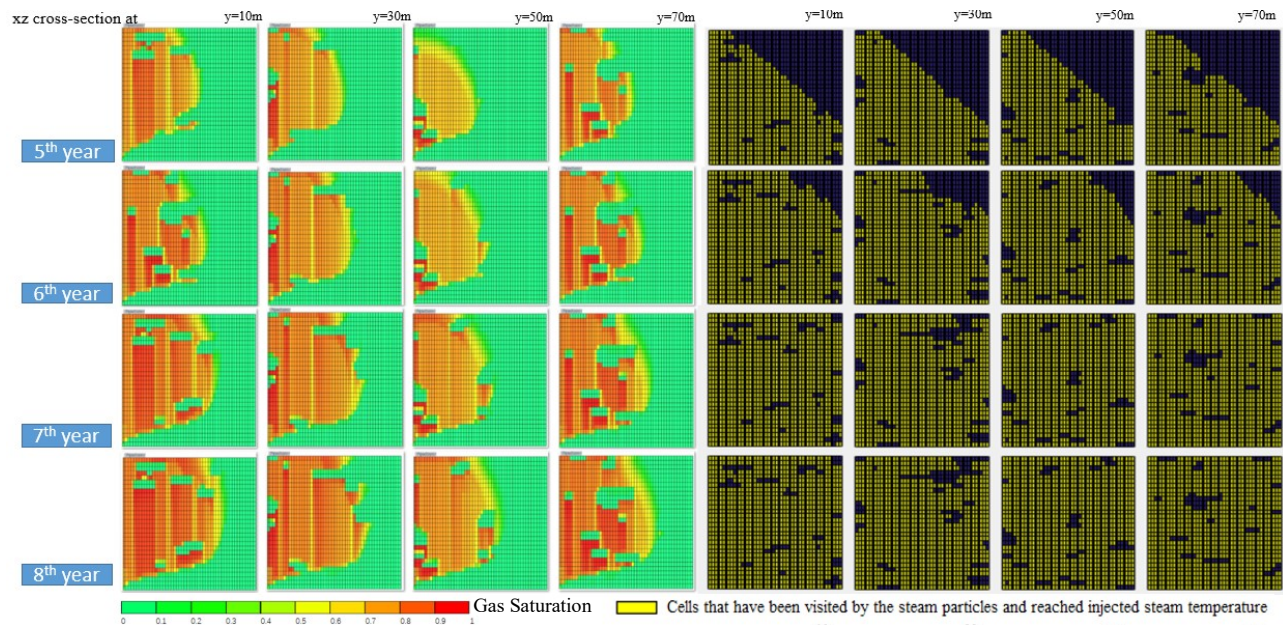
Figure 12-14. Steam chamber evolution over the 5ᵗʰ to 8ᵗʰ year corresponding to the heterogeneous model Case 39.
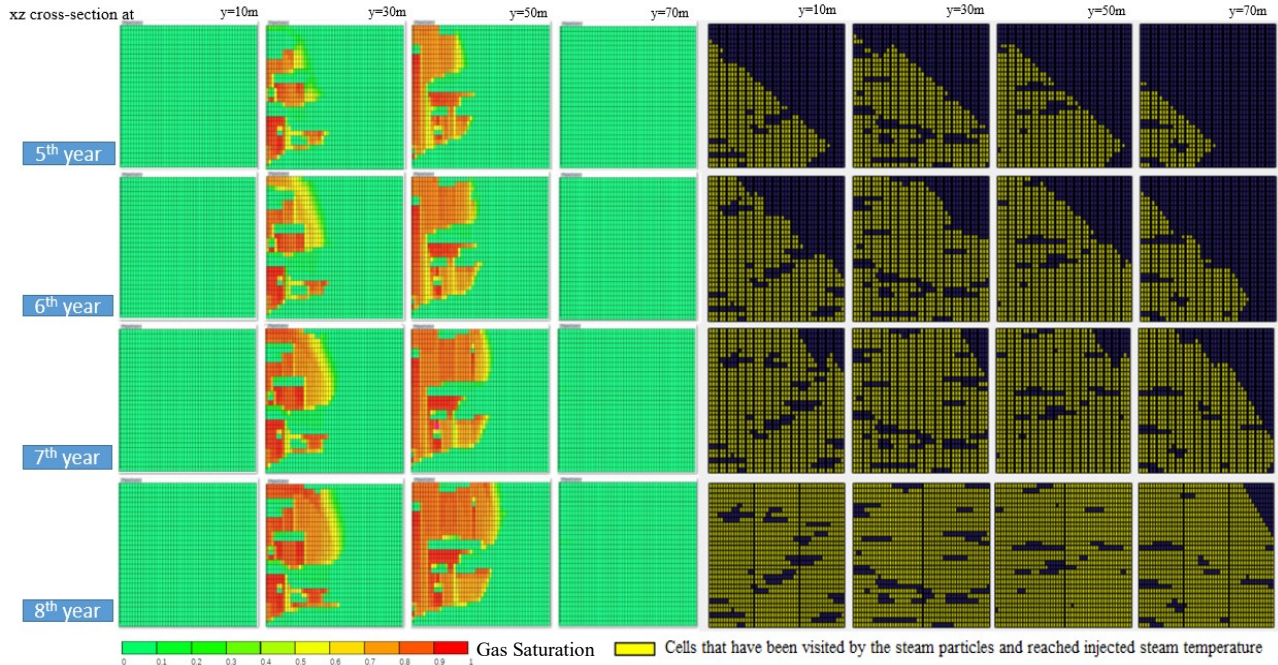
Figure 12-15. Steam chamber evolution over the 5th to 8th year corresponding to the heterogeneous model Case 43.
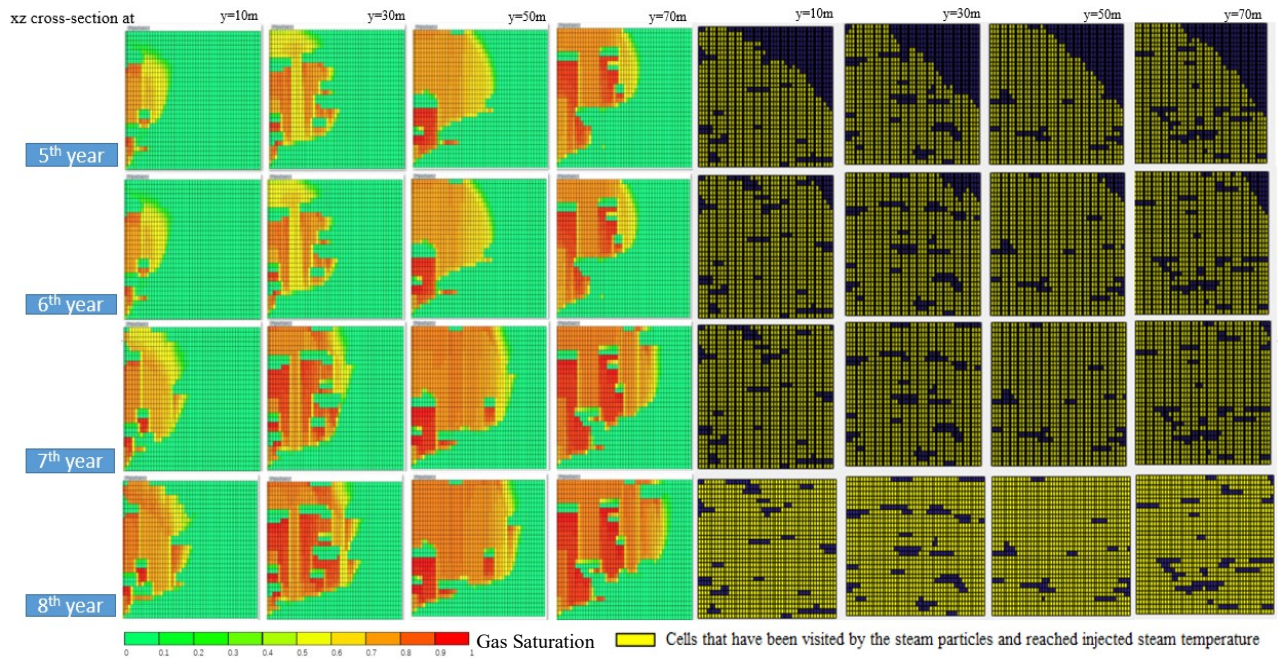
Figure 12-16. Steam chamber evolution over the 5th to 8th year corresponding to the heterogeneous model Case 49.

5.4 Detailed Examination of the Clustering Result obtained from detailed numerical simulations vs. Particle-Tracking Modeling

In this section, a more detailed examination of the clustering results is presented. The comparison between the particle-tracking and flow simulation results is shown in Figure 12-17. 91% of the cases in cluster 1 are predicted correctly using either the particle-tracking model or detailed numerical simulation. There is a small portion of the cases (9%) being identified as cluster 1 following the particle-tracking model, while corresponding to cluster 2 according to the detailed numerical simulation analysis. Similarly, for cluster 2, 80% of the cases in this cluster are correctly identified using either the particle-tracking or flow simulation analyses. The remaining 20% of the cases are misidentified as cluster 2 using the particle-tracking model, as they should belong to cluster 3 based on the detailed numerical simulation analysis. As explained in section 3.2, these misclassified cases often represent situations where there is limited connectivity between the well pair in one particular segment, and it is negatively impacting the chamber evolution; however, the steam particles may find a way to travel around the shale barriers at some point, resulting in little distortion in the final chamber profile, as predicted by the particle-tracking modeling. As for cluster 3, there is a perfect correspondence between the particle-tracking and flow simulation results. Therefore, it is concluded that the particle-tracking model is capable of capturing the key influences of shale barriers with respect to steam chamber development. Minor discrepancies are noted and deemed reasonable, considering that only simplified physics are involved. The particle-tracking simulation offers an efficient alternative to quantify the influences of shale barriers, facilitating the formulation of a flow-based distance measure that can be used to assess the (dis)similarity among different heterogeneous models.
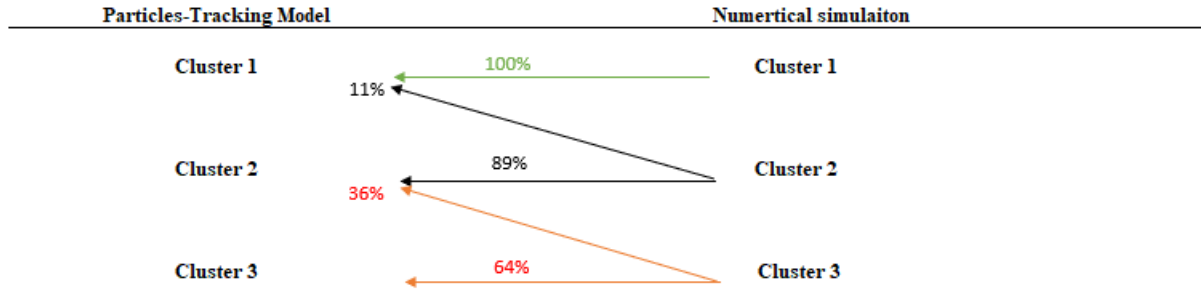
Particles-Tracking Model		Numertical simulaiton

Cluster 1 — little effect of shale barriers, good connectivity between the well ;
Cluster 2 — limited effect of shale barriers, limited connectivity between the well pair in some segments along the well length
Cluster 3 — most noticeable impacts of shale barriers, limited connectivity between the well pair in most segments along the well length

Figure 12-17. Comparison of the clustering results obtained from detailed numerical simulations vs. particle tracking modeling and the Hausdorff distance method, as well as the static quality calculation.

CHAPTER 6: Comparison of Clustering Results Corresponding to Different Distance Measures

In this chapter, four cases (cases 24, 37, 43 and 49) from model type 2 are selected to analyze the different heterogeneities captured by each distance measures method. Table 13-1 summarizes the clustering result for each selected case using detailed flow simulation, particle-tracking model, static quality measure and Hausdorff distance, respectively. Cases belong to cluster 1 are considered as good cases with little effect of shale barriers. Cases belong to cluster 2 are considered as medium cases with some effect of the shale barriers. Cases belong to cluster 3 are considered as bad cases with severe effect of shale barrier. Cases denoted in A/B/C are cases with different spatial distribution of shale barriers. Table 13-2 summarizes the shale barrier characteristics for the four selected cases. Table 13-3 summarizes the reservoir heterogeneities captured by each distance measures method. Figure 13-1 to Figure 13-5 presents the MDS and clustering results for the particle-tracking modeling, Hausdorff distance and statice quality calculation, compared with flow simulation, respectively. The four heterogeneous realizations are shown in Figure 13-6; and the steam chamber evolution profiles for these four cases over the 8 production years for detailed flow simulation and the particle-tracking model, as well as expected drainage volume estimate by the static quality within different window sizes, are presented in Figure 13-7 to Figure 13-10, respectively.

As shown in Figure 13-6 and Table 13-2, cases 24, 37, and 43 contain situation where there is presence of shale barriers in between the well pair which hinders the communication between well pairs, result limit/no steam injection in those locations, and locally limit the steam chamber development; whereas case 49 are scenarios with several shale barrier presents near the injector and one moderate sits right above the injector. All these cases are considered as either a medium or bad

case based on detailed flow simulation's clustering result. The clustering result based on the detailed flow simulation informs how many/in which portions of the well length the steam chamber can effectively expand far away from the well pair. As presented by Table 13-1 and Table 13-3, as well as Figure 13-1 to Figure 13-5, there are discrepancies among the four sets of clustering results. This is due to the physics implement in or formulation(s) use for each distance measures method is different.

As discussed in section 5.3, for the particle tracking method, due to the neglect of fluid movement, its clustering result is primarily based on the connectivity assessment during the preheating period. Additionally, due to the neglect of gravity effect, it is only able to inform any presence of medium/long shale barriers located in between the well pair. Thus, for cases with small shale barriers located in between the well pair (case 37) or for cases where there are many shales around the well(s) and/or with the presence of shale barriers located right next to the injection wells (case 49), the proposed particle tracking method cannot distinguish them separately from other cases. However, it is still able to capture most of the key influences of shale barriers with respect to steam chamber development.

For the static quality, as discussed in section 3.5.3, during the calculation, the injection well's position is not taken into account; and hence, the model is not able to inform the presence of shale barriers in between the well pair, and fails to capture the key impacts of shale barriers on the steam chamber development. However, since the local connectivity is evaluated during the static quality calculation, as shown in Figure 13-7 to Figure 13-10, this method is still capable to captures some minor influences of shale barriers on the oil production performance, such as the proportion and size/continuity of shale barriers in the near- well (producer) region.

Similarly, for Hausdorff distance, as discussed in section 3.5.4, the formulation mainly

focus on the spatial distribution of shale barriers, and does not incorporate the relative locations of shale barriers to either injection well or the production well; thus, this method also failed to capture the key impacts of shale barriers on the production performance. Additionally, since the steam chamber evolution highly sensitive to locations of certain shale barriers in relation to the well pair, this method is effective in capturing any impact of shale barriers on the dynamic evolution of a steam chamber.

Table 13-1. Summary of clustering results of the selected cases for the four models selected from base model type 2.

	Numerical Simulation	**Particle-Tracking Proxy Model**	**Static Quality Measure (Small Window Size)**	**Static Quality Measure (Large Window Size)**	**Hausdorff Distance Model**
Case 24	Cluster 2	Cluster 2	Cluster 3	Cluster 2	Cluster C
Case 37	Cluster 3	Cluster 2	Cluster 1	Cluster 1	Cluster A
Case 43	Cluster 3	Cluster 3	Cluster 3	Cluster 3	Cluster C
Case 49	Cluster 2	Cluster 1	Cluster 2	Cluster 2	Cluster A

Table 13-2. Summary of shale barrier characteristics for the four models selected from base model type 2.

	Small/ discontinuous shale barriers in between the well pair	Moderate shale barriers in between the well pair	Long/ continuous barriers in between the well pair	Shale barriers right next to a well (injector/ producer)	Many shale barriers in the near-well region	Extensive/ continuous shale barriers in the near-well region
Case 24	No	Yes	No	No	Yes	No
Case 37	Yes	Yes	No	No	No	No
Case 43	Yes	Yes	Yes	Yes	Yes	Yes
Case 49	No	No	No	Yes	Yes	No

Table 13-3. Summary of shale barrier characteristics captured by each model.

	Numerical Simulation	Particle-Tracking Proxy Model	Static Quality Measure (Small Window Size)	Static Quality Measure (Large Window Size)	Hausdorff Distance Model
Small/discontinuous shale barriers in between the well pair	Yes	No	No	No	No
Moderate shale barriers in between the well pair	Yes	Yes	No	No	No
Long/continuous barriers in between the well pair	Yes	Yes	No	No	No
Shale barriers right next to a well (injector/producer)	Yes	No	No	No	No
The proportion of shale barriers in the near-well region	Yes	No	Yes	Yes	No
Size/Volume of shale barriers in the near-well region	Yes	No	Yes	Yes	No
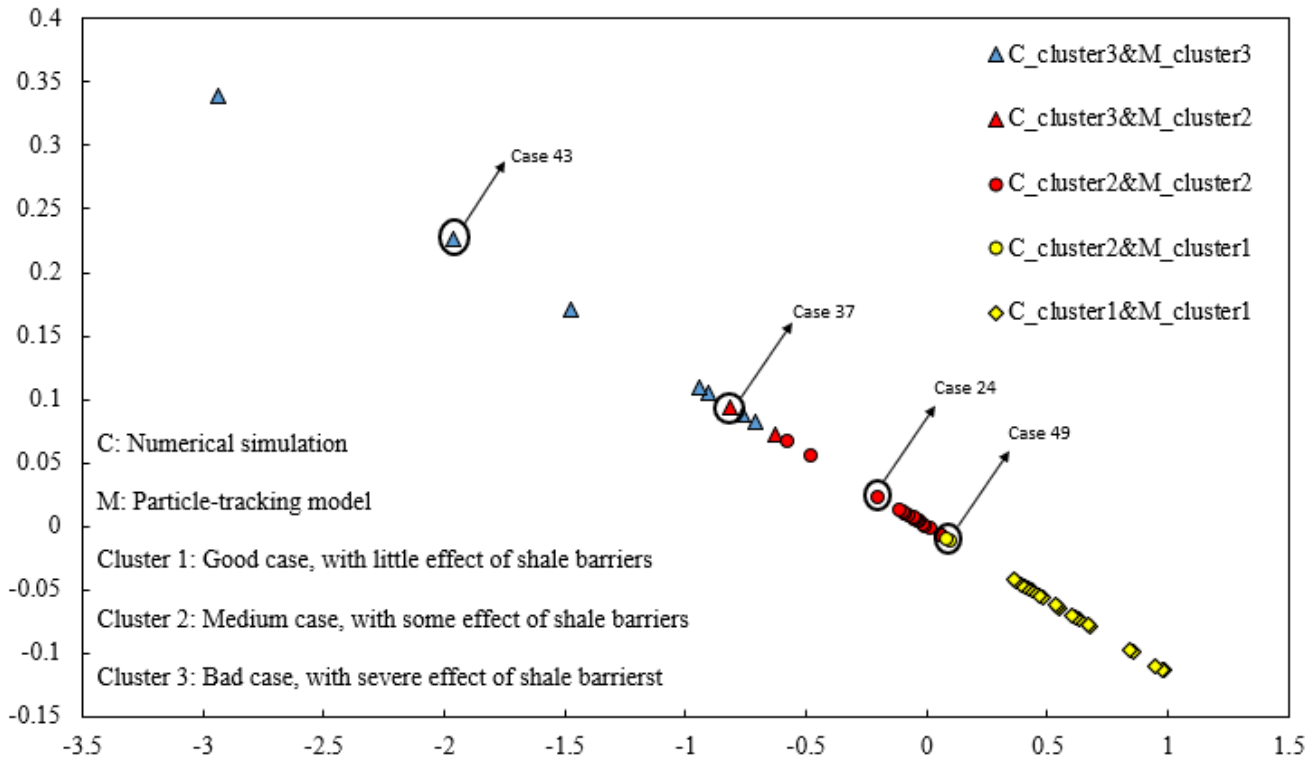
Figure 13-1. MDS and clustering results corresponding to the particle-tracking simulation for the production period – clustering results based on the flow simulations are compared, demonstrating a significant correlation between the two methods.
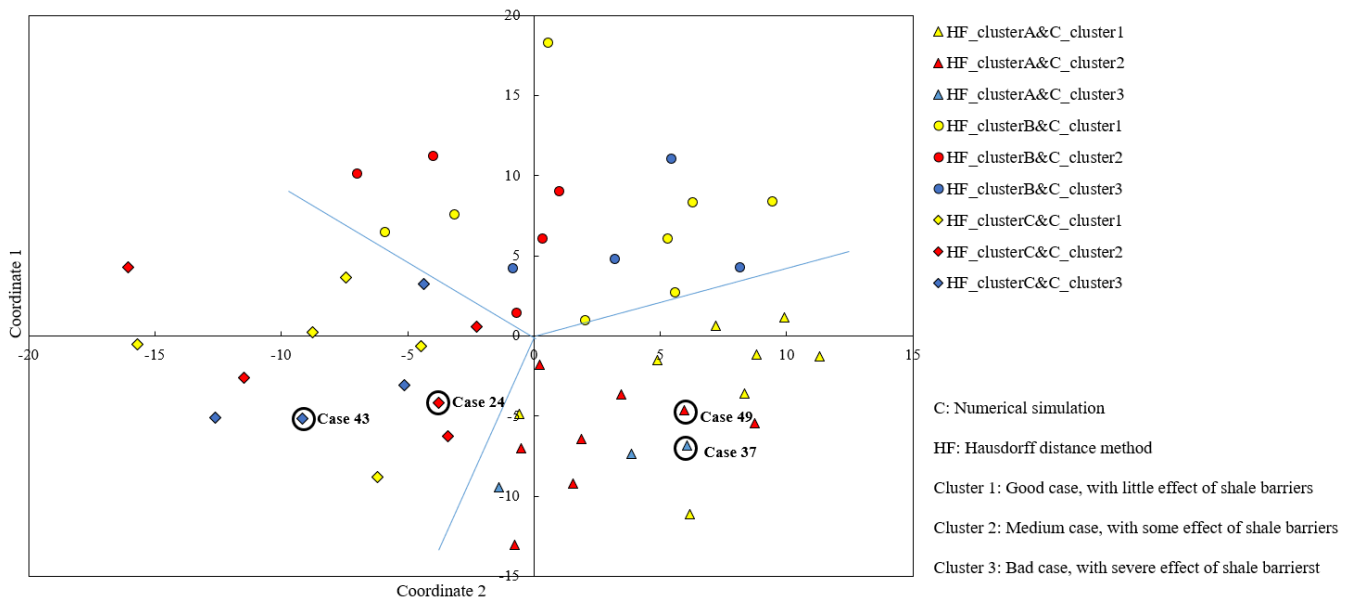
Figure 13-2. MDS and clustering results corresponding to the Hausdorff distance for base

model type 2 – clustering results for the flow simulations are compared; noticeable differences are noted comparing the two methods.
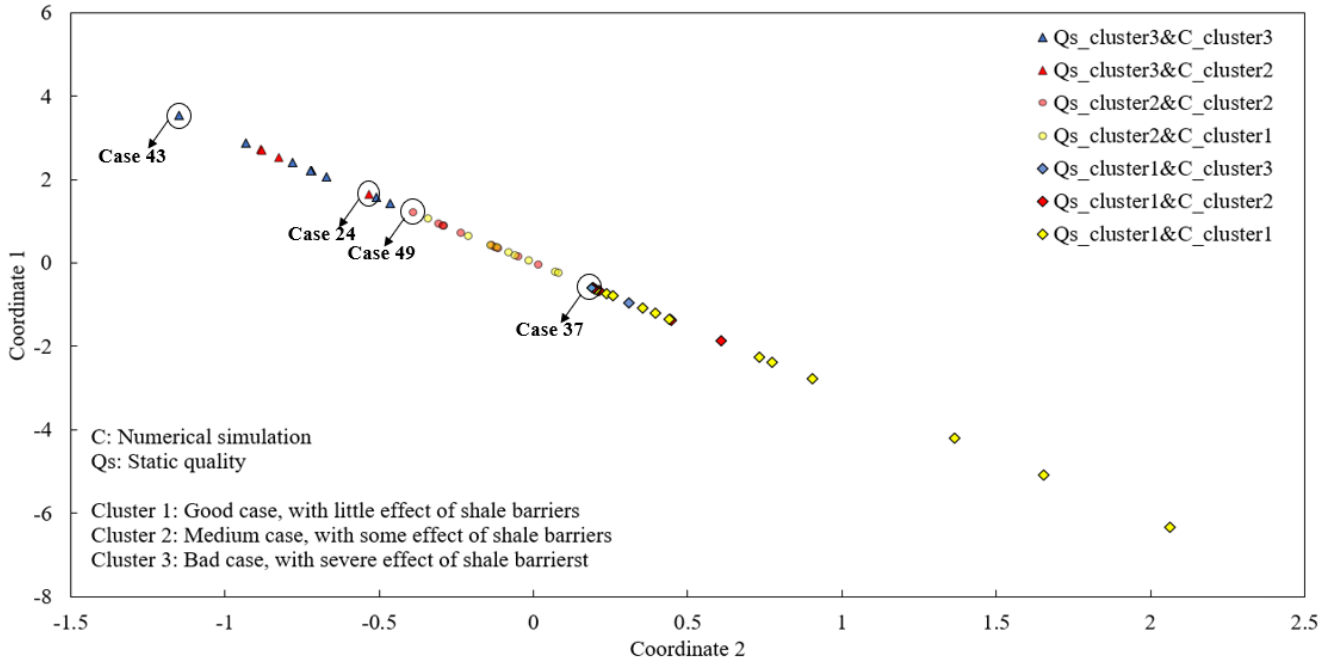
Figure 13-3. MDS and clustering results corresponding to the static quality (Qs) with a window size of 5m for base model type 2 – clustering results for the flow simulations are compared; noticeable differences are noted comparing the two methods.
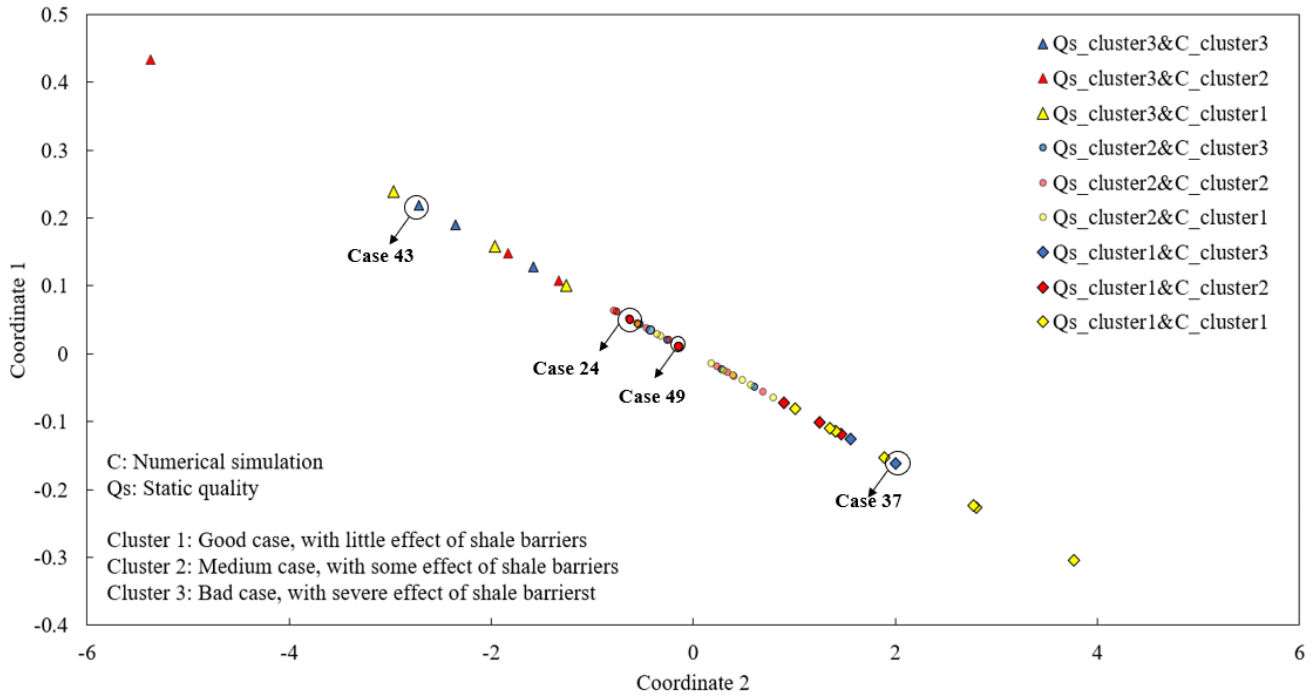
Figure 13-4. MDS and clustering results corresponding to the static quality (Qs) with a window size of 15m for base model type 2 – clustering results for the flow simulations are compared; noticeable differences are noted comparing the two methods.
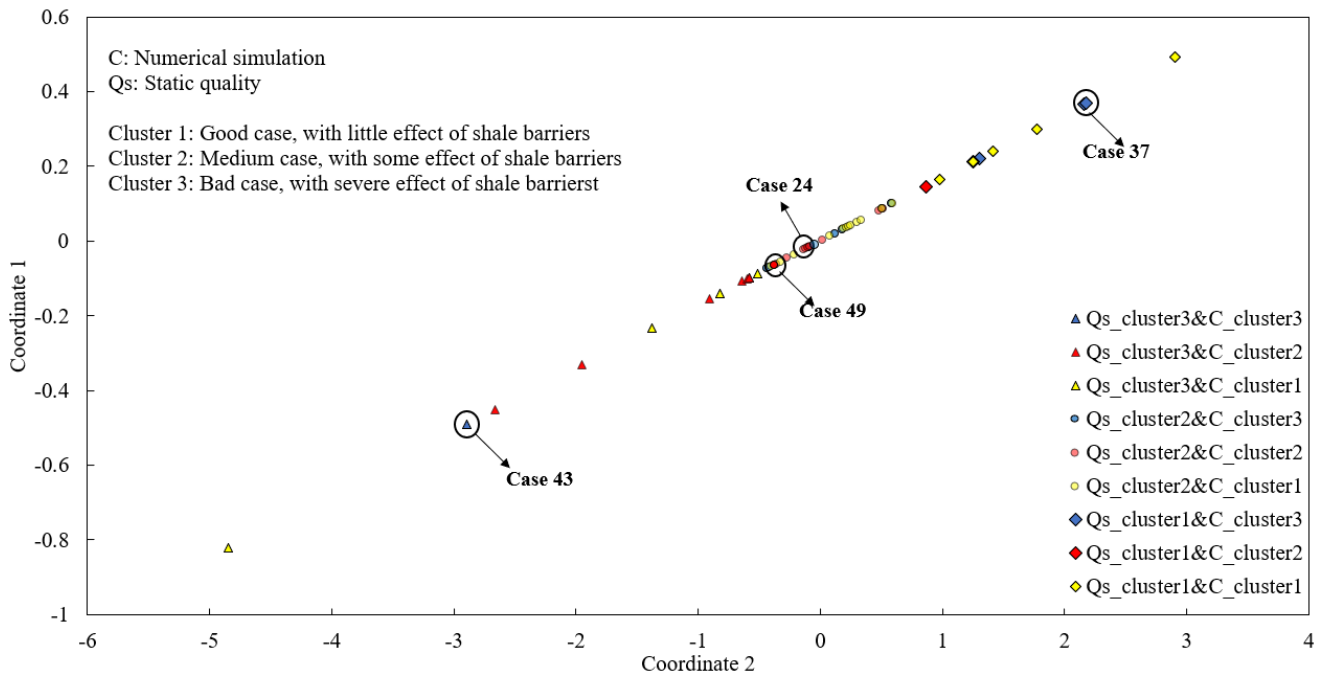
Figure 13-5. **MDS and clustering results corresponding to the static quality (Qs) with a window size of 25m for base model type 2 – clustering results for the flow simulations are compared; noticeable differences are noted comparing the two methods.**
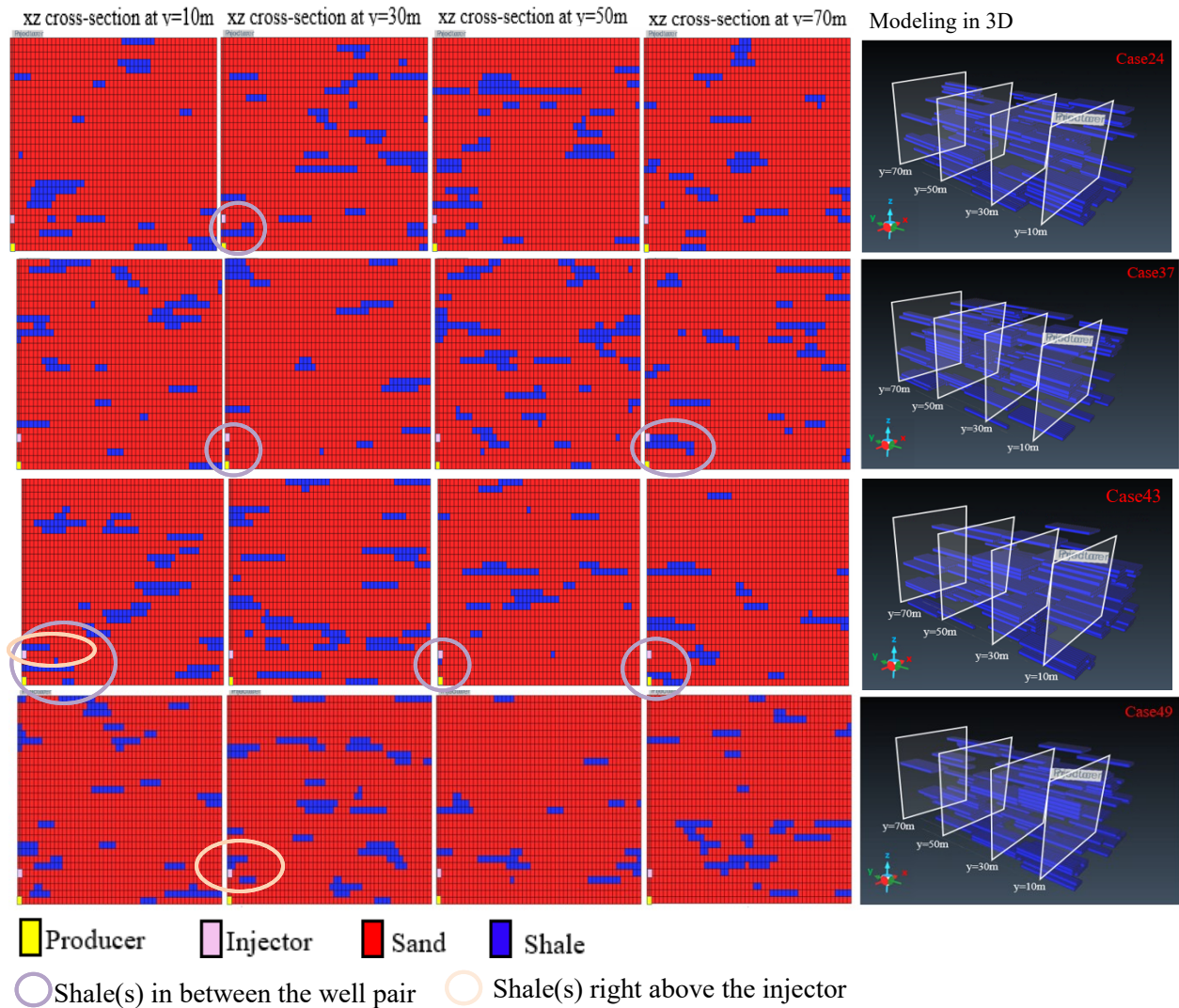
Figure 13-6. Four selected heterogeneous realizations: the first four columns correspond to the four segments along the *y*-axis, and the last column illustrates the shale barrier configuration in 3D.

xz cross-section at y=10m y=30m y=50m y=70m y=10m y=30m y=50m y=70m

Steam Chamber

Steam Chamber

1st year

2nd year

3rd year

4th year

xz cross-section at y=10m y=30m y=50m y=70m y=10m y=30m y=50m y=70m

5th year

6th year

7th year

8th year

Gas Saturation | 0 0.1 0.2 0.3 0.4 0.5 0.6 0.7 0.8 0.9 1

Cells that have been visited by the steam particles and reached injected steam temperature

Window size=5m

Window size=15m

Window size=25m

Locally connected cell
Non-net cell
Net cell
Net cell
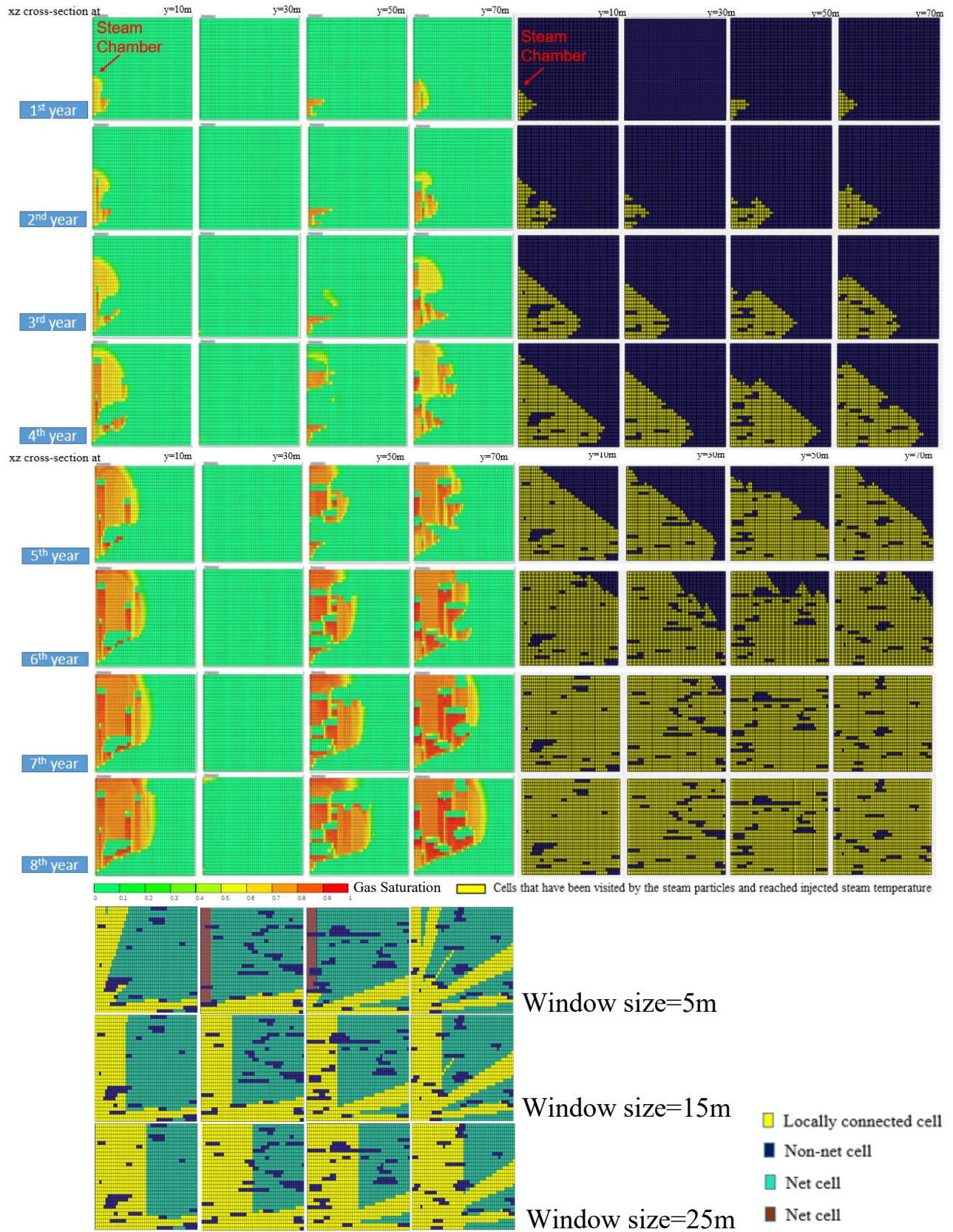
Figure 13-7. Steam chamber evolution over the initial 8-year period corresponding to the heterogeneous model Case 24 for detailed flow simulation and the particle-tracking model, as well as expected drainage volume estimate by the static quality.

xz cross-section at

y=10m y=30m y=50m y=70m y=10m y=30m y=50m y=70m

Steam Chamber

Steam Chamber

1st year

2nd year

3rd year

4th year

xz cross-section at

y=10m y=30m y=50m y=70m y=10m y=30m y=50m y=70m

5th year

6th year

7th year

8th year

Gas Saturation
0   0.1 0.2 0.3 0.4 0.5 0.6 0.7 0.8 0.9 1

Cells that have been visited by the steam particles and reached injected steam temperature

Window size=5m

Window size=15m

Window size=25m

Locally connected cell
Non-net cell
Net cell
Net cell

114
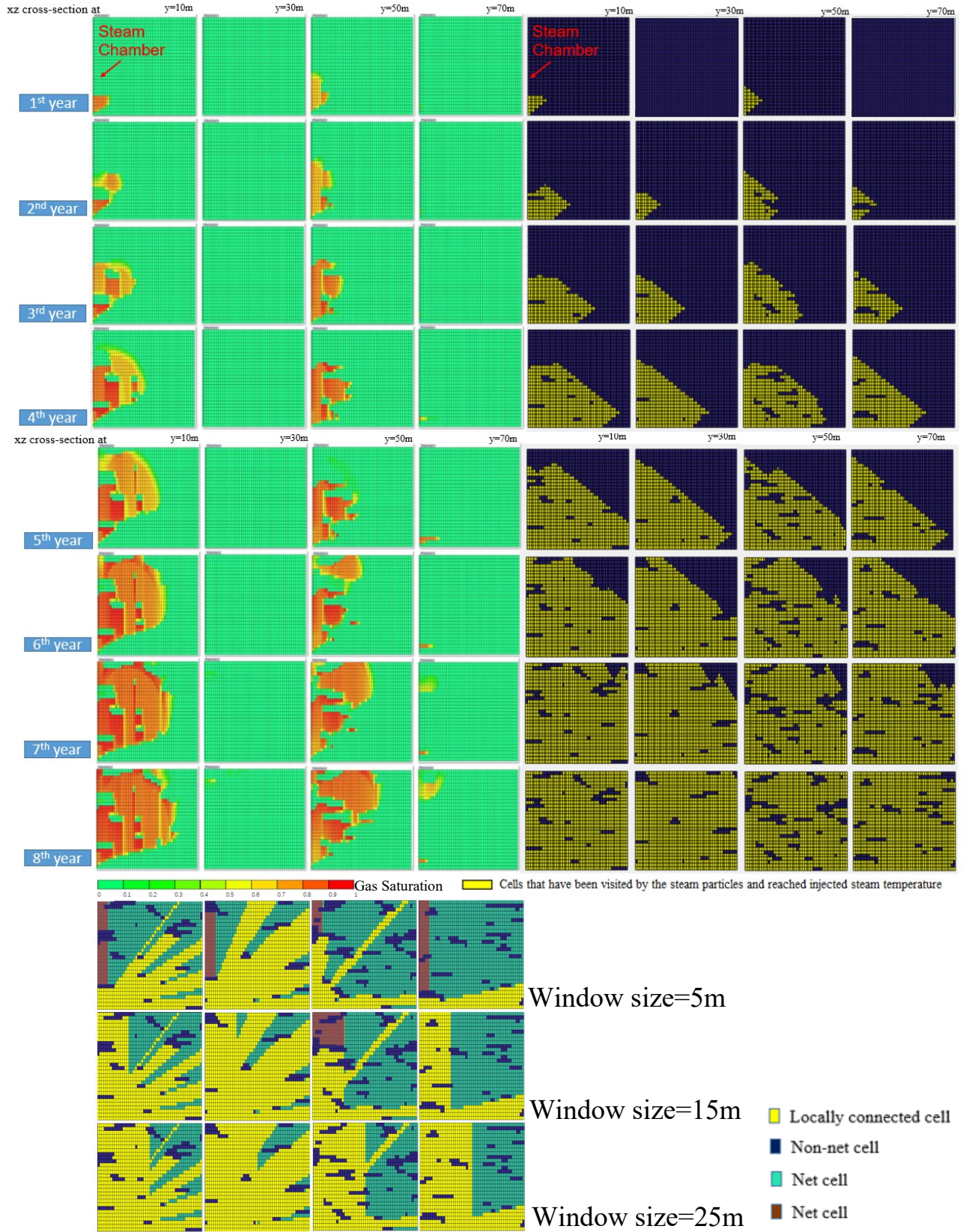
Figure 13-8. Steam chamber evolution over the initial 8-year period corresponding to the heterogeneous model Case 37 for detailed flow simulation and the particle-tracking model, as well as expected drainage volume estimate by the static quality.

xz cross-section at

| | y=10m | y=30m | y=50m | y=70m | | y=10m | y=30m | y=50m | y=70m |

Steam Chamber

Steam Chamber

1st year

2nd year

3rd year

4th year

xz cross-section at

| | y=10m | y=30m | y=50m | y=70m | | y=10m | y=30m | y=50m | y=70m |

5th year

6th year

7th year

8th year

Gas Saturation   Cells that have been visited by the steam particles and reached injected steam temperature

Window size=5m

Window size=15m

Window size=25m

Locally connected cell
Non-net cell
Net cell
Net cell
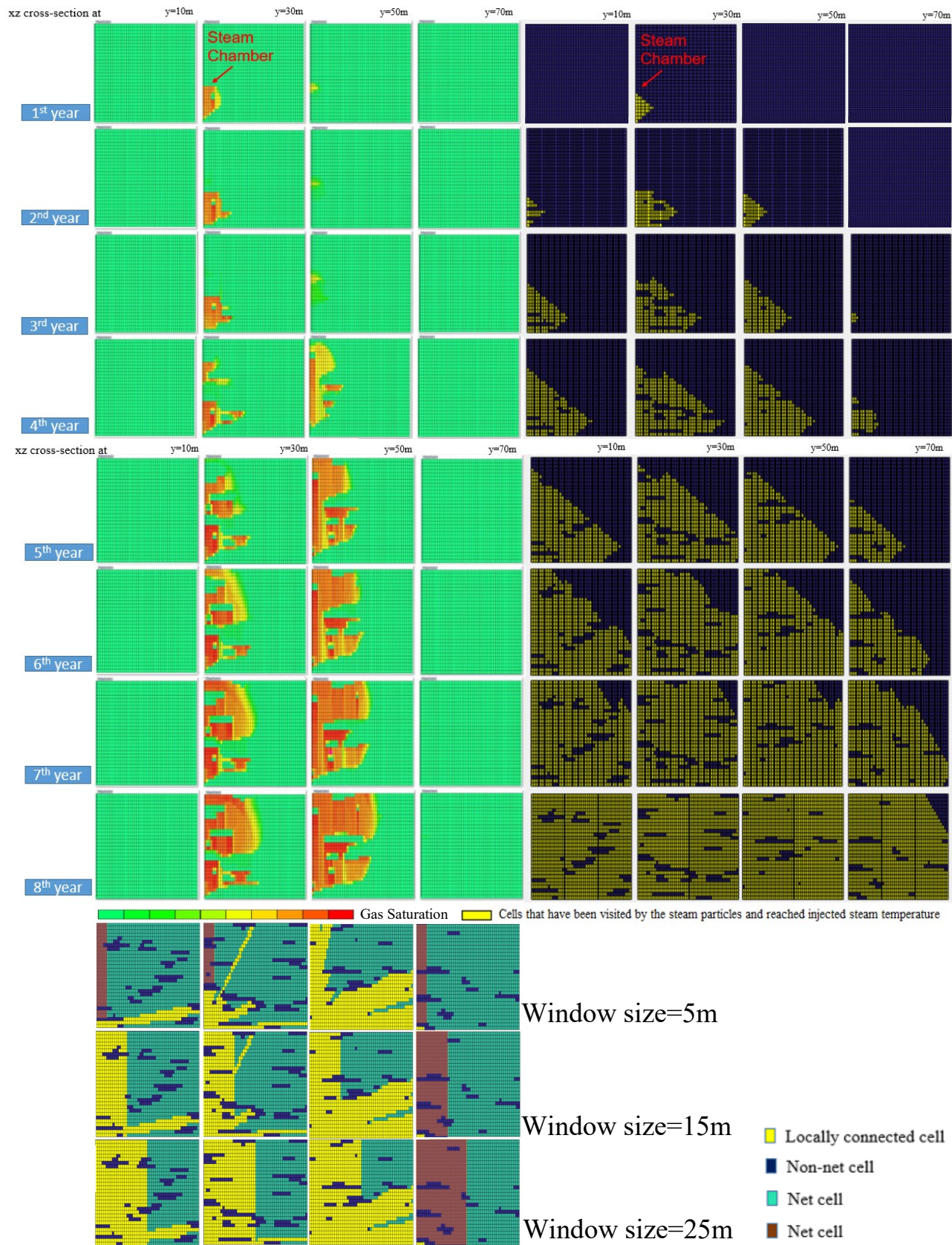
Figure 13-9. Steam chamber evolution over the initial 8-year period corresponding to the heterogeneous model Case 43 for detailed flow simulation and the particle-tracking model, as well as expected drainage volume estimate by the static quality.

Gas Saturation: 0 0.1 0.2 0.3 0.4 0.5 0.6 0.7 0.8 0.9

Cells that have been visited by the steam particles and reached injected steam temperature

Window size=5m

Window size=15m

Window size=25m

Locally connected cell
Non-net cell
Net cell
Net cell
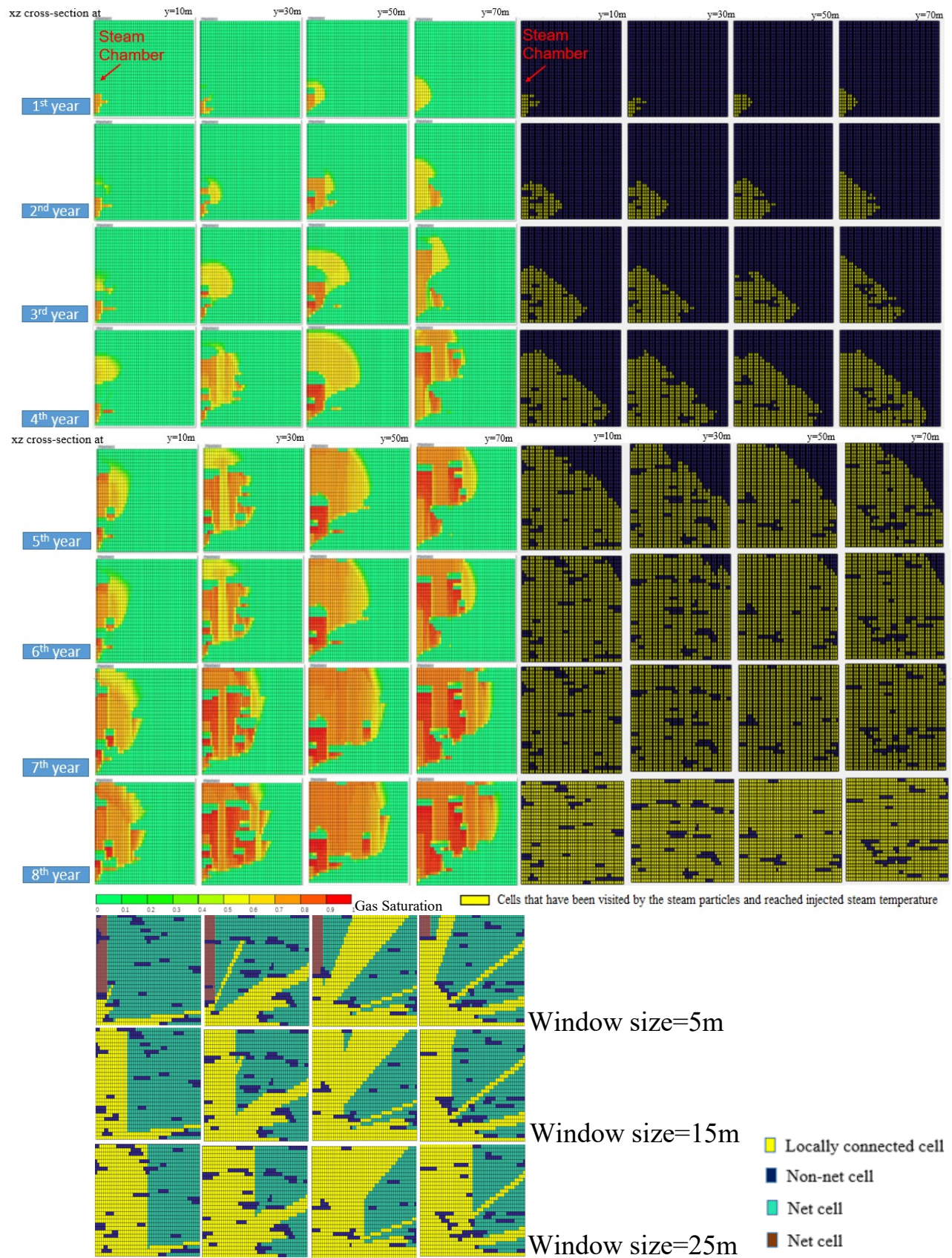
Figure 13-10. Steam chamber evolution over the initial 8-year period corresponding to the heterogeneous model Case 49 for detailed flow simulation and the particle-tracking model, as well as expected drainage volume estimate by the static quality.

CHAPTER 7: CONCLUDING REMARKS

7.1   Summary and Conclusions

A workflow is developed to fast screen through a large set of realizations and categorize these reservoir models into different groups in accordance with their spatial properties or other forms which reflect the production response of a SAGD recovery process. This workflow can be utilized as a preprocessing tool for assembling training data sets for many data-driven proxy analyses. A suite of 3D models is constructed using representative petrophysical properties and operating constraints extracted from several pads in Suncor's Firebag project.

The distance measures are used to partition the models into different groups. The static quality is utilized to estimate the potential recoverable volume of a SAGD reservoir. Due to the neglection of the injector's position, this method is incapable to capture the key influence of shale barriers with respect to the steam chamber evolution and the oil production performance, However, since the calculation incorporates the relative location of shale barriers to the production well, static quality is able to inform some minor influence of shale barriers to the production performance, such as the proportion and size/volume of shale barriers in the near-well region, as well as the relative distance of a shale barrier to the producer. The Hausdorff distance is also utilized to provide a static distance measure, but its effectiveness cannot be demonstrated. Two particular drawbacks are noted. First, all objects, irrespective of their locations relative to the well pair, are weighted equally. Second, salient features of the underlying physical mechanisms are ignored.

In order to demonstrate the key influence associated with the dynamic evolution of a steam chamber, a novel physics-based particle-tracking proxy is introduced. This simple dynamic flow simulation incorporating the energy balance and Darcy's law is developed to simulate the

dynamic SAGD chamber evolution. Steam particles are released into the formation and their locations are tracked. The time series of volume chamber size is calculated.

With the proposed simplified flow model based on the particle-tracking algorithm, the proposed workflow for investigating the effect of shale barrier configurations on the SAGD production behavior is optimal. The workflow consists of 3 steps. First, quantify the (dis)similarity between any two synthetic reservoir model by applying the proposed particle-tracking proxy. Next, identify internal clusters among the reservoir models using MDS and K-mean clustering analysis. Last, subject these models to detailed numerical flow simulators to predict the actual chamber evolution and the production profiles.

The particle-tracking results correspond reasonably well with those obtained from detailed flow simulation, particularly during the early time. Some minor discrepancies are noted, as connectivity issues due to insufficient drainage cannot be fully captured by the particle-tracking technique, since fluid flows and gravity effects are not explicitly modeled. What is more, the particle-tracking method is much more computationally efficient (80× speed up), in comparison to detailed 3D flow simulation. Thus, it can be used to efficiently rank or screen a large number of heterogeneous models.

A case study is conducted for all four simulations: detailed numerical flow simulation, the proposed particle-tracking model, Hausdorff distance, and static quality calculation. Only the clustering results according to the proposed flow-based distance measures match reasonably well to those obtained from detailed flow simulations. The developed particle-tracking method can facilitate the efficient screening of multiple heterogeneity realizations and the categorization of these models into different groups in accordance with their steam chamber development and shale barrier characteristics. On the other hand, clustering results from both static measures again

confirm that flow-based proxy and distance measures are often needed to capture the essential features associated with the underlying physical mechanisms.

7.2   Contributions

The main contributions are summarized as follows:

(1) Steam-assisted gravity drainage (SAGD) process is strongly impacted by the distributions of shale heterogeneities, which tend to impede the development of a steam chamber and potentially reduce oil production. Detailed compositional flow simulators are often employed to assess the impacts of reservoir heterogeneities on the steam chamber growth and to forecast production. To reduce the computational costs, machine learning techniques have been widely proposed in recent studies to develop various data-driven models. In all cases, a training data set consisting of many (>1000) synthetic simulation cases are required to achieve reasonable accuracy, especially in the case of 3D models. A suitable training data set should be large enough to sufficiently span the parameter space without exhaustively sampling cases with similar production characteristics. A novel physics-based proxy is proposed to approximate key SAGD production features in heterogeneous reservoirs

(2) The proposed model can help better understand the impacts of heterogeneity during the SAGD recovery process. The simulation results reveal that shale barriers that are located in the near well region would have a more pronounced impact, especially the ones located in between the well pair. Additionally, increasing the number and/or size of the shale barriers in the near-well region may delay the steam chamber development.

(3) The proposed model also presents a significant potential to be integrated with other data-driven

approaches or workflows for rank/screen a large number of heterogeneous models, due to its run time is much less than the conventional simulations. What is more, it significantly reduces the computational load typically associated with detailed flow simulations involving multiple heterogeneous reservoir realizations.

(4) Another challenge is to quantify the (dis)similarities among a large set of (>1000) realizations with various shale barriers configuration, particularly if 3D models are involved. In this work, a workflow is proposed to visualize/screen a large number of heterogeneity realizations and categorization into different groups in accordance with their steam chamber development behavior and shale barrier characteristics (proportions and positions of shale barriers in the near-well region). This workflow illustrates a framework for optimizing a training data set by systematically adding/removing realizations, with the intent of maximizing the spanning of the model parameter space and without exhaustively sampling similar realizations.

(5) The proposed workflow can be used to efficiently screen a large number of reservoir models and facilitate the classification of these models into groups with distinct shale heterogeneity characteristics; so that, instead of running a large set of unknown clustering cases, we can now pick certain number realizations from a certain group to do a detail simulation. Thus, it can be applied as a pre-processing tool to construct a training data set with less redundancy for data-driven proxy.

7.3 Limitations and Recommendations

(1) In this work, only two specific rock types, sands and shale, are considered. Although it is capable to represent the characteristics of shale barriers, for future work, the reservoir model should incorporate more rock types. Additionally, the spatial correlation of the shale

configurations is not taken into account. In future studies, it is recommended to include the spatial correlation, such as variogram, and other conditioning information as constructing the synthetic models.

(2) For the synthetic models employed in this study, in consideration of the trade-off between the model resolution and problem complexity, only 80 m along the *y*-direction and 50 m along *x*-direction are modeled. Although, according to horizontal GR logs, the continuity of a shale barrier is generally within this range, a larger reservoir dimension could be taken into consideration in the future study.

(3) In this study, for the proposed workflow, multiple static distance measures (Hausdorff distance, static quality (Qs) –the preliminary formulation is the connected hydrocarbon volume (CHV)) and dynamic flow simulations (proposed particle-tracking proxy, detailed numerical flow simulator) have been successfully implemented for the purpose of classification. There are more other distance measures, such as tracer measures and streamline simulations, are available, but they are not utilized in this study. Similarly, for the clustering purpose of this workflow, beside the K-mean clustering analysis, other clustering techniques, such as Kernel transformation, principal component analysis, can also be applied. In future studies, other options could be investigated to further optimize the workflow.

BIBLIOGRAPHY

Akin, S. (2005). Mathematical modeling of steam assisted gravity drainage. *SPE Reservoir Evaluation & Engineering*, *8*(05), 372-376

Alpak, F.O., Barton, M.D. & Caers, J., (2010). A flow-based pattern recognition algorithm for rapid quantification of geologic uncertainty. *Computational Geosciences*. **14**(4), 603-621. https://doi.org/10.1007/s10596-009-9175-5.

Amirian, E., Leung, J. Y., Zanon, S., D., J., & Dzurman, P., J., (2014). Integrated cluster analysis and artificial neural network modeling for steam-assisted gravity drainage performance prediction in heterogeneous reservoirs. *Expert Systems with Applications.*

Arpat, G. B., (2005). Sequential simulation with patterns. PhD dissertation, Stanford University, USA, 166p.

Ates, H., Bagar, A., and Mohsen, S., 2003. Ranking and Upscaling of Geostatistical Reservoir Models Using Streamline Simulation, *Society of Petroleum Engineers (SPE)*, Paper 81497.

Bagci, A., S., (2006). Experimental and simulation studies of SAGD process in fracture reservoirs. Paper presented at the SPE/DOE symposium on improved oil recovery, Tulsa, Okalahoma, USA.

Birrel G. E., & Putnam P. E. (2000). A study of the influence of reservoir architecture on SAGD steam chamber development at the Underground Test Facility, northeaster Alberta, Canada, using a graphical analysis of temperature profiles. Paper presented at the *Petroleum Society's Canadian International Petroleum Conference*, Calgary, AB, Canada.

Borg, I., & Groenen, P. J., (2005). Modern multidimensional scaling: *Theory and applications* (second edition). Springer Science & Business Media, New York, USA.

Bresenham, J., (1987). Ambiguities in incremental line rastering. *IEEE Computer Graphics and Applications*. **7**(5), 31-43.

Butler, R., McNab, G., & Lo, H. (1981). Theoretical studies on the gravity drainage of heavy oil during in-situ steam heating. *The Canadian Journal of Chemical Engineering*. **59** (4), 445-460.

Butler, R. M. (1985). A new approach to the modelling of steam-assisted gravity drainage. *Journal of Canadian Petroleum Technology*, *24*(03), 42-51.

Butler, R., McNab, G., (2004). The behavior of non-condensable gas in SAGD-A realization. *Journal of Canadian Petroleum Technology*. **43** (1), 28-34.

Chen, Q., Gerritsen, M., G., & Kovscek, A., R., (2008). Effects of reservoir heterogeneities on the steam-assisted gravity-drainage process. *SPE Reservoir Evaluation & Engineering*. **11**(05). 921-932.

CMG, 2019. STARS: Users' Guide, advanced processes & thermal reservoir simulator (Version 2019), Calgary, Alberta, Canada: Computer Modeling Group Ltd.

Cox, T. F., & Cox, M. A. (2001). Multidimensional scaling (second edition). Chapman and Hall, London, UK.

Edmunds N.R. (1998). Investigation of SAGD steam trap control in two and three dimensions. Paper presented at the SPE International Conference on Horizontal Well Technology, Calgary, Canada.

Deutsch, C.V. & Srinivasan, S., (1996). Improved Reservoir Management through Ranking Reservoir Models, *Society of Petroleum Engineers (SPE)*, Paper 35411.

Fenik D. R., Nouri A., & Deutsh C.V., (2009). Criteria for ranking realizations in the investigation of SAGD reservoir performance. Paper presented at SPE Canadian International Petroleum Conference (CIPC), Calgary, Canada.

Gao, C., Ma, Z., & Leung, J.Y. (2018). A novel particle-tracking based proxy for capturing SAGD production features under reservoir heterogeneity, Paper presented at SPE Western Regional Meeting, San Jose, California, USA.

Gao, C., & Leung, J.Y. (2020). Techniques for fast screening of 3D heterogeneous shale barrier configurations and their impacts on SAGD production behavior, Paper presented at SPE Canada Heavy Oil Technical Conference, Calgary, AB, Canada.

Gilman, J., Meng, H., Uland, M., Dzurman, P., & Cosic, S., 2005. Statistical Ranking of Stochastic Geomodels Using Streamline Simulation: A Field Application, *Society of Petroleum Engineers (SPE)*, Paper 77374.

Hausdorff, F., (1914) Grundzuge der Mengenlehre. Am Math Soc.

Honarkhah, M., & Caers, J. (2010). Stochastic simulation of patterns using distance-based pattern modeling. *Mathematical Geosciences*, **42**(5), 487-517. https://doi.org/10.1007/s11004-010-9276-7.

Idrobo, E.A., et al, 2000. Swept Volume Calculations and Ranking of Geostatistical Reservoir Models Using Streamline Simulation, *Society of Petroleum Engineers (SPE)*, Paper 62557.

Kisman K. E., & Yeung K. C. (1995). Numerical study of the SAGD process in the Burnt Lake Oil Sands Lease. Paper presented at the *SPE International Heavy Oil Symposium*, Calgary, AB, Canada

Laurel, D.K., Hovadik, J.M., 2006. Connectivity of Channelized reservoirs: a modelling approach. *Pet. Geol*. **12**(4), 291–308, http://dx.doi.org/10.1144/ 1354-079306-699

Le Borgne, T., Bolster, D., Dentz, M., de Anna, P., & Tartakovsky, A., (2011). Effective pore-scale dispersion upscaling with a correlated continuous time random walk approach. *Water Resources Research*. **47** (12), W12538.

Le Ravalec, M., Morlot, C., Marmier, R., & Foulon, D. (2009). Heterogeneity impact on SAGD process performance in mobile heavy oil reservoir. *Oil & Gas Science and Technology – Rev. IFP*, *64* (4), 469-476.

Lee, H., Jin, J., Shin, H., & Choe, J. (2015). Efficient Prediction of SAGD Productions Using Static Factor Clustering. *Journal of Energy Resources Technology*, *137*(3), 032907.

Lee, K., Lim, J., Choe, J., & Lee, H. S., (2017). Regeneration of channelized reservoirs using history-matched facies-probability map without inverse scheme. *Journal of Petroleum Science and Engineering*, **149**, 340-350. https://doi.org/10.1016/j.petrol.2016.10.046

Li, S. L., Deutsch, C. V., & Si, J. H., (2012). Ranking geostatistical reservoir models with modified connected hydrocarbon volume. Paper presented in Ninth International Geostatistics Congress, Oslo, Norway.

Ma, Z., Leung, J. Y., Zanon, S., & Dzurman, P. (2015a). Practical implementation of knowledge-based approaches for steam-assisted gravity drainage production analysis. *Expert System with Applications.* **42** (21). 7326-7343.

Mccarthy, J.F., 1993. Reservoir Characterization: Efficient Random-Walk Methods for Upscaling and Image Selection, *Society of Petroleum Engineers (SPE)*, Paper 25334.

McLennan, J. A., & Deutsch, U., (2005). Ranking geostatistical realizations by measures of connectivity. *Society of Petroleum Engineers (SPE).* Paper 98168. Presented at the 2005 SPE International Thermal and Operations and Heavy Oil Symposium, 1-3 November 2005, Calgary, Alberta, Canada.

McKenna, S.A., Akhriev, A., & Echeverría Ciaurri, D. et al., (2019). Efficient uncertainty quantification of reservoir properties for parameter estimation and production forecasting. *Mathematical Geosciences*. https://doi.org/10.1007/s11004-019-09810-y.

National Energy Board. (2006). Canada's oil sand: opportunities and challenges to 2015: an energy market assessment. *National Energy Board.* **35** (32).

Niu, H., Li, Z., Lee, K., & Kepkay, P. (2011). Modeling the transport of oil-mineral-aggregate (OMAs) in the marine environment and assessment of their potential risks. Environmental Modeling & Assessment. **16** (1), 61-75.

Ochi, J., & Vernoux, J. F. (1999). A two dimensional network model to simulate permeability decrease under hydrodynamic effect of particle release and capture. *Transport in porous media*. **37** (3), 303-325.

Park, K., & Caers, J. (2007). History Matching in Low-Dimensional Connectivity Vector Space. Paper presented in EAGE Petroleum Geostatistics 2007 Conference, Cascais, Portugal.

Pooladi-Darvish, M., & Ali, S. M. (1994). Steam heating of fractured formations containing heavy oil: basic premises and a single-block analytical model. Paper presented at the *SPE Annual Technical Conference and Exhibition*, New Orleans, LA, USA.

Reis, J. C. (1992). A steam-assisted gravity drainage model for tar sands: linear geometry. *Journal of Canadian Petroleum Technology*, *31*(10), 14-20.

Rose, P. E. (1993). *The steam-assisted gravity drainage of oil sand bitumen*. Doctoral dissertation, The University of Utah, USA.

Saad, Y., (1996). Iterative methods for sparse linear system (first edition). Society for Industrial and Applied Mathematics.

Saad, N., & Maroongroge, V. (1996). Ranking Geostatistical Using Tracer Production Data, *Society of Petroleum Engineers (SPE)*, Paper 35494

Sharma, J., & Gates, I. D. (2010). Multiphase flow at the edge of a steam chamber. *The Canadian Journal of Chemical Engineering*, *88*(3), 312-321.

Scheidt, C., & Caers, J. (2009). Representing spatial uncertainty using distances and kernels. *Mathematical Geosciences*, **41**(4), 397-419. https://doi.org/10.1007/s11004-008-9186-0

SGeMs, (2009). Applied Geostatistics with SGeMS: A User's Guide. Cambridge: Cambridge University Press. doi:10.1017/CBO9781139150019

Shin, H., & Polikar, M. (2006). Experimental investigation of the Fast-SAGD process. Paper presented at the Petroleum Society's 7th Canadian International Petroleum Conference, Calgary, Canada.

Siqueira, A. G., Bonet, E. J., & Shecaira, F. S. (2003). A 3D network model of rock permeability impairment due to suspended particles in injection water. Paper presented at 2003 SPE European Formation Damage Conference, Hague, Netherlands.

Srinivasan, S., & Deutsch, C.V., (1996a). Improved Reservoir Management Through Ranking Stochastic Reservoir Models. SPE Paper 35411 presented at the SPE/DOE Tenth Symposium on Improved Oil Recovery, Tulsa, OK., USA.

Srinivasan, S., Deutsch, C.V., & Mo., Y., (1996b) "Geostatistical Reservoir Modeling Accounting for the Scale and Precision of Seismic Data", SPE Paper 36497 prepared for the 1996 SPE Annual Technical Conference and Exhibition held in Denver, Colorado, USA

Srinivasan, G., Tartakovsky, D. M., Dentz, M., Viswanathan, H., Berkowitz, B., & Robinson, B.A. (2010). Random walk particle tracking simulations of non-Fickian transport in heterogeneous media. *Journal of Computational Physics*. **229** (11), 4304-4314.

Suzuki, S., & Caers, J., (2006). History matching with an uncertain geological scenario. Paper presented at the 2006 SPE Annual Technical Conference and Exhibition, San Antonio, Texas, USA.

Suzuki, S., & Caers, J. (2008). A distance-based prior model parameterization for constraining solutions of spatial inverse problems. *Mathematical Geosciences*, *40*(4), 445-469.

Suzuki, S., & Caers, J. (2008). A distance-based prior model parameterization for constraining solutions of spatial inverse problems. Mathematical Geosciences, **40**(4), 445-469. https://doi.org/10.1007/s11004-008-9154-8

Tang, H., & Liu, N. (2008). Static connectivity and heterogeneity (sch) analysis and dynamic uncertainty estimation. Paper presented at 2008 International Petroleum Technology Conference, Kuala Lumpur, Malaysia.

Tavakoli, R., Srinivasan, S., & Wheeler, M. F. (2014). Rapid updating of stochastic models by use of an ensemble-filter approach. SPE Journal, **19**(03), 500-513.

The MathWorks. (2019b). MATLAB User's Guide. The MathWorks, Inc., Natick, MA.

Vishal, V. and Leung, J.Y. (2015). Modeling impacts of subscale heterogeneities on dispersive solute transport in subsurface systems. Journal of Contaminant Hydrology **182**, 63-77.

Vishal, V., Leung, J.Y. (2017). Statistical framework for scale-up of dispersivity in multi-scale heterogeneous media. Environmental Earth Sciences **76**, 624.

Vishal, V. & Leung, J.Y. (2018). A novel framework for integration of random-walk particle-tracking simulation in subsurface multi-phase flow modeling. Transport in Porous Media. **125**(3), 609-631.

Wagner et al., (2000), The IAPWS industrial formulation 1997 for the thermodynamic properties of water and steam. *ASME Journal of Engineering: Gas Turbines Power.* **122** (1). 150-182.

Wang, Y. Kovscek., 2002. Streamline Approach for Ranking Reservoir Models that Incorporates Production History, *Society of Petroleum Engineers (SPE)*, Paper 77377.

Wang, C. and Leung, J.Y. (2014). Characterizing the effects of lean zones and shale distribution in SAGD recovery performance. Paper presented at the SPE heavy oil conference-Canada, Calgary, Alberta, Canada.

Wang, C. and Leung, J.Y. (2015). Characterizing the effects of lean zones and shale distribution in steam-assisted-gravity-drainage recovery performance. *SPE Reservoir Evaluation & Engineering* **18**(3), 329-345.

Wang, C., Ma, Z., Leung, J. Y., & Zanon, S. D. (2018). Correlating stochastically distributed reservoir heterogeneities with steam-assisted gravity drainage production. *Oil & Gas Sciences and Technology–Revue d'IFP Energies nouvelles*, **73**, 9.

Wilde, B., J., & Deutsch, C. V., (2012). Calculating an improved connected hydrocarbon volume with line-of sight for ranking realizations by SAGD performance. *CCG Annual Report 14*. Paper 205.

Yang, C., & Butler, R. M. (1992). Effects of reservoir heterogeneities on heavy oil recovery by steam- assisted gravity drainage. *Journal of Canadian Petroleum Technology.* **31**(08), 37-43.

Zhang W., Youn S., & Doan Q. (2005). Understanding reservoir architectures and steam chamber growth at Christina Lake, Alberta, by using 4D seismic and crosswell seismic imaging. Paper presented at the *SPE/PS-CIM/CHOA International Thermal Operations & Heavy Oil Symposium*, Calgary, AB, Canada

Zheng, J., Leung, J.Y., Sawatzky, R.P., and Alvarez, J.M. (2018a). An AI-based workflow for estimating shale barrier configurations from SAGD production histories. *Neural Computing and Applications*. https://doi.org/10.1007/s00521-018-3365-9.

Zheng, J., Leung, J. Y., Sawatzky, R. P., & Alvares, J. M., (2018b). A cluster-based approach for visualizing and quantifying the uncertainty in the impacts of uncertain shale barrier

configurations on SAGD production. Paper presented at the SPE Canada Heavy Oil Technical

Conference, Calgary, Canada.